ANITA LEITGEB

Contributions to the Advancement of Ruthenium Based Initiators for Olefin Metathesis

Applications in ROMP

DOCTORAL THESIS

Dissertation

zur Erlangung des akademischen Grades einer Doktorin der technischen Wissenschaften an der Technischen Universität Graz

Betreuung: Assoc. Prof. Dipl.-Ing. Dr.techn. Christian Slugovc
Institut für Chemische Technologie von Materialien

Jänner 2012

ACKNOWLEDGEMENT

ABSTRACT

The Nobel Prize for Chemistry in 2005, caused another boost in research on olefin metathesis. As a powerful C–C bond forming reaction, metathesis allows for economic synthetic pathways in fine chemical or pharmaceutical industry. With the development of highly active, robust ruthenium based catalysts, ring opening metathesis polymerization (ROMP) has gained much attention - mainly in the field of material design, where tailored specialty polymers are requested. Modifications of the employed initiators can have a decisive influence on the resulting polymer. This work contributes to the advancement of new ruthenium based olefin metathesis initiators for their applications in two diametrically opposed ROMP application fields: "**App$_{act}$**", the controlled synthesis of well-defined ROM polymers with highly active initiators, and "**App$_{lat}$**", thermally triggered polymerization with latent initiators. **App$_{lat}$** is particularly interesting for industrial processes like ink-jet-printing or reaction injection molding, and has herein been investigated upon bulk polymerization of the commodity material dicyclopentadiene (DCPD).

Steric and electronic impacts of three N-heterocyclic carbene ligands – **SIMes** (1,3-dimesityl-4,5-dihydroimidazole-2-ylidene), **SIPr** (1,3-di(2,5-di-isopropyl-phenyl)-4,5-dihydroimidazole-2-ylidene) and **SI-o-Tol** (1,3-di(*ortho*-tolyl-4,5-dihydro-imidazole-2-ylidene) – on initiation and propagation behavior of 2nd and 3rd generation ruthenium initiators have been investigated. Resulting polymers have been compared regarding the *cis/trans* ratio of double bonds and molecular weight distributions, revealing considerable deviations. The unexpected bimodality in the context of highly active SIPr-initiators is discussed. A series of apparently very similar initiators based on the Hoveyda concept of chelating carbene ligands has been investigated. Highly active species **extHov1** (Dichloro-(κ^2(C,O)-((3-isopropoxynaphthalen-2-yl)methylene)(1,3-bis(2,4,6-trimethylphenyl)-4,5-dihydroimidazol-2-ylidene)ruthenium) was found suitable for **App$_{act}$**, whereas **App$_{lat}$** is shown to be feasible with "sibling species" **extHov2** (Dichloro-(κ^2(C,O)-((2-isopropoxynaphthalen-1-yl)methylene)(1,3-bis(2,4,6-trimethylphenyl)-4,5-dihydroimidazol -2-ylidene)ruthenium). Commercially available initiators **M2** (1,3-Bis(2,4,6-trimethylphenyl)-2-imidazolidinylidene)-dichloro-(3-phenyl-*1H*-inden-1-ylidene)(tricyclohexylphosphine)ruthenium) and **M22** (1,3-Bis(2,4,6-trimethylphenyl)-2-imidazolidinylidene)-dichloro-(3-phenyl-*1H*-inden-1-ylidene)(tri-isopropylphosphite)-ruthenium) have been evaluated regarding **App$_{lat}$** for DCPD for the first time. Mechanical testing of shoulder test bars from poly(DCPD) revealed tensile strengths in the range of respective values from literature. Commercially available initiator **M31** (1,3-Bis(2,4,6-trimethylphenyl)-2-imidazolidinylidene)dichloro-(3-phenyl-*1H*-inden-1-ylidene)(pyridyl)ruthenium) was employed in two different mixed ROMP-ATRP approaches for the synthesis of new, well-defined organic-inorganic hybrid graft-co-polymers.

ZUSAMMENFASSUNG

Der Nobelpreis für Chemie 2005 führte zu einem immensen Forschungsaufschwung in der Olefinmetathese. Die C-C bindungsbildende Reaktion ermöglicht ökonomische Synthesen für die Herstellung von z.B. Feinchemikalien oder Pharmazeutika. Durch die Entwicklung hochaktiver, stabiler Ruthenium-Initiatoren hat vor allem die Ring öffnende Metathesepolymerisation (ROMP) profitiert, besonders im Bereich maßgeschneiderter Polymere für die Materialentwicklung. Modifizierungen der hierfür verwendeten Initiatoren können den Polymerisationsverlauf und somit auch die Eigenschaften des Polymers entscheidend verändern. Die vorliegende Arbeit beschäftigt sich mit Weiterentwicklungen neuer Ruthenium-Initiatoren für Anwendungen in ROMP in zwei diametral entgegengesetzten Anwendungsgebieten: „**App**$_{act}$", die kontrollierte Synthese von wohldefinierten ROM Polymeren mit hochaktiven Initiatoren, und „**App**$_{lat}$", die thermisch schaltbare Polymerisation mit latenten Initiatoren. **App**$_{lat}$ ist besonders für industrielle Prozesse (Ink-jet-printing oder Spritzguss) interessant, und wurde hier hauptsächlich am Beispiel der Polymerisation von Dicyclopentadien (DCPD), einem großtechnisch wichtigen Material, untersucht. Sterische und elektronische Einflüsse dreier N-hetrocyclischer Carbenliganden – **SIMes** (1,3-Dimesityl-4,5-dihydroimidazol-2-yliden), **SIPr** (1,3-Di(2,5-di-isopropylphenyl)-4,5-dihydroimidazol-2-yliden) und **SI-o-Tol** (1,3-Di(*ortho*-tolyl-4,5-dihydroimidazol-2-yliden) auf Initiations- und Propagierungsverhalten von Ruthenium-Initiatoren der 2. und 3. Generation wurde untersucht. Die entstandenen Polymere wurden hinsichtlich des *cis/trans* Verhältnisses der Doppelbindungen, sowie Molekulargewichtsverteilung verglichen, wobei deutliche Abweichungen festgestellt wurden. Die unerwartete Bimodalität im Zusammenhang mit hochaktiven SIPr-Initiatoren wird erörtert. Eine Reihe augenscheinlich ähnlicher Hoveyda-Typ Initiatoren wurde untersucht: Der hochaktive **extHov1** (Dichloro-(κ^2(C,O)-((3-isopropoxy-naphthalen-2-yl)methylene)(1,3-bis (2,4,6-trimethylphenyl)-4,5-dihydroimidazol-2-yliden)ruthenium) ist für **App**$_{act}$ geeignet, wohingegen "Bruderkomplex" **extHov2** (Dichloro-(κ^2(C,O)-((2-isopropoxy-naphthalen-1-yl)-methylene)(1,3-bis(2,4,6-trimethyl-phenyl)-4,5-dihydroimidazol-2-yliden)ruthenium eine gute Wahl für **App**$_{lat}$ zu sein scheint. Die kommerziell erhältlichen Initiatoren **M2** (1,3-Bis(2,4,6-trimethylphenyl)-2-imidazolidinyliden)-dichloro-(3-phenyl-*1H*-inden-1-yliden)(tricyclohexyl-phosphine)-ruthenium) und **M22** (1,3-Bis(2,4,6-trimethylphenyl)-2-imidazolidinylidene)-dichloro-(3-phenyl-*1H*-inden-1-yliden)(tri-isopropylphosphite)ruthenium), wurden erstmals hinsichtlich **App**$_{lat}$ für DCPD evaluiert. Bei der Zugprüfung hergestellter Schulterstäbe aus poly(DCPD) wurden literaturübliche Werte für die Zugfestigkeit erreicht. Der kommerziell erhältliche Initiator **M31** (1,3-Bis(2,4,6-trimethylphenyl)-2-imidazolidinylidene) dichloro-(3-phenyl-*1H*-inden-1-yliden)(pyridyl)ruthenium) wurde erfolgreich für die Synthese neuer, wohldefinierter organisch-anorganischer Hybrid-graft-co-Polymere eingesetzt.

TABLE of CONTENTS

1 PREFACE

The following work was accomplished within the EUMET project, sponsored by the European Commission within the 7th frame work program (**FP7 no CP-FP 211468-2**). The project itself aims at design, development, utilization and commercialization of olefin metathesis catalysts.

The EUMET consortium is composed of six academic research groups (universities) and three industrial partners spread in Europe. Universities involved are:

- University of St Andrews, Scotland (Prof. Steven P. Nolan)
- University of Salerno, Italy (Prof. Luigi Cavallo)
- University of Warsaw, (Prof. Karol Grela
- Leibniz University of Hannover, Germany (Prof. Andreas Kirschning)
- Technical University of Graz, Austria (Prof. Christian Slugovc)
- École Nationale Supérieure de Chimie de Rennes, France (Dr. Marc Mauduit)
- Umicore, Germany (Dr. Angelino Doppiu)
- Janssen Pharmaceutica, Belgium (Dr. Andras Horvath)
- IFP Energies nouvelles, France (Dr. Hélène Olivier-Bourbigou)

The project comprises several work packages whereas the herein presented work is located in two of them: **WP1 – Catalyst Synthesis**: Development and synthesis of new ligands and the corresponding ruthenium complexes; and **WP3 – Catalysis**: Testing of the newly developed catalysts in olefin metathesis reactions. Regarding WP3, Graz University of Technology (respectively the author of this work) is mainly involved in ring opening metathesis polymerization (ROMP). ROMP is a special variety of olefin metathesis where the term catalyst does not adequately describe the role of the ruthenium complexes. Rather, the term **initiator** shall be used in the following.

This work is composed of several individual parts that are all linked via the EUMET project, and most of them have been realized as cooperation with one or several project partners. However, obtained results will herein always be presented exclusively from the "ROMP-point-of-view" but discussed in full context when necessary for clarity.
The INTRODUCTION will give general background information on the chemistry involved in this work. A short historical overview on olefin metathesis chemistry and initiator development is given, emphasizing on ROMP. It is aimed at contouring the

different core themes, so that a comprehensive overview is provided without getting lost in details.

The part "INITIATOR DESIGN AND TESTING IN ROMP" treats development and syntheses of new metathesis initiators that have been accomplished for this work. Structural implications on the activity in ROM polymerization are evaluated and discussed.

Chapter 4 and chapter 5 deal with commercially available initiators M2, M22 and M31 (whereas M22 has been developed within the EUMET project at the University of St. Andrews), and their respective use in diverging application fields of ROMP.

A comprehensive CONCLUSION will critically summarize obtained results and also mention remaining issues.

In the EXPERIMETNAL PART synthetic details, experiment setups, interpretation of spectra etc. are provided.

2 INTRODUCTION

2.1 Olefin Metathesis: A Nobel Prize Winning Reaction

Olefin Metathesis is a transition metal catalyzed, C – C double bond forming reaction. This reaction has never been observed in nature. As for chemistry, olefin metathesis has emerged as a powerful tool facilitating the synthesis of molecules that are hardly accessible by other means. The mechanism of olefin metathesis allows a large pool of substrates including linear olefins and (α,ω)-di-olefins, acrylates, vinyl compounds and a cyclic olefins. Many of these substrates can be taken from natural products (e.g. unsaturated fatty acid esters) or from petro industry products (branched, linear or cyclic alkenes). Hence, olefin metathesis gives access to a broad variety of products and has therefore been established in organic chemistry as well as oleo chemistry and polymer chemistry. In 2005 the Nobel Prize for Chemistry was awarded to Yves Chauvin, Robert H. Grubbs, and Richard R. Schrock for "the development of the metathesis method in organic synthesis".[1]
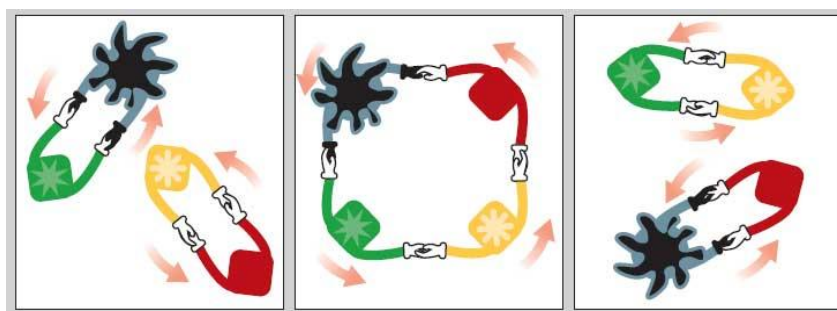
Figure 1: Olefin metathesis as a dance with changing partners[1]

2.1.1 From Ill-Defined Heterogeneous Catalysts to Tailored Transition Metal Complexes

The olefin metathesis reaction was already discovered in the late 1950s, when also the Ziegler-Natta polymerization of ethylene was disclosed.[2] Olefin metathesis products were observed when using several ill-defined heterogenous catalytic systems, mostly involving transition metal halides and alkylation reagents. The first targeted works on olefin metathesis were published in the 1960, when norbornene was polymerized by

---

[1] http://www.nobelprize.org/nobel_prizes/chemistry/laureates/2005/press.html; (Press Release and supplementary information; The Nobel Prize in Chemistry 2005) 2011, Nov 16
[2] Ziegler, K.; Holzkamp, E.; Breil, H.; Martin, H. *Angew. Chem.* **1955**, *67*, 426.

ROMP with a catalytic system of $TiCl_4$-$LiAl(hep)_4$.[3] But it was not before 1971 that the mechanism had been disclosed by Yves Chauvin et al.[4] Chauvin proposed a reversible [2+2] cycloaddition mediated by a transition metal carbene proceeding via a metallacyclobutane intermediate (*cf.* Scheme 1). This mechanism nowadays is still considered to be what actually happens in olefin metathesis.
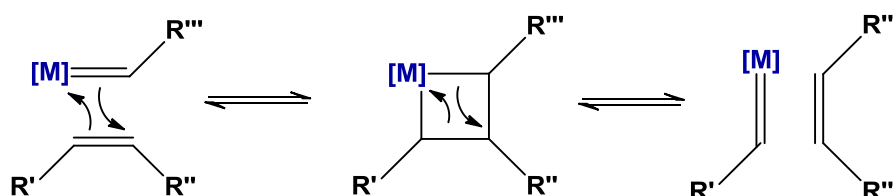
Scheme 1: Chauvin mechanism for olefin metathesis

The first well defined homogenous catalytic systems were introduced by Richard Schrock, employing tungsten and molybdenum alkylidene complexes with various ligands in 1990 (Figure 2).[5] These complexes of the general formula $M(NAr)(CHR)(OR')_2$ (M=Mo, W; Ar=aryl, R = aryl or alkyl; R' = CMe_3, CMe_2CF_3, $CMe(CF_3)_2$, $C(CF_3)_2$, aryl) facilitated controlled olefin metathesis reactions with high initiation and propagation rates and often enable living polymerization.[6] However, these systems suffered from high sensitivity towards oxygen and moisture and only limited functional group tolerance which severely restricted application possibilities.[7]
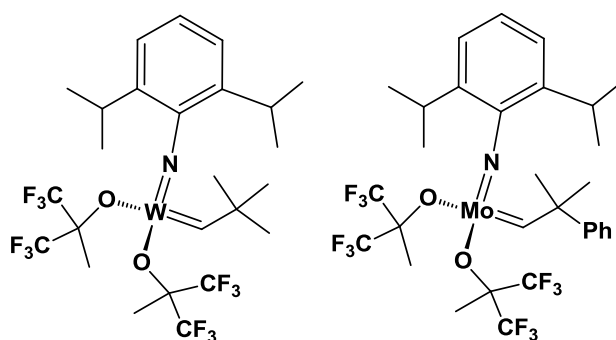
Figure 2: First well defined homogenous catalysts for olefin metathesis

[3] (a) Truett, W. L.; Johnson, D. R.; Robinson, I. M.; Montague, B. A. *J. Am. Chem. Soc.* **1960**, 82, 2337-2340. (b) Calderon, N.; Chen, H. Y.; Scott, K. W. *Tetrahedron Lett.* **1967**, *34*, 3327-3329.

[4] Hèrisson, J. L.; Chauvin, Y. *Makromol. Chem.* **1971**, *141*, 161-176.

[5] Schrock, R.R. *Acc. Chem. Res.* **1990**, *23*, 158-165.

[6] (a) Schrock, R.R.; Hoveyda, A.H.; *Angew. Chem.* **2003**, *115*, 4740-4782; (b) Schrock, R.R. *Angew. Chem. Int. Ed.* **2003**, *42*, 4592-4563.

[7] Slugovc, C. *Macromol. Rapid Commun.*, **2004**, *25*, 1283-1297.

Table 1: reactivity of different transition metal carbene complexes towards various substrates[8]

Ti	W	Mo	Ru	reactivity
acids	acids	acids	**olefins**	
alcohols, water	alcohols, water	alcohols, water	acids	
aldehydes	aldehydes	aldehydes	alcohols, water	↑
ketones	ketones	**olefins**	aldehydes	
esters, amides	**olefins**	ketones	ketones	
olefins	esters, amides	esters, amides	esters, amides	

Grubbs et al. subsequently introduced ruthenium based alkylidene initiators that yielded to a downright rebirth of olefin metathesis.[8] Most prominent, the so-called Grubbs 1st generation complex featuring two neutral phosphine ligands (**G1**: $(PCy_3)_2(Cl)_2Ru=CHPh$; Figure 3, left) solved the above described problems of the Schrock catalysts to a high extent and olefin metathesis polymerization could be extended to ambient conditions and even protic media (*cf*. reactivity trends in Table 1). However, this advantage had to be paid with the high prize of tremendously reduced activity. Ligand variation eventually led to the development of 2nd generation ruthenium complexes that are characterized by an *N*-heterocyclic carbene ligand (NHC) replacing one of the phosphines from **G1**. The NHC ligand H_2IMes (N,N-bis(mesityl)-4,5-dihydroimidazol-2-lidene) is a strongly binding σ-donor ligand and provides **G2** $((H_2IMes)-(PCy_3)(Cl)_2Ru=CHPh$; Figure 3, middle) with a completely different activity profile. A high propagation rate is opposed to a very slow initiation step compared to **G1**, which is prohibiting the possibility of living polymerization. On the other side, functional group tolerance of **G2** is even higher than of **G1**.[9] Slugovc et al. published a systematic test series where the effects of various donor additives had been studied upon comparing molecular weights and weight distributions of resulting ROMP monomers.[10] In course of these studies a highly active initiator was formed (yielding low M_n and PDI-values) upon the addition of pyridine. At about the same time, **G3** $((H_2IMes)(py)_2(Cl)_2Ru=CHPh)$; Figure 3, right) and its 3-bromopyridine derivative was

[8] Schwab, P.; Grubbs, R. H.; Ziller, *J. W. J. Am. Soc.*, **1996**, *118*, 100-110.

[9] (a) Sanford, M. S.; Love, J. A.; Grubbs, R. H. *J. Am. Chem. Soc.* **2001**, *123*, 6543-6554. (b) Trnka, T. M.; Grubbs, R.H. *Acc. Chem. Res.* **2001**, *34*, 18-29; (c) Buchmeiser, M. R.; *Chem. Rev.* **2000**, *100*, 1565-1604; (d) Frenzel, U.; Nuyken, O.; *J. Polym. Sci. Part A: Polym. Chem*. **2002**, *40*, 2895-2916; (e) Fürstner, A.; *Angew. Chem* **2000**, *112*, 3140-3172; *Angew. Chem. Int. Ed*. **2000**, *39*, 3012-3043; (f) Roy, R.; Das, S. J.; *Chem. Commun*. **2000**, *519-529*; (g) Jorgensen, M.; Hadwiger, P.; Madsen, R.; Stütz, A. E.; Wrodnigg, T. M. *Curr. Org. Chem*. **2000**, 4, 565-588; (h) Maier, M. E.; *Angew. Chem*. **2000**, *112*, 2153-2157; *Angew. Chem. Int. Ed*. **2000**, *39*, 2073-2077; (i) Schrock, R. R. *Tetrahedron* **1999**, *55*, 8141-8153; (j) Hoveyda, A. J.; Gillingham, D. G.; VanVeldhuizen, J. J.; Kataoka, O.; Garber, S. B.; Kingsbury, J. S.; Harrity, J. P. A. *Org. Biomol. Chem*. **2004**, *2*, 8-23; (k) Marciniec, B.; Pietraszuk, C. *Curr. Org. Chem*. **2003**, *7*, 691-735.

[10] Slugovc, C.; Demel, S.; Riegler, S.; Hobisch. J.; Stelzer, F. *Macromol. Rapid. Commun.* **2004**, *25*, 475–480.

published by Grubbs et al.[11] The introduction of pyridine as labile ligand led to fast and complete initiation and eventually to an increase of activity by six orders of magnitude.[10,11]
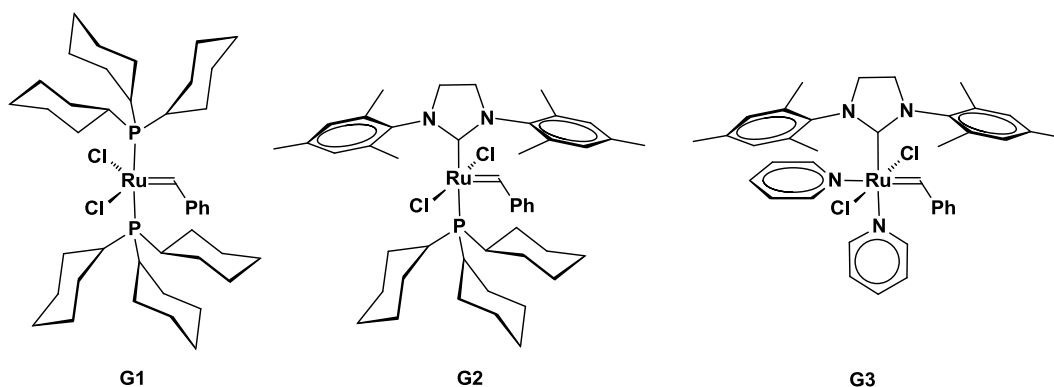
Figure 3: The so-called Grubbs catalysts 1st, 2nd and 3rd generation G1, G2 and G3 (left to right)

With the ruthenium benzylidene complexes (**G1**-**G3**) a new era of olefin metathesis had begun. The paramount functional group tolerance and broad application spectrum of course inspired for further improvement and development of olefin metathesis catalysts. Within the last decade, an alternative system to the Grubbs type complexes was established. Very efficient ruthenium allenylidene complexes for ring closing metathesis reactions by several groups turned out to in fact be ruthenium-indenylidene species arising from in situ isomerization.[12] In due course these complexes were further investigated and a mechanism for the isomerization was established by studying η^6-arene-ruthenium complexes [RuCl$_2$ (p-cymene)]$_2$ or Wilkinson catalyst [Ru(Cl$_2$(PPh$_3$)$_4$] reacting with propargylic alcohol (3,3-diphenylpropyn-3-ol) and a proton source (Scheme 2).[13] A key feature differentiating the resulting ruthenium indenylidene complexes from Grubbs-type complexes is the quaternary carbene carbon C$_\alpha$.

[11] Love, J. A.; Morgan, J. P.; Trnka, T. M.; Grubbs, R. H. *Angew. Chem*. **2002**, *114*, 4207-4209.

[12] (a) Jafarpour, L.; Schanz, H.-J.; Stevens, E. D.; Nolan, S. P. *Organometallics* **1999**, *18*, 5416–5419; (b) Fürstner, A.; Thiel, O. R.; Ackermann, L.; Schanz, H.-J.; Nolan, S. P. *J. Org. Chem.* **2000**, *65*, 2204–2207; (c) Fürstner, A.; Guth, O.; Düffels, A.; Seidel, G.; Liebl, M.; Gabor, B.; Mynott, R. Chem. Eur. J. **2001**, *7*, 4811–4820.

[13] (a) Castarlenas, R.; Vovard, C.; Fischmeister, C.; Dixneuf, P. H. *J. Am. Chem. Soc*. **2006**, *128*, 4079-4089. (b) Antonucci, A.; Bassetti, M.; Bruneau, C.; Dixneuf,P. H.; Pasquini, C. *Organometallics* **2010**, *29*, 4524–4531.
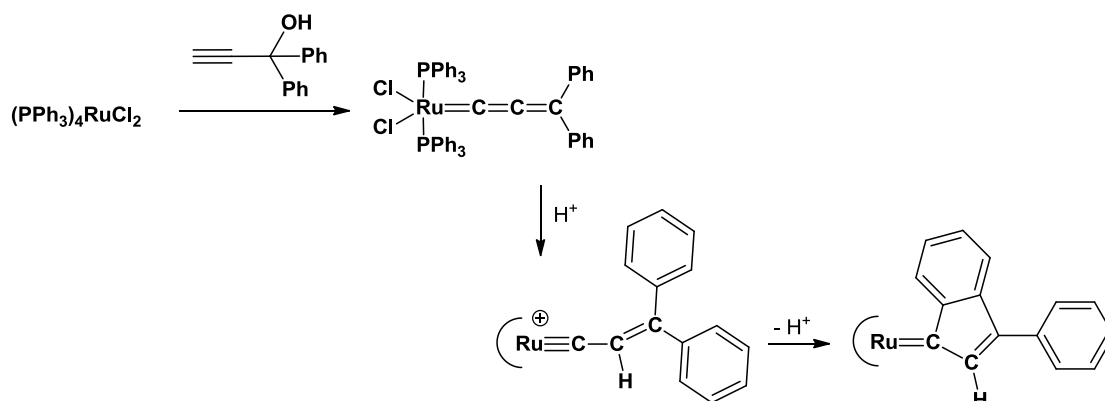
Scheme 2: Synthesis ruthenium indenylidene complexes from Wilkinson catalyst[13]

Today, indenylidene carbenes as alternatives to Grubbs' benzylidenes are well established in ruthenium olefin metathesis catalysts.[14] Numerous variations regarding ancillary ligands have been described and shown to be highly active in various metathesis reactions, yet maintaining an extremely high stability at ambient conditions.[12,15] Meanwhile, an extensive library of such complexes is commercially available in Europe.[16] Most prominent members are analogues to **G1**, **G2** and **G3**, namely **M1**, **M2** and **M31** respectively. Notably, 3rd generation indenylidene complex **M31** only bears one pyridine ligand instead of two (Figure 4). The **M**-series can substitute high-priced Grubbs complexes regarding their applicability to a large extent. [14,17] Hence indenylidene complexes got more and more attractive for ongoing research on olefin metathesis, both as actual catalysts but also as precursors for new complexes.

[14] (a) Leitgeb, A.; Burtscher, D.; Bauer, T.; Slugovc, C. *Chim. Oggi*. **2009**, *27*, 30-32.

[15] (a) Opstal, T.; Verpoort, F. *Angew. Chem., Int. Ed.* **2003**, 42, 2876–2879. (b) Clavier, H.; Nolan, S. P. *Chem.;Eur. J.* **2007**, 8029–8036; (c) Stjin, M; Drozdzak, R.; Dragutan, V.; Dragutan, I.; Verpoort, F. Eur. *J. Inorg. Chem*. **2008**, 432–440.

[16] Umicore Precious Metal Refining, Hanau, Germany

[17] (a) Burtscher, D.; Lexer, C.; Mereiter, K.; Winde, R.; Karch, R.; Slugovc C. *J. Polym. Sci. Part A: Polym. Chem.* **2008**, *46*, 4630-4635. (b) de Frément, P.; Clavier, H.; Montembault, V.; Fontaine, L.; Nolan, S. P. *J. Mol. Catal. A,* **2008**, *283*, 108-113.
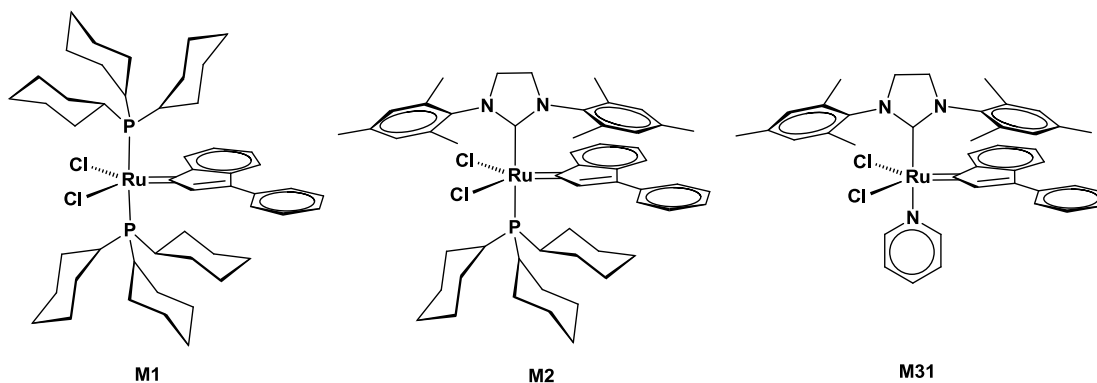
Figure 4: Analogues to Grubbs' catalysts featuring an indenylidene carbene

Another variation of the benzylidene ligand of Grubbs initiators was made by Hoveyda et al. by functionalizing it with an ether moiety in *6*-position. As a consequence, the labile ligand (phosphine or pyridine respectively) is kicked out and a ruthenium complex featuring a chelating carbene ligand results. Complexes **Hov-1**[18] and **Hov-2**[19] (Figure 5) can be synthesized by a metathesis reaction of 1-isopropoxy-2-vinylbenzene with **G1** and **G2** respectively in presence of CuCl as phosphine scavenger. Especially phosphine-free complex **Hov-2** revealed surprising characteristics superior to **G2** in terms of stability and initiation rates. Regarding ring opening metathesis polymerization this results in lower molecular weights and PDI values within shorter time. Yet, living polymerization is not feasible with most monomers and PDI values are around 1.3 for monomers that prohibit chain degradation by backbiting.[7] This new architecture employing chelating ligands was to immensely influence catalyst design. In particular for olefin metathesis polymerization a concept making use of this feature will be discussed in chapters 0 and 0.
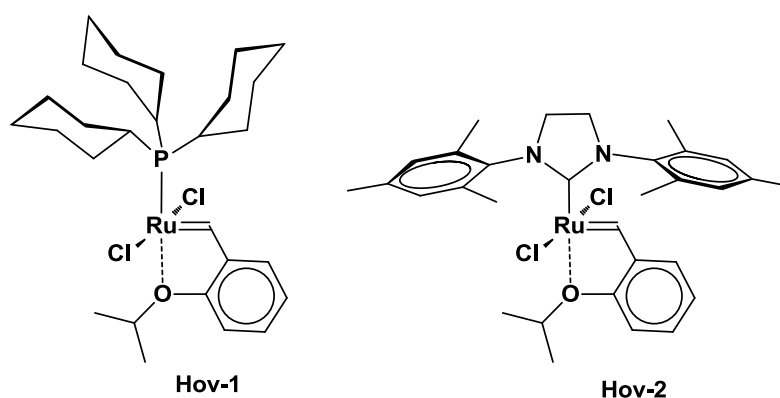
Figure 5: 1ˢᵗ and 2ⁿᵈ generation Hoveyda catalysts featuring a chelating carbene ligand

[18] Kingsbury, J. S.; Harrity, J. P. A.; Bonitatebus, P. J. Jr.; Hoveyda, A. H. *J. Am. Chem. Soc.* **1999**, 121, 791–799.

[19] Garber, S. B.; Kingsbury, J. S.;Gray, B. L.; Hoveyda, A. H. *J. Am. Chem. Soc.* **2000**, 122, 8168–8179.

2.1.2 Olefin Metathesis Reactions

The development of new initiator systems has facilitated a large scope of various metathesis reactions, most important ring closing metathesis (RCM), ring opening metathesis polymerization (ROMP), cross metathesis (CM), acyclic diene metathesis polymerization (ADMET) and en-yne metathesis (Figure 6). This again extremely broadened the application spectrum of olefin metathesis which today many fields of chemistry, technology and life science, as schematically shown in Figure 7.
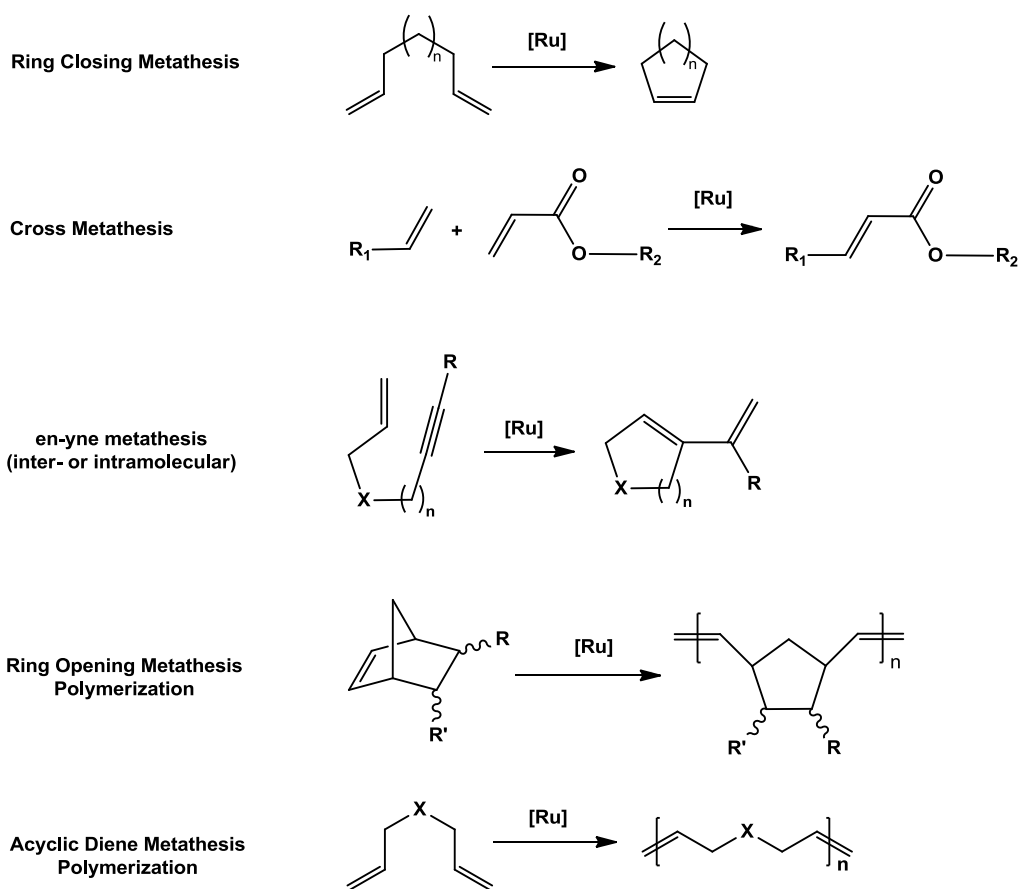
Figure 6: Scope of olefin metathesis with ruthenium catalysts

Pladienolide D: R′ = H

Kanada, Itoh, et al *Angew. Chem. Int Ed.* **2007**, *46,* 4350

S. Kovačič, P. Krajnc and C. Slugovc; *Chem. Commun.*, **2010**, *46*, 7504.

Fraunhofer IAP
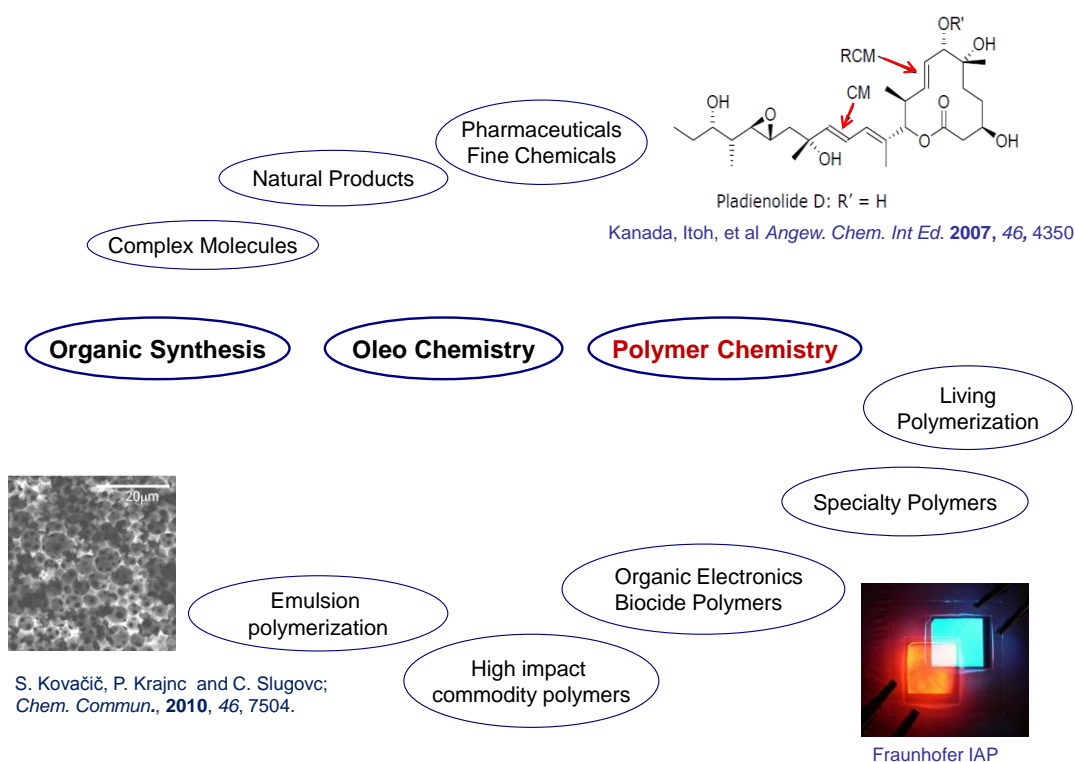
Figure 7: Application fields of olefin metathesis

2.2 Ring Opening Metathesis Polymerization (ROMP)

This chapter focuses on ring opening metathesis polymerization that constitutes the heart of this work. ROMP is an extraordinary polymerization method in many ways. Apart from its application for the synthesis of specialty polymers (for the moment mostly in academia), ROMP is also used for industrial scale production of several polymers. Moreover, ROMP is a viable tool for the characterization of metathesis initiators.

2.2.1 ROMP in Industry

In 1976 CdF Chimie launched the ROMP product poly(norbornene) under the trade name Norsorex® which was later produced by Zeon Europe (Germany). Today Norsorex® is produced by the Austrian company AstroTech in Vienna for numerous and widely varied applications, such as oil absorption, vibration and noise dampers for railways and tires, body protection sports equipment, footwear, a.s.o. The high molecular weight polymer (> 3 000 000 g/mol) has a high affinity to hydrocarbons and

can absorb around 10 times of its own weight of oil. Also 300 phr (parts per hundred parts of rubber) of various fillers can be added, giving a reasonable rubber compound.[9d,20] Vestenamer® is ROM polymerized cyclooctene, produced by Evonik Degussa. Vestenamer® is a semicrystalline rubber and acts as processing aid in rubber industry e.g. for the recycling of waste rubber or as additive in asphalt for easier processing and prevention of unwanted formation of hazardous vapors. [21] Dicyclopentadiene is industrially ROM polymerized by the Metton process by the companies Metton and Telene. Dicyclopentadiene exhibits two strained rings and yields therefore cross-linked thermosets after ROMP. With reaction injection molding (RIM) large pieces for e.g. automotive sector can be produced.[22]
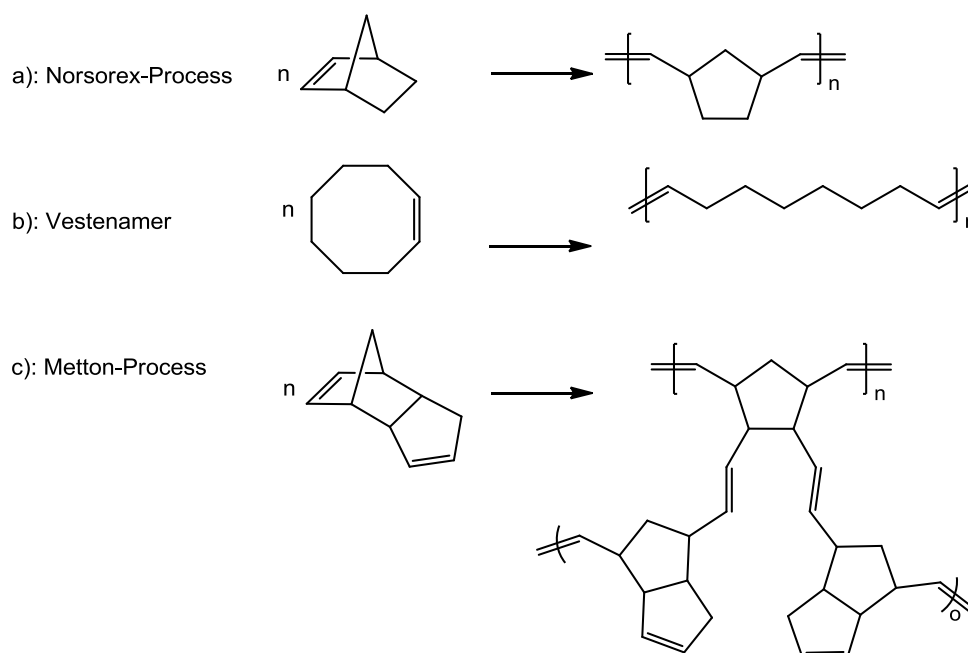
Scheme 3: Industrial applications of ROMP

For all of the industrial processes described above tungsten or molybdenum based catalysts are used, e.g. WCl_6/Et_3Al.[9d,23] Up to now the low costs for these systems outperform ruthenium initiators for industrial applications despite their low functional group tolerance and ill-definedness.

[20] http://astrotech.at/index.php/home.html (2011, Nov 18)

[21] http://www.degussa-hpp.com/eng/products/rubber/ (2011, Nov 21)

[22] (a) http://www.telene.com, (2011, Nov 21); (b) http://www.metton.com/index.html, (2011, Nov 21)

[23] Janiak, C.; Klapötke, T. M.; Meyer, H.-J. *Moderne anorganische Chemie*, **1999**, Gruyter Verlag Berlin, ed. (Erwin Riedel)
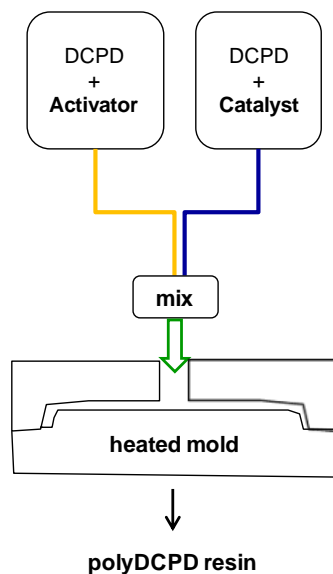
Figure 8: The Metton process for reaction injection molding of DCPD with 2-component-catalysts

2.2.1.1 Dicyclopentadiene (DCPD)

Dicyclopentadiene is available as a cheap by-product from petrochemical industry. In the C_5-fraction of oil refineries cyclopentadiene (CPD) is one of the products. After dimerization via a Diels-Alder reaction[24] at elevated temperatures (~100°C) it can be separated as dicyclopentadiene (DCPD) from the stream by distillation in about 90% purity. This raw product constitutes also the transportable form of CPD. Further purification of DCPD is accomplished by vacuum distillation at specific conditions. A purity of 96% yields a greasy colourless solid at room temperature, exhibiting a density of 0.98 g*mL^{-1}, a melting point of 32°C and a boiling point of 170°C (*endo* isomer).[25] In most processes a purity of 98 % and higher is required. Dicyclopentadiene exists in two isomers, *endo* and *exo* (*cf*. Figure 9), whereas the *endo* isomer is thermodynamically more stable and hence representing the main share in commercially available DCPD (ratio of *endo* isomer > 95 %).[26]

---

[24] Diels, O.; Alder, K. *Liebigs Annalen der Chemie*. **1928**, *460*, 98–122.

[25] (a) Ullmann's Encyclopedia of Industrial Chemistry. P*henol Derivatives/Cyclopentadiene and Cyclopentene (Online Version)* DOI: 10.1002/14356007 (2011, Nov 21); (a) Yamazaki, M. *J. Mol. Catal. A*, **2004**, *213*, 81–87.

[26] NMR spectra of SigmaAldrich DCPD given in Figure 66.

endo DCPD   exo DCPD
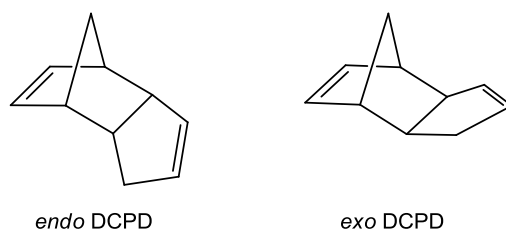
Figure 9: Isomers of DCPD

The *exo* isomer can be obtained upon elaborate thermal and pressurized treatment[27] which is usually not accomplished due to the high effort. However, the *exo* isomer is much more reactive in metathesis.[28] This has been impressively shown by Kessler for the ROM polymerization of DCPD followed by dynamic scanning calorimetry (DSC) employing Grubbs 1st generation initiator **G1**.[29] At different scanning rates (2 to 15 K*min[-1]) the *endo* isomer yielded broad exothermic polymerization peaks with their respective maxima between 42°C and 80°C. In contrast, the *exo* isomer reacted at lower temperatures with comparatively sharp peaks between 35°C and 45°C in the same temperature program. It is to be noted that in the latter case a second, rather broad peak was observed in each curve in the range of the respective *endo* peak (*cf.* Figure 10, right). This was attributed to the cross-linking reaction where the cyclopentene ring is opened. Other than for the more favoured cleavage of the norbornene structure, no considerable differences between *exo* and *endo* isomer are to be expected for this second step.[28]
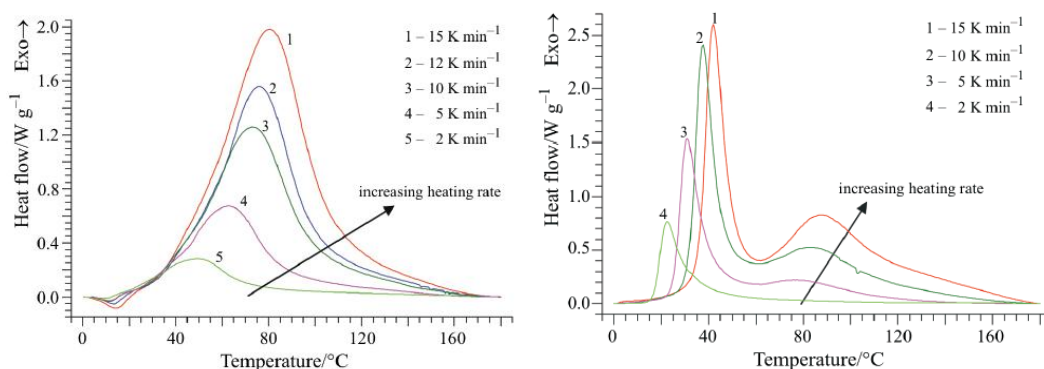
Figure 10: ROMP of *endo* DCPD (left) and *exo* DCPD (right) with G1 (taken from reference 29)

[27] (a) Nelson, G. L.; Kuo, C. L. *Synthesis*, **1975**, *105-106;* (b) Fisher, R. A.; Grubbs, R. H. *Makromolekulare Chemie- Macromolecular Symposia,* **1992***, 63* 271-277. (c) Zhang, X. W.; Jiang, K.; Jiang, Q.; Zou, J. J.; Wang, L.; Mi, Z. T. *Chin. Chem. Lett*. **2007**, *18*, 673-676.
[28] Rule, J. D.; Moore, J. S. *Macromolecules* **2002**, *35,* 7878-7882.
[29] Kessler, M. R.; Larin, G. E.; Bernklau, N. ; *J. Therm. Anal. Cal*. **2006**, *85* 7–12.

Polymers from DCPD are highly cross-linked thermosets featuring the following typical physical properties:[30]

Table 2: physical properties of polyDCPD

Property	Value
Density	1.03 g*cm^{-3}
Tensile strengths (at yield)	47 MPa
Youngs modulus	1850 MPa
Elongation (at yield)	5 %

The favorable physical properties, easy post processability (drilling, threading, sanding etc.) of polyDCPD and its compatibility with a broad range of materials (inorganic fillers, colors, glass or carbon fibers etc.) would make processing modes other than RIM (nitrogen conditions due to sensitivity of catalysts) attractive. Ruthenium initiators provide enough stability for attractive processes at ambient conditions like filament winding, rotational molding or spray casting. However, due to high costs these systems have not yet been implemented in commercial processes.[30(b)] Within this thesis several ruthenium initiators have been tested for their applicability for ROMP of DCPD (chapter 4). DCPD is also employed for special applications in smaller scale such as self-healing materials and highly porous materials. These issues will be treated in the following chapter.

2.3 ROMP in Research for Advanced Applications

ROMP is an extremely versatile polymerization method that can be tuned and adapted almost unrestrictedly upon required needs. In 2004, Slugovc published a comprehensive feature article on state-of-the art ROMP pointing out how to best exploit beneficial characteristics of various ruthenium initiators and presenting a broad library of functional monomers.[7] Parameters addressed in this so-called ROMP-Toolbox are initiators, monomers, solvent and additive effects as well as reaction parameters temperature and time. Initiators will be treated in an extra chapter

---

[30] (a) http://www.matweb.com/search/datasheetText.aspx?bassnum=O3190; MatWeb entry on pDCPD (2011, Nov 22); (b) *PU Magazine International*, **2009**, *5*, 258-264.

emphasizing on ligand modification relevant for this work. In order to draw on the previous chapter, the first part of this section is dealing with special applications of DCPD.

2.3.1 DCPD for Special Applications

2.3.1.1 Self-Healing Polymers

In the early 1980s the concept of self-healing polymers was proposed for the first time.[31] Since then many different methods for self-healing polymeric materials have been published. Due to their diverging (mechanical) properties, thermoplastics and thermosets require different modes of healing. For thermosets, strategies like molecular interdiffusion, photo-induced healing, recombination of chain ends, self-healing via reversible bond formation, or self-healing by nanoparticles, were established. For thermosets a self-healing agent is incorporated into the polymer matrix in form of hollow fibers or microcapsules.[32] White et al were the first to use ROMP for self-healing materials.[33] In case of a crack in the material, healing is accomplished by the release of microencapsulated *endo*-DCPD into the polymer matrix, where I gets into contact with a ROMP initiator (**G1**) and polymerize, thus filling the crack. (*cf*. Figure 11).
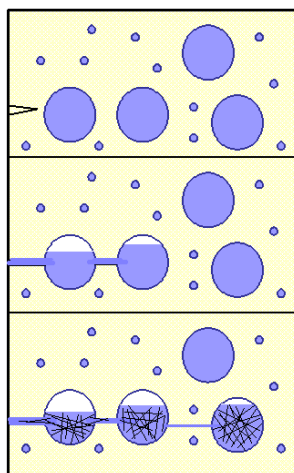
Figure 11: Concept of self-healing using encapsulated healing agents and ROMP initiators. Redrawn from reference 33

[31] Jud, K.; Kausch, H. H.; Williams, J. G. *J Mater Sci* **1981**, *16,* 204-210.

[32] Wu, D. Y.; Meure, S.; Solomon, D. *Prog Polym Sci* **2008**, *33*, 479-522.

[33] White, S. R.; Sottos, N. R.; Geubelle, P. H.; Moore, J. S.; Kessler, M. R.; Sriram, S. R.; Brown, E. N.; Viswanathan, S. *Nature* **2001**, *409*, 794-797.

This preliminary system suffers from some major drawbacks. Firstly, *endo* DCPD exhibits a rather low activity for in situ polymerization which makes high initiator loadings necessary (2.5 %).[33] This again increases costs dramatically. Secondly, the melting point of DCPD is as high as 32°C, making the healing process impossible at room temperature. In order to overcome these problems, 5-ethylidene-2-norbornene (ENB) was investigated as healing agent. This monomer combines high polymerization activity and a low melting point at -80°C. Benefits from DCPD (cross-linked thermoset with high toughness and strength) nevertheless cannot be accomplished by ENB. Hence, a mixture of ENB with a norbornene-based cross-linker was used.[34] Thus, reduced gelation time and resulting in lower initiator loadings could be achieved.

2.3.1.2 Porous ROM Polymers

Porosity of functional materials plays a major role for many applications and highly porous materials have been subject of intensive research during the last years. Properties such as good mechanical strength combined with light weight and large surface serve well for applications such as insulation, solid support for heterogenous reactions or chromatography.[35] There are three ways to obtain highly porous materials via ROMP: (i) concentrated emulsions (ii) phase separation and (iii) secondary processes. (i) The preparation of highly porous polymeric materials via concentrated emulsions is a templating process. Water-in-oil emulsions exhibiting a ratio of internal phase up to 80% (high internal phase emulsions -HIPEs) provide the scaffold for the polymerization. The monomer is located in the organic phase and polymerized while basically maintaining the emulsion's structure, yielding so-called poly(HIPE)s. Due to minor shrinking during the curing process pores are opened by interconnecting windows, a characteristic feature of polyHIPEs.[36] In initial investigations by Deleuze, three different norbornene based monomers for the preparation of porous foams have been tested: tetracyclo [6,2,1^{3,6},0^{2,7}]dodeca-4,9-diene (BVD), dicyclopentadiene (DCPD) and tetracyclodecen.[37] Using initiator **G1**, HIPE structures could only obtained with BVD and DCPD did not yield any porous material under the tested conditions. However, recent developments at Graz University of Technology prove applicability of DCPD for the synthesis of polyHIPEs exhibiting outstanding mechanical properties. Monoliths and membranes of different porosity (50-80%) were prepared with initiator **M2** and a suitable surfactant. [38]

---

[34] Sheng, X.; Lee, J. K.; Kessler, M. R. *Polymer* **2009**, *50*, 1264-1269.
[35] Buchmeiser, M. R. *J Sep Sci* **2008**, *31,* 1907-1922.
[36] Cameron, N. R. *Polymer* **2005**, *46*, 1439-1449.
[37] (a) Deleuze, H.; Faivre, R.; Herroguez, V. *Chem Commun* **2002**, 2822-2823. (b) Benmachou, K.; Deleuze, H.; Heroguez, V. *Reactive and Functional Polymers* **2003**, *55*, 211-217.
[38] Kovacic, S.; Krajnc, P.; Slugovc, C. *Chem. Commun.* **2010**, *46*, 7504-7506.
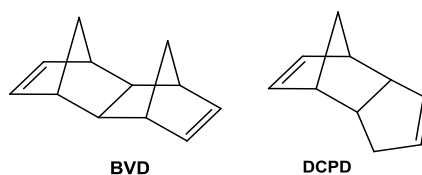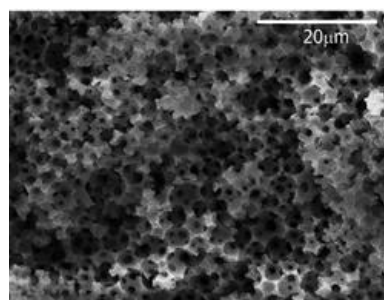
Figure 12: ROMP monomers for polyHIPEs

Figure 13: TEM picture of polyHIPE structure from DCPD (80% pore volume) achieved with M2[38]

Shoulder test bars were produced from these polyHIPEs for tensile strength tests and remarkable results have been accomplished.[39]

2.3.2 Frequently Used ROMP Monomers

As for monomers, olefin metathesis polymerization is also feasible with linear dienes, which are then transformed to ADMET (acyclic diene metathesis polymerization) polymers. However, α,ω-dienes are usually employed in ring closing metathesis (RCM) reactions. For ring opening metathesis polymerization, strained cyclic olefins are most useful. Release of the ring strain in the first step of the metathetic cycle will serve as driving force of the reaction and turn it irreversible. Bicyclic norbornene derivatives are the most prominent monomers for ROMP. They are comparatively easily accessible by Diels Alder reactions of cyclopentadiene and the respective 2-butene compound, and in general they are stable due to ring strain in the right range (27.2 kcal/mol).[40] Moreover, this monomer class can be functionalized upon needs at many positions. In their 2- and 3-position, norbornenes can be either *exo* or *endo* substituted. Regarding the tendency to coordinate towards a metathesis initiator and undergo ring opening, the *exo* isomer is much more active. As the two isomers are hard to separate and mixtures thereof will considerably decrease control over the polymerization progress, the 2,3-*exo,endo*-disubstituted isomer is to be favored. This can be accomplished by using fumaric acid derivatives or other trans-2-butene derivatives for the Diels-Alder

---

[39] Kovačič, S.; Jeřabek, K.; Krajnc, P.; Slugovc, C. *Polym. Chem.* **2012**, *in press.*
[40] Schleyer, P. R.; Williams, J. E.; Blanchard, K.R. *J Am Chem Soc* **1970**, *92*, 2377-2386.

reaction (*cf.* Scheme 4). Another common architecture for specially functionalized monomers is the dicarboximide that is obtained from the norbornene dicarboxylic acid anhydride by amidation. In this monomer class the imide's nitrogen acts as anchor for further groups. 2-Aza-norbornenes are another monomer class that has recently been paid more attention due to its potential applications in biocide polymers.[41]
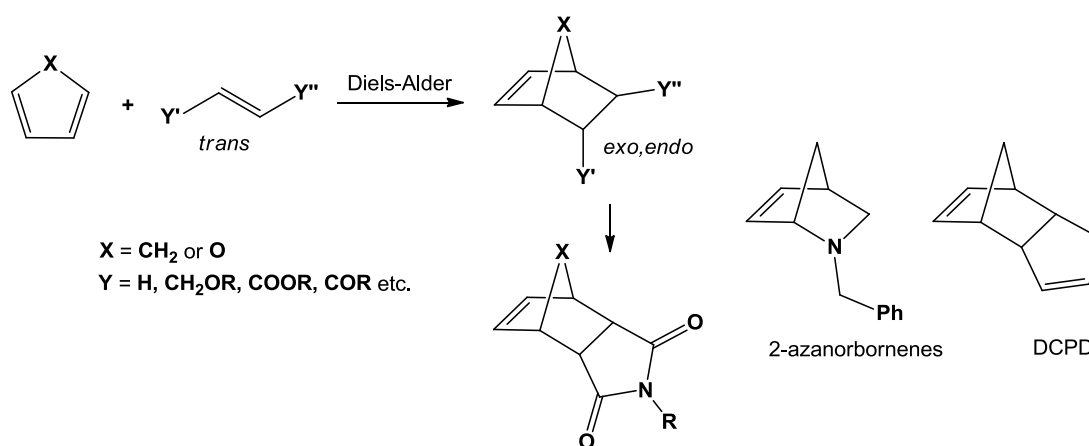
Scheme 4: Typical synthesis and exemplary structures for norbornene based ROMP monomers

Besides of norbornene derivatives also cyclooctene and cyclooctadiene are used for ROMP (*cf.* chapter 2.2.1). However, these monomers yield linear, unsaturated polymer chains that are prone to be attacked by active initiators. Thus the polymer chains are degraded during polymerization and cannot be polymerized in a controlled manner, which results in broad molecular weight distributions (high PDI values). Also, some norbornene derivatives (including neat norbornene) show this behavior. The so-called backbiting is prohibited by sufficient steric encumbrance that usually is guaranteed in 2,3-disubstituted norbornenes.[7] For mono- or unsubstituted monomers, backbiting can be reduced by polymerization at very low temperature, as shown by Grubbs et al. with the polymerization of norbornene with **G3**. The PDI value was reduced from 1.65 (at room temperature) to 1.08 (at -20°C). [42]

---

[41] Gstrein, C. Master Thesis, **2011**, „Synthesis and Characterization of Poly(azanorbornene)s via Ring-Opening Metathesis Polymerization using Ruthenium-based Initiators"

[42] Choi, T.-L.; Grubbs, R. H. *Angew. Chem.* **2003**, *115*, 1785-1788; *Angew. Chem. Int. Ed*. **2003**, *42*, 1743-1746.

2.3.3 Tailored Specialty Polymers: ROMP Is the Tool of Choice

Since the beginning of the 21st century ROMP has developed from a "one-of-many"-polymerization method the tool of choice for the synthesis of advanced macromolecular structures. Research has been focused on obtaining tailored precision polymers for highly demanding purposes in many areas. With the proper choice of monomer and initiator, living polymerization is feasible, which is conditional for well-defined block copolymers featuring various functionalities. A review on recent developments on this sector has been realized in within the PhD-period, which clearly illustrates the applicability of ROMP for smart materials.[43] In the following chapters some selected examples thereof will be discussed in order to demonstrate the paramount nature of ROMP, schematically depicted in Figure 14.
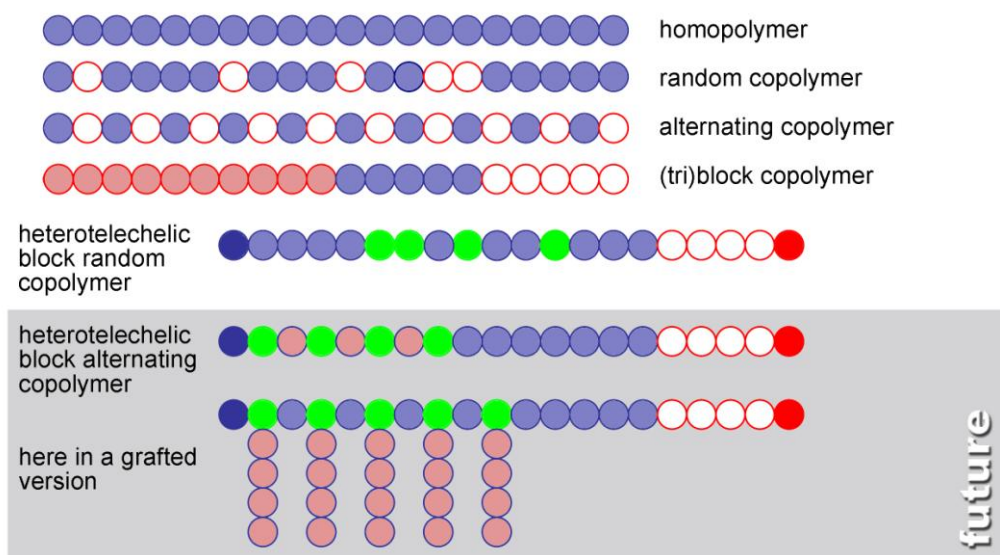
Figure 14: Polymer architectures accessible by ROMP[43]

2.3.3.1 Random and Block-Co-Polymers

Donor-acceptor materials for their application in polymer-based solar cells were accessed by random copolymerization of monomers bearing phthalocyanine and fullerene (C-60).[44] Also for photovoltaic applications, Swager et al. prepared a

---

[43] Leitgeb, A.; Wappel, J.; Slugovc, C. *Polymer* **2010**, *51*, 2927-2946.

[44] De la Escosura, A.; Martinez-Diaz, M. V.; Torres, T.; Grubbs, R. H.; Guldi, D. M.; Neugebauer, H.; Winder, C.; Drees, M.; Sariciftci, N. S. *Chem. Asian J.* **2006**, *1*, 148-154.

precursor ROM block copolymer functionalized with phenylene-thiophene or phenylene-furan moieties. In this approach, the tendency of block copolymers to phase-separate is used to build up nano-structured conducting polymers. A conjugated and thus conductive network by electrochemical means is formed and the conductive moieties will align along the initial backbone.[45] ROMP derived host-guest systems employing phosphorescent platinum(II)[46] or iridium(III)[47] complexes were used for organic light emitting devices (OLEDs). For example, Niedermair et al. used random copolymers of host (carbazole functionalized monomer) and guest (polymerizable platinum complex). The random structure prevents self-quenching. Moreover, this statistic block was implemented in an amphiphilic tribloc-co-polymer that self-aggregates to micelles in selected solvents. Energy transfer from the host to the guest leads to red phosphorescence.[48] Other examples for this type of micelle forming polymer architecture were realized for sensing issues, incorporating pH-sensitive dyes like eosin and fluorescein.[49]
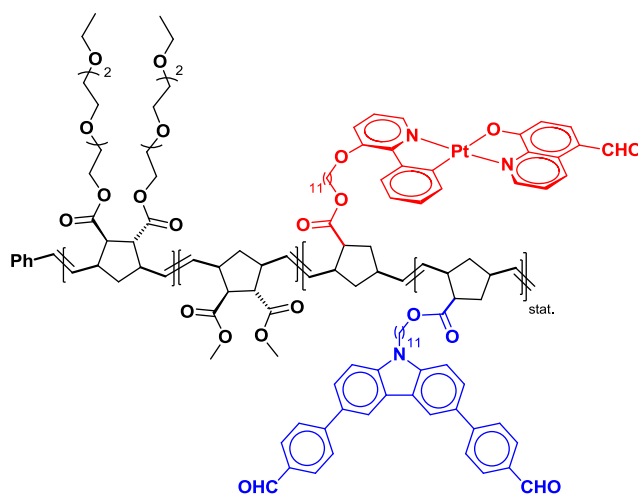

Figure 15: ROM triblock-co-polymer for organoelectronics[48b]

[45] Kang, H. A.; Bronstein H. E.; Swager T. N. *Macromolecules* **2008**, *41*, 5540-5547.

[46] Cho, J. Y.; Domercq, B.; Barlow, S.; Suponitsky, K. Y.; Li, J.; Timofeeva, T. V.; Jones, S. C.; Hayden, L. E.; Kimyonok, A.; South, C. R.; Weck, M.; Kippelen, B.; Marder, S. R. *Organometallics* **2007**, *26*, 4816-4829.

[47] (a) Kimyonok, A.; Weck, M. *Macromol. Rapid Commun.* **2007**, *28,* 152-157; (b) Haldi, A.; Kimyonok, A.; Domercq, B.; Hayden, L. E.; Jones, S. C.; Marder, S. R.; Weck, M.; Kippelen, B. *Adv. Funct. Mater.* **2008**, *18,* 3056-3062. (c) Kimyonok, A.; Domercq, B.; Haldi, A.; Cho, J. Y.; Carlise, J. R.; Wang, X. Y.; Hayden, L. E.; Jones, S. C.; Barlow, S.; Marder, S. R.; Kippelen, B.; Weck, M. *Chem. Mater.* **2007**, *19,* 5602-5608.

[48] (a) Niedermair, F.; Stubenrauch, K.; Pein, A.; Saf, R.; Ingolić, E.; Grogger, W.; Fritz-Popovski, G.; Trimmel, G.; Slugovc, C. *J. Mater. Chem*. **2011**, *21*, 15183–15185. (b) Niedermair, F.; Sandholzer, M.; Kremser, G.; Slugovc, C. *Organometallics* **2009**, *28*, 2888-2896.

[49] (a) Sandholzer, M.; Fritz-Popovski, G.; Slugovc, C. *J Polym Sci Part A: Polym. Chem.* **2008**, *46,* 401–413; (b) Sandholzer, M.; Slugovc, C. *Macromol. Chem. Phys.* **2009**, *210,* 651-658.

Amphiphilic ROMP block-copolymers have also found their way for biochemical/biomedical applications. Sleiman and Bazzi synthesized multi-functional amphiphilic triblock-copolymers with 3rd generation initiator **G3**. Resulting micelles can bind to biological target molecules via specific recognition units, whereas gathered flurescent transition metal complexes in the core of the micelles will act as signal amplifiers.[50] Thus, a detecting, sensing and amplifying tool for biological applications was developed.
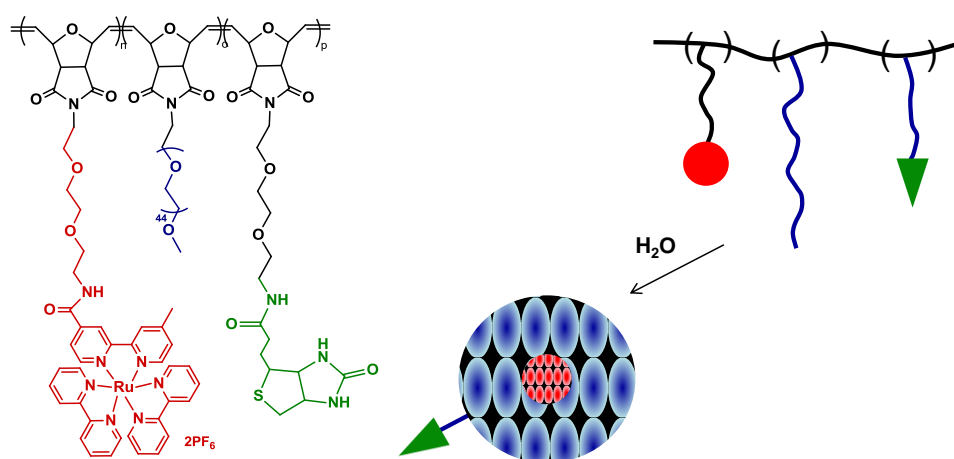

Figure 16: ROMP block-copolymers self-assembling to micelles exhibiting a luminescent core (red), a biocompatible PEG shell (blue), and biotin as biological recognition unit in the periphery (green); redrawn from reference 50

2.3.3.2 End Group Functionalization

Polymers exhibiting exactly defined end groups are valuable tools in manifold applications in polymer science. Obviously, end group functionalization is not limited to ROMP, but can be accomplished in a satisfying way with all living polymerization techniques. However, possibilities for metathesis polymerization shall here be briefly discussed. Functionalization can be accomplished either on only one chain end (semitelechelic) or on both chain ends (telechelic). Telechelic polymers can be classified into homotelechelics (equal functional groups) and heterotelechelics (unequal functional groups). The functional group can be introduced by (i) using a metathesis initiator bearing a functional carbene, (ii) using chain transfer agents during

---

[50] Sankaran, N. B.; Rys, A. Z.; Nassif, R.; Nayak, M. K.; Metera, K.; Chen, B.; Bazzi, H. S.; Sleiman, H. F. *Macromolecules* **2010**, *43,* 5530–5537.

polymerization, or (iii) using a terminating agent.[51] Apart from being used as analytical tool, proper end-group functionalization paves the way for combining ROMP with radical polymerization techniques such as RAFT (reversible addition–fragmentation chain transfer polymerization)[52] or ATRP (atom transfer radical polymerization)[53] which immensely enlarges the scope of accessible polymer architectures.
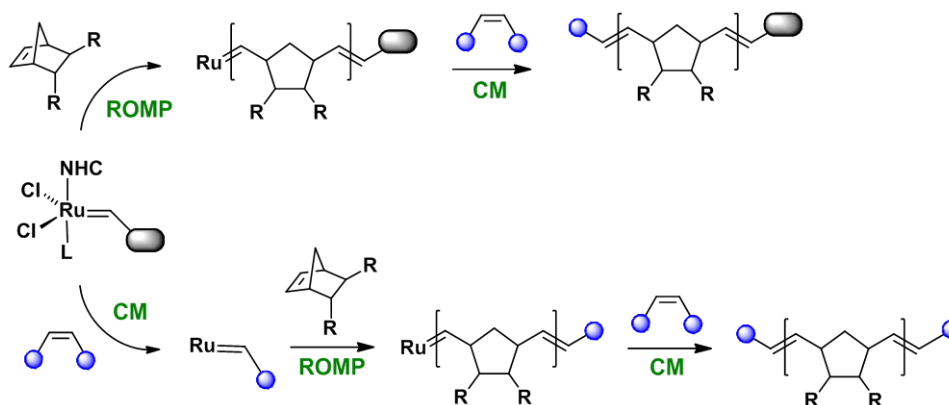
Scheme 5: Synthesis of telechelic and semitelechelic polymers using a chain transfer agent (from reference 51)

2.3.3.3 Grafted Polymers

Graft copolymers (brush, hyperbranched or dendronized co-polymers) are supramolecular structures (*cf*. Figure 14) that exhibit a more precise nanoscale morphology in comparison to self-assembling block copolymers.[54] In principle, three routes are feasible: (i) "grafting onto": attachment of ready side chains to ready backbone; (ii) "grafting through": homo- or copolymerization of macromonomers exhibiting side chains; (iii) "grafting from": side chains are polymerized from the ready backbone.[43] Various polymerization methods can be applied (and mixed) depending on the synthetic strategy, however the combination of ROMP with ATRP turned out to be rather attractive due to their versatility in many ways. Usually, the "grafting from"

[51] Hilf, S.; Kilbinger, A. F. M. *Nature Chemistry* **2009**, *1*, 537-546.

[52] (a) Barner-Kowollik, C.; Buback, M.; Charleux, B.; Coote, M. L.; Drache, M.; Fukuda, T.; Goto, A.; Klumperman, B.; Lowe, A. B.; McLeary, J. B.; Moad, G.; Monteiro, M. J.; Sanderson, R. D.; Tonge, M. P.; Vana, P. *J. Polym. Sci. Part A: Polym. Chem.* **2006**, *44*, 5809-5831; (b) Mahanthappa, M. K.; Bates, F. S.; Hillmyer, M. A. *Macromolecules* **2005**, *38,* 7890-7894.

[53] (a) Wang, J.-S.; Matyjaszewski, K. *J Am Chem Soc.* **1995**, *117,* 5614-5615; (b) Matson, J. B.; Grubbs, R. H. *Macromolecules* **2008**, *41*, 5626-5631.

[54] (a) Lord, S. J.; Sheiko, S. S.; LaRue, I.; Lee, H. I.; Matyjaszewski, K. *Macromolecules* **2004**, *37,* 4235–4240; (b) Boyce, J. R.; Shirvanyants, D.; Sheiko, S. S.; Ivanov, D. A.; Qin, S.; Borner, H.; Matyjaszewski, K. *Langmuir* **2004**, *20,* 6005–6011.

strategy is employed and norbornene-based monomers are ROM polymerized, before side chains like poly(acrylic acid) or polystyrene are grafted by ATRP.[55] A challenging, mixed "grafting-through-grafting-from" approach was presented by Xie et al., using hetero-difunctionalized norbornene macromonomers that provide two initiating sites, namely a hydroxyl group (branch A: ROP of ε-caprolactone) and a 2-bromoisobutyryloxymethyl group (branch B: ATRP of amino functionalized methacrylate), *cf.* Scheme 6.[56] However, for such complicated polymer architectures major losses in terms of conversion and livingness have to be faced.
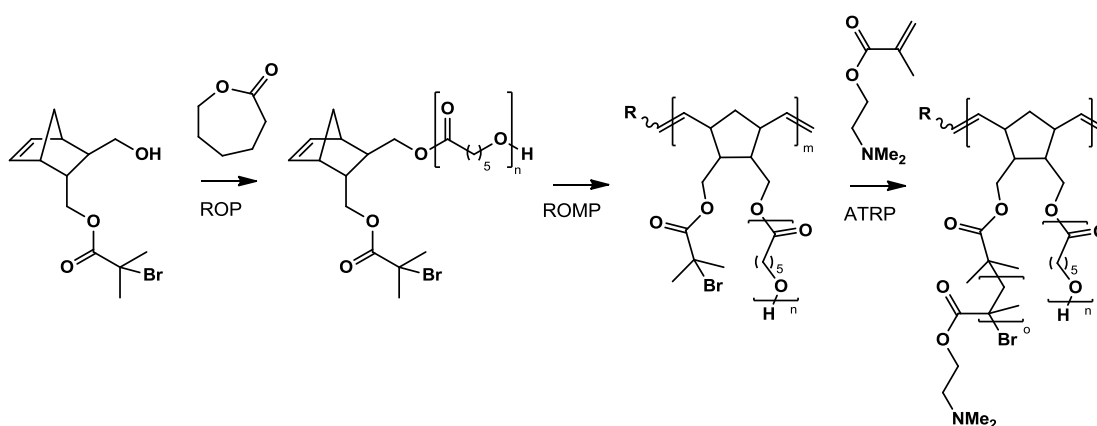
Scheme 6: Brush copolymer achieved by combination of ROP, ROMP and ATRP[56]

## 2.3.3.4 *Stereo and Sequence Selective ROM Polymerization*

Besides of the monomeric composition within the chain (copolymer, block-copolymer) also the mutual stereochemistry of the monomers is of importance, respectively interesting to be controlled. As for norbornene derivatives that represent the most frequently used ROMP monomers, a whole bunch of possible configurations arise from the bicyclic structure and its various functionalization patterns: (i) *cis/trans* of the exocyclic doublebonds, (ii) configuration of the allylic bridgehead-carbons (RS-RS, RS-SR) and (iii) linkage of unsymmetrically substituted monomers (head-head, tail-tail, head-tail, tail-head).[57] Control over the microstructure of ROMP polymers has not yet

[55] (a) Nomura, K.; Abdellatif, M.M. *Polymer* **2010**, *51*, 1861-1881. (b) Kriegel, R. M.; Rees, W.S. Jr.; Weck, M. *Macromolecules* **2004**, *37,* 6644-6649; (c) Runge, M. B.; Dutta, S.; Bowden, N.B. *Macromolecules* **2006**, *39*, 498-508; (d) Charvet, R.; Novak, B.M. *Macromolecules* **2004**, *37*, 8808-8811.

[56] Xie, M.; Dang, J.; Han, H.; Wang, W.; Liu, J.; He, X.; Zhang, Y. *Macromolecules* **2008**, *41*, 9004-9010.

[57] (a) Delaude, L.; Demonceau, A.; Noels, A. F. *Macromolecules* **1999**, *32,* 2091-2103; (b) Delaude, L.; Demonceau, A.; Noels, A. F. *Macromolecules* **2003**, *36*, 1446-1456. More detailed discussion in chapter 3.2.6

been satisfyingly achieved. Schrock and Hoveyda recently presented promising results with molybdenum or tungsten based for *cis* selective ROMP of norbornadienes and cyclooctene[58]. However, for the convenient ruthenium systems only minor progress on the matter can be reported. A *trans* content of more than 90% was achieved by Noels et al. employing the bimetallic [RuCl$_2$(*p*-cymene)]$_2$ pre-initiator system that is activated by TMSD (trimethylsilyldiazomethane). The success was attributed to the bidentate coordination of the monomer that is possible due to the absence of phosphines as it would be the case for **G1** or **G2** analogues (*cf.* Scheme 7).[57(a)] The necessary activator constitutes a severe limitation of this system as the actual initiation of the metathesis (that influences the molecular weight distribution) can hardly be controlled. Also, the reported stereoregularity is restricted to selected monomers.
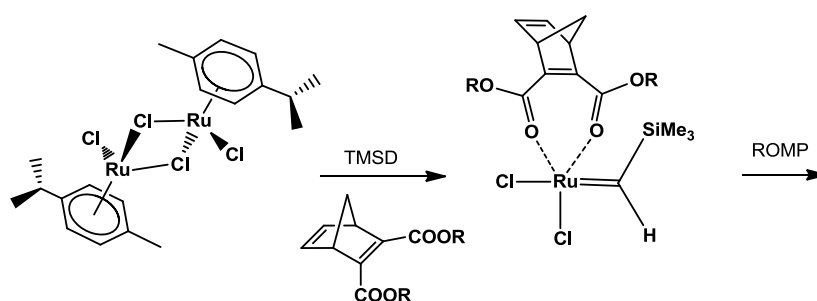
Scheme 7: Activation of cymene precataylst for stereoselective ROMP

Anyway, the example clearly points out that both, initiator and monomer have to be considered when searching for selectivity. This is also the case for selectivity of ruthenium initiators towards different double bonds (resp. different monomers) that is necessary for the synthesis of strictly alternating ROM copolymers. Generally, an alternating preference towards two monomers is hardly conceivable. However, with the combination of an unsymmetrical NHC ligand and two monomers exhibiting a clearly different ring strain, Blechert and Buchmeiser et al. managed to get alternating co-polymers of norbornene (highly active in metathesis) and cyclooctene (less active). The key issue in this approach is steric prohibition of consecutive insertion of two norbornene monomers in a row (*cf.* Figure 17).[59]

---

[58] Flook, M. M.; Jiang, A. J.; Schrock, R. R.; Müller, P.; Hoveyda, A. H. *J. Am. Chem. Soc.* **2009**, *131*, 7962-7963.

[59] (a) Vehlow, K.; Wang, D.; Buchmeiser, M. R.; Blechert, S. *Angew. Chem. Int. Ed.* **2008**, *47*, 2615-2618; (b) Lichtenheldt, M.; Wang, D.; Vehlow, K.; Reinhardt, I.; Kühnel, C.; Decker, U.; Blechert, S.; Buchmeiser, M. R. *Chem. Eur. J.* **2009**, *15*, 9451-9457.
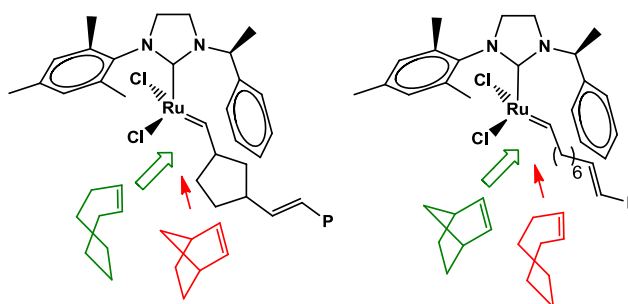
Figure 17: Steric control in alternating ROMP

2.4 Initiator Development for ROMP

The previous chapters only roughly covered some recent aspects of ROMP and completely excluded other olefin metathesis reactions like ring closing- (RCM), cross- (CM), en-yne or ring rearrangement metathesis (RRM). Still, it can be clearly seen how important the choice of right initiator for the respective application is. Breaking it down to two main interests, ROMP initiators should be either (i) fast initiating complexes for living polymerization of tailored specialty polymers, or, (ii) latent initiators that can be switched on upon an external trigger (heat, light, acid…)[60] for applications where the monomer-initiator mixture has to be processed before polymerization. A broad range of ruthenium metathesis initiators has been developed since the introduction of the Grubbs-type initiators, and a considerable amount is commercially available. Still, many questions remain undisclosed. Comparatively little is known about the influence of the respective ligands in the initiation step and during metathesis polymerization. Upon ligand variation some effects can be studied. For Grubbs-type initiators, there are mainly four "construction sites", which are the (i) anionic ligands **X** – mostly halides, (ii) the neutral inert ligand **L$_{inert}$** – phosphine or NHC, (iii) the neutral leaving ligand **L$_{labile}$** and (iv), the carbene active in metathesis **=C-R** (*cf.* Figure 18, left). This work will deal with initiator design and the resulting impacts for ROMP regarding two different ligand systems, namely the NHC ligand (*cf.* chapter 0) and chelating carbene ligands (*cf.* chapters 0 and 0), as indicated in Figure 18 middle and right, respectively.

---

[60] Diesendruck, C. E.; Tzur, E.; Lemcoff, N. G. *Eur. J. Inorg. Chem.* **2009**, 4185–4203.
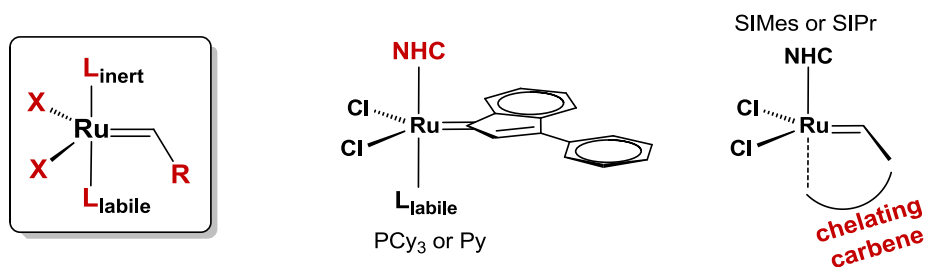
Figure 18: Construction sites in Grubbs type initiators treated within this work

2.4.1 The N-heterocyclic Carbene Ligand (NHC)

The N-heterocyclic carbene ligand is known to severely influence the initiators stability and activity in olefin metathesis.[61] Most well established and commercially available ruthenium olefin metathesis initiators bear a SIMes ligand that is also present in **G2**. However, tuning of sterical and electronic properties of this ligand turned out to be an interesting field, not only for disclosure and evaluation of new complexes, but also for gaining a deeper understanding of metathesis mechanisms. In the following some crucial ROMP relevant aspects for NHC ligands will be summarized that have been published in reference 61[62]

2.4.1.1 Various Design Motives

Generally, all herein relevant NHC ligands consist of an imidazole derived carbene that is equipped with various functionalities. The backbone of the imidazole moiety can be tuned upon hydrogenation or other functionalization maintaining the double bond. The fragments bound to the imidazole's nitrogens can be of various shapes and, be either symmetrical or different at each side. The favourable mesityl group present in **G2** combines considerable steric bulk and flatness of the phenyl rings which is advantageous when attaching the ligand to the ruthenium complex. Therefore **IMes** (1,3-dimesityl-imidazole-2-ylidene) and its saturated analogue **SIMes** were among the first described NHC ligands used in ruthenium based olefin metathesis catalysts/initiators.[62]

---

[61] N-Heterocyclic Carbenes in Transition Metal Catalysis and Organocatalysis, *Springer*, Cazin, C. S. J. (Ed.) 1st Edition., **2011**, p.63ff.

[62] Leitgeb, A.; Slugovc C., chapter 3.2 :"NHC Bearing Ruthenium Carbene Complexes as Initiators for Ring Opening Metathesis Polymerisation" in reference 62.
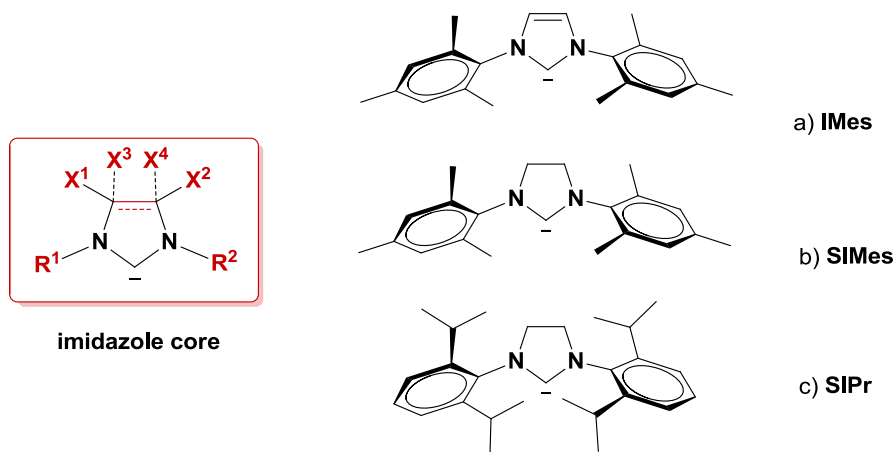
Figure 19: Principle layout (left) and commonly used derivatives of NHC ligands: (a) IMes: 1,3-dimesityl-imidazole-2-ylidene; (b) SIMes: 1,3-dimesityl-4,5-dihydroimidazole-2-ylidene; (c) SIPr: 1,3-di(2,5-di-isopropylphenyl)-4,5-dihydroimidazole-2-ylidene

One way to describe the steric influence of the NHC ligand on the ruthenium complex is the buried volume V_{Bur} as suggested by Cavallo et al. V_{Bur} can be calculated from the bond parameters obtained from crystal structures of the respective complexes. At https://www.molnac.unisa.it/OMtools/sambvca.php an according web application (sambVca) has been provided.[63]
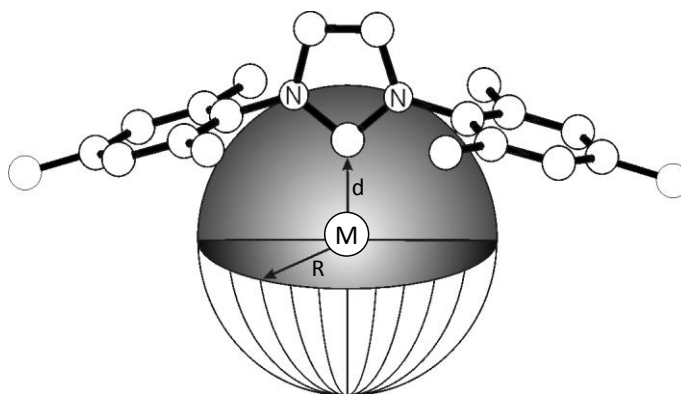

Figure 20: Graphical representation of the sphere used to calculate the %V_{Bur}[63]

2.4.1.1.1 IMes, SIMes and SIPr^i in ROMP

2nd generation initiators featuring the abovementioned NHC ligands have been tested in ROMP of 1,5-cyclooctadiene (COD). Time-conversion plots reveal the striking

---

[63] Poater, A.; Cosenza, B.; Correa, A.; Giudice, S.; Ragone, F.; Scarano, V.; Cavallo L, *Eur. J. Inorg. Chem.* **2009**, *13*, 1759-1766.

superiority of the saturated systems. 50% conversion was reached with SIMes and SIPr within only 1 min and after less than 10 min complete conversion was accomplished. In contrast, the less electron-donating IMes ligand led to a deceleration of the initiator that now took 20 min for 50 % conversion and more than 1 h for complete polymerization.[64] This example shows in an impressively clear way, that a minor change on first sight can have major effects on the polymerization characteristics.
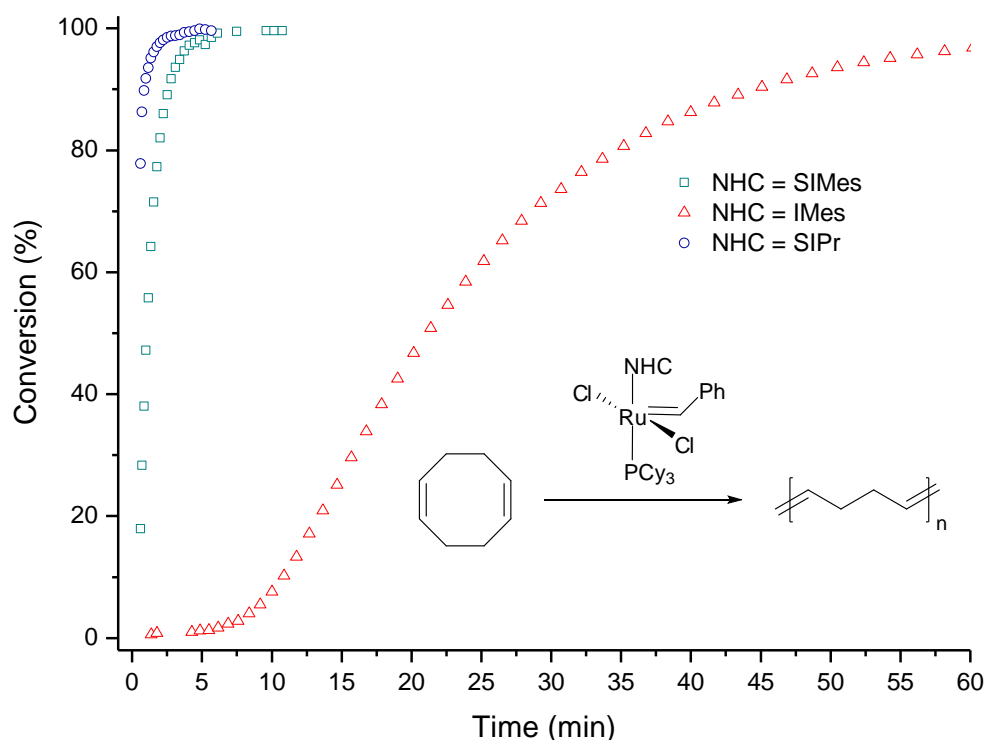

Figure 21: ROMP of COD: conversion vs. time plot comparing 2nd generation catalysts bearing the NHC ligands SIMes , IMes and SIPr; redrawn from ref. 64a

On the other hand, the steric modification of SIMes to SIPr has an accelerating effect, the bulkier *iso*-propyl substituents induce a further increase of activity to the initiator. Especially at lower temperatures up to 30°C, it outperforms **G2**. At elevated temperatures the steric bulk obviously causes increased sensibility and faster degradation of the initiator.[64a,65] A thorough discussion of SIPr and SIMes NHC ligands

---

[64] (a) Ritter, T.; Hejl, A.; Wenzel, A. G.; Funk, T. W.; Grubbs, R. H. *Organometallics*, **2006**, *25*, 5740-5745; (b) Demel, S.; Schoefberger, W.; Slugovc, C.; Stelzer, F. *J. Mol. Catal. A*, **2003**, *200*, 11-19.
[65] (a) Dinger, M. B.; Mol, J. C. *Adv. Synth. Catal.* **2002**, *344*, 671-677; (b) Courchay, F. C.; Sworen, J. C.; Wagener, K. B. *Macromolecules* **2003**, *36*, 8231-8239.

in ROMP will is accomplished in chapter 0), as a closer examination of these systems was a major part of this work.[66]

2.4.1.1.2 Asymmetric NHC Ligands

For some applications, asymmetrical NHC ligands might be useful. For example, the asymmetry introduces chirality at the active center which will supposedly influence the *cis/trans* selectivity of the complex. For example, Grubbs et al. presented some modified 2nd generation complexes exhibiting one mesityl group and a fluorine substituted benzene on the other side of the NHC ligand. Compared to **G2**, these complexes showed increased E/Z selectivity in the cross metathesis of allyl benzene with *cis*-1,4-diacetoxy-2-butene (>60 %).[67] Also for metathesis polymerization asymmetric NHC ligands can be advantageous, e.g. for gaining sequential control as already described in chapter 2.3.3.4, (*cf.* Figure 17). Ring expansion metathesis polymerization (REMP), a variety of ROMP, makes use of initiators exhibiting a bi-dentate bi-carbene ligand.[68] A Grubbs type pre-catalyst exhibiting a ω-unsaturated side chain at the NHC will start the reaction upon metathesizing its own ligand: a metallacycle-carbene is formed. Consecutive ROMP with monomers such as COD will expand this ring until it is cleaved off (again by intramolecular metathesis). Thus, the catalyst is recovered and a macrocyclic polymer is yielded (Scheme 8). Initially, these experiments were performed with an unsaturated NHC backbone, which led to rather low activity. The unsaturated SIMes analogue accelerated the reaction's half-life (50% conversion) from 120 to 12 min.[69]

---

[66] Urbina-Blanco, C. A.; Leitgeb, A.; Slugovc, C.; Bantreil, X.; Clavier, H.; Slawin, A. M. Z.; Nolan, S. P. *Chem. Eur. J.* **2011**, *17*, 5045-5053.

[67] Vougioukalakis, G. C.; Grubbs, R. H. *Chem. Eur. J.* **2008**, *14*, 7545 – 7556.

[68] (a) Fürstner, A.; Ackermann, L.; Gabor, B.; Goddard, R.; Lehmann, C. W.; Mynott, R.; Stelzer, F.; Thiel, O. R. *Chem. Eur. J.* **2001**, *7*, 3236-3653; (b) Bielawski, C. W.; Benitez, D.; Grubbs, R. H. *Science* **2002**, *297*, 2041-2044.

[69] Boydston, A. J.; Xia, Y.; Kornfield, J. A.; Gorodetskaya, I. A.; Grubbs, R. H. *J. Am. Chem. Soc.* **2008**, *130*, 12775-12782.
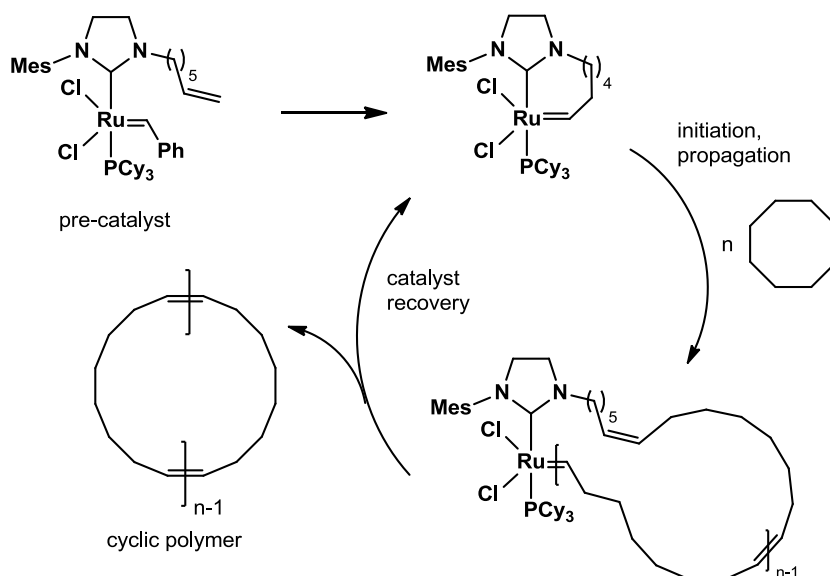
Scheme 8: REMP yields cyclic polymers upon intramolecular metathesis

2.4.2 Chelating Carbene Ligands for Thermally Switchable Initiators

The incredible stability and functional group tolerance of ruthenium based metathesis initiators (*cf.* chapter 2.1, Table 1) made them attractive applicants for applications where initiator-monomer formulations can be stored or processed without polymerization until needed. This is the case for RIM processes of e.g. DCPD (*cf.* Figure 8) or ink jet printing. In this context, the idea of an external trigger that will allow polymerization only after a certain switching event has been a major subject in initiator design.[70] Various strategies to introduce latency to metathesis initiators have been investigated – many of them following a thermal trigger concept. The most promising design motif therefore is to block the free coordination site of the initiator with a strongly chelating ligand, preferably the carbene ligand involved in the metathetic cycle. Thus, fast propagation will be maintained after retarded initiation, as schematically shown in Scheme 9.

---

[70] (a) Slugovc, C.; Burtscher, D.; Mereiter, K.; Stelzer, F.; O*rganometallics,* **2005**, *24*, 2255-2258. (b) Gstrein, X.; Burtscher, D.; Szadkowska, A.; Barbasiewicz, M.; Stelzer, F.; Grela, K.; Slugovc, C. *J. Polym. Sci., Part A: Chemistry* **2007**, *45*, 3494-3500.
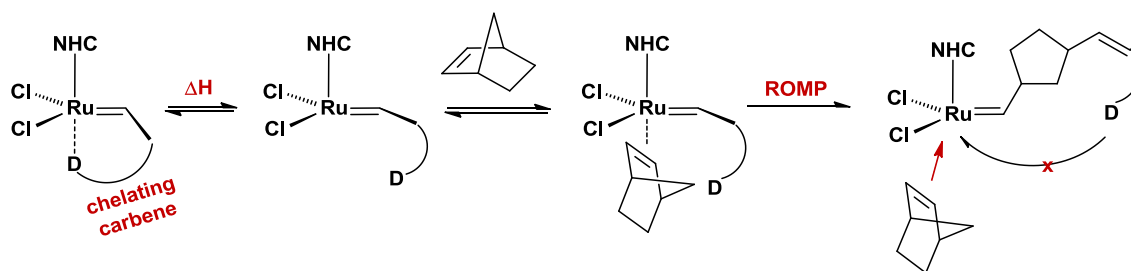
Scheme 9: Thermally triggered ROMP with a chelating carbene initiator

Chelating carbene ligands were introduced with **Hov** initiators featuring an isopropoxy-benzylidene ligand (*cf*. Figure 5).[18,19] However, the chelation of the benzylidene ether moiety is not strong enough to prevent metathesis at ambient conditions and **Hov** happens to be a very active initiator for olefin metathesis, respectively for ROMP.[71] Exchanging the ether moiety for an ester has considerably augmented latency, even more so when the aldehyde derivative was used.[72] Beside of activity effects, the ester complexes turned out to feature a *cis* geometry of the chloride ligands.

2.4.2.1 Excursus: Geometry of Chloride Ligands in Complexes Featuring Chelating Carbenes

Most well established and commercially available initiators (e.g. **G1-G3, Hov**) exhibit a square pyramidal coordination geometry with the benzylidene carbene ligand forming the apex, the base is formed by two chloride ligands in *trans* configuration and the two neutral ligands, also in mutual *trans* configuration. However, some complexes featuring chelating carbene ligands exhibit *cis* dichloro structure, where the chlorides and respectively the neutral ligands are in mutual *cis* configuration (*cf*. Figure 22). It has been found that many *cis* dichloro complexes can isomerize into their *trans* dichloro counterparts and vice versa under specific conditions that vary from complex to complex. Fürstner et al. found isomerization from *trans* to *cis* upon treatment with silica for two benzylidene complexes.[73] Lemcoff et al. disclosed detailed investigations on *trans* to *cis* izomerizations of sulfur chelating benzylidene complexes dissolved in

[71] (a) Michrowska,A.; Bujok,R.; Harutyunyan,S.; Sashuk,V.; Dolgonos, G.; Grela, K. *J. Am. Chem. Soc.* **2004**, *126*, 9318-9325; () Wappel, J.; Urbina-Blanco, C. A.; Abbas, M.; Albering, J. H.; Saf, R.; Nolan, S. P.; Slugovc, C. *Beilstein J. Org. Chem.* **2010**, *6*, 1091–1098.

[72] (a) Slugovc, C.; Burtscher, D.; Mereiter, K.; Stelzer, F. *Organometallics*, **2004**, *23*, 3622-3626; (b) Zirngast, M.; Pump, E.; Leitgeb, A.; Albering, J. H.; Slugovc, C. *Chem. Commun.* **2011**, *47*, 2261-2263.

[73] Prühs, S.; Lehmann, C. W.; Fürstner, A. *Organometallics* **2004**, *23*, 280-287.

dichloromethane.[74] It is believed that *cis* dichloro complexes are generally inactive in olefin metathesis and only activated upon (thermally induced) isomerization to the *trans* counterpart. Regarding possible mechanistic pathways for this isomerization, theoretical studies by Poater *et al*. and Benitez et al. found considerably high activation energies for a concerted mechanism or a mechanism based on the hemi-lability of the chelating ligand.[75] Only recently, Slugovc et al. disclosed a new pathway including the formation of a cationic intermediate that is preferable formed in presence of donor ligands.[72b] The activity of the complexes was compared by means of ROMP conversion and was determined to be considerably higher for the cationic species than for the *cis* dichloro species, which supports the abovementioned hypothesis.
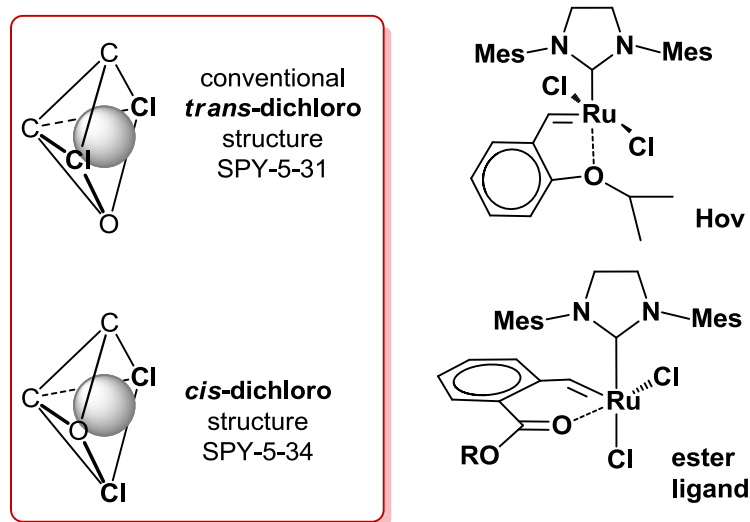

Figure 22: *cis* and *trans* dichloro complexes

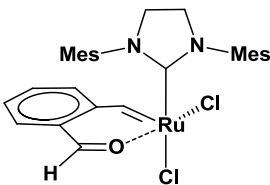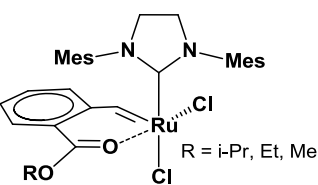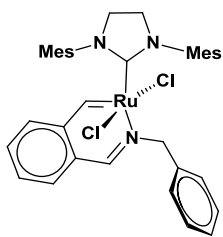### 2.4.2.2 Different Design Motives for Chelating Carbene Ligands
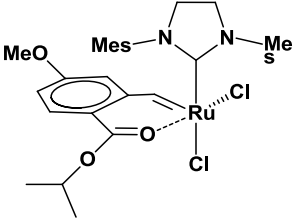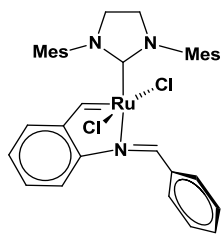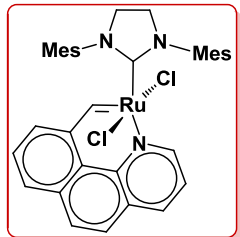
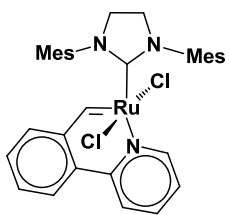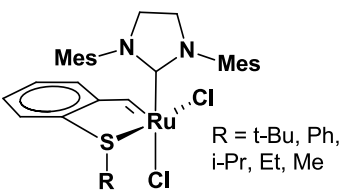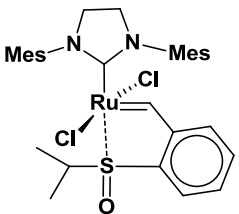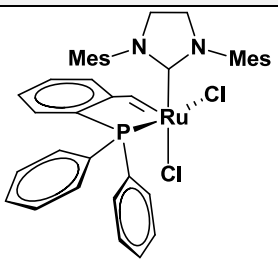The side effect of changing the chelate's ring size from a five-membered to a six-membered ring (*cf*. Figure 22) has also been investigated separately regarding its influence on latency, revealing a slightly more pronounced latency for six-membered rings.[70a] Modification of the ligand scaffold itself and variation of the chelating atom

---

[74] Aharoni, A.; Vidavsky, Y.; Diesendruck, C. E.; Ben-Asuly, A.; Goldberg, I.; Lemcoff, N. G. *Organometallics*, **2011**, *30*, 1607-1615.

[75] (a) Poater, A.; Ragone, F.; Correa, A.; Szadkowska, A.; Barbasiewicz, M.; Grela, K.; Cavallo, L.; *Chem. Eur. J.* **2010**, 16, 14354-14364; (b) D. Benitez and W. A. Goddard III, *J. Am. Chem. Soc.*, 2005, **127**, 12218-12219.

has led to numerous alternative approaches for increasing or also decreasing latency of ruthenium complexes featuring chelating carbene ligands.[76]

Table 3: Exemplary latent ruthenium metathesis initiators featuring chelating carbene ligands with various donor atoms; framed in red: extremely latent SIMes-benzoquinoline complex

Oxygen donor ligands: aldehyde and ester derivatives[72]

Nitrogen donor ligands: Schiff base ligands[70a]; benzoquinoline and benzylpyridine[77]

Sulfur Donor Ligands: sulfide[76g] and sulfoxide[76f]	**Phosphor Donor Ligands** [76k]

[76] (a) Gstrein, X.; Burtscher, D.; Szadkowska, A.; Barbasiewicz,M.; Stelzer, F.; Grela, K.; Slugovc,C.; *J. Polym Sci. Part A: Polym. Chem*. **2007**, *45*, 3494-3500; (b) Burtscher, D.; Perner, B.; Mereiter, K.; Slugovc, C. *J. Organomet. Chem.* **2006**, *691*, 5423-5430; (c) Ung, T.; Hejl, A.; Grubbs, R. H.; Schrodi, Y. *Organometallics* **2004**, *23*, 5399-5401; (d) Hejl, A.; Day, M. W.; Grubbs, R. H. *Organometallics* **2006**, *25*, 6149-6154. (e) Diesendruck, C. E.; Vidavsky, Y.; Ben-Asuly, A.; Lemcoff, N. G. *J. Polym. Sci. Part A: Polym. Chem.* **2009**, *47*, 4209-4213; (f) Szadkowska, A.; Makal, A.; Wozniak, K.; Kadyrov, R.; Grela, K. *Organometallics* **2009**, *28*, 2693-2700; (g) Kost, T.; Sigalov, M.; Goldberg, I.; Ben-Asuly, A.; Lemcoff, N. G. *J. Organomet. Chem.* **2008**, *693*, 2200-2203; (h) Ben-Asuly, A.; Tzur, E.; Diesendruck, C. E.; Sigalov, M.; Goldberg, I.; Lemcoff, N. G. *Organometallics* **2008**, *27*, 811-813; (i) Diesendruck, C. E.; Tzur, E.; Ben-Asuly, A.; Goldberg, I.; Straub, B. F.; Lemcoff, N. G. *Inorg. Chem.* **2009**, *48*, 10819–10825; (j) Tzur, E.; Szadkowska, A.; Ben-Asuly, A.; Makal, A.; Goldberg, I.; Wozniak, K.; Grela, K.; Lemcoff, N. G. *Chem.-Eur. J.* **2010**, *16*, 8726-8737; (k) Lexer, C.; Burtscher, D.; Perner, B.; Tzur,E.; Lemcoff, N. G.; Slugovc C. *J. Organomet. Chem*. **2011**, *696*, 2466-2470.

An impressive example for thermally switchable metathesis initiators is the **SIMes-benzoquinoline** complex framed in red in Table 3. (SPY-5-31)-Dichloro-(κ^2(C,N)-2-(benzo[h]quinolin-10-yl)methylidene)(1,3-bis(2,4,6-trimethylphenyl)4,5-dihydroimidazol-2-ylidene)ruthenium is virtually inert at room temperature and extremely stable also in solution and under ambient conditions in presence of ROMP monomers. Polymerization (and other metathesis reactions) is only accomplished above 100°C.[77] Such pronounced latency makes the complex interesting for ink-jet-print-applications, e.g. for curing of conductive inks on printed circuit bords (PCB).[78] In a comparative work by Grela and Slugovc et al., the rigidity of the chelating benzoquinoline ligand was declared responsible for obtaining this high latency (the more flexible benzylpyridine ligand resulted in a switching temperature of 50°C).[77]
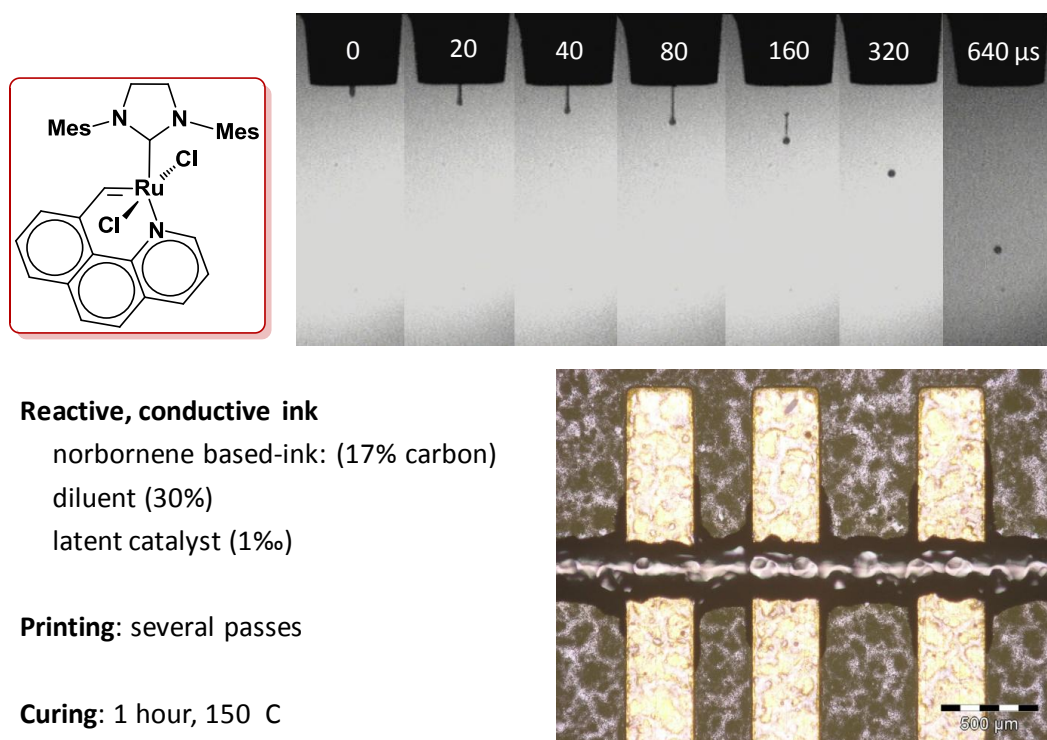

Reactive, conductive ink
   norbornene based-ink: (17% carbon)
   diluent (30%)
   latent catalyst (1‰)

Printing: several passes

Curing: 1 hour, 150 C

Figure 23: Application of latent ROMP initiators for ink-jet-printing on printed circuit boards[78]

Besides of geometry, ring size and rigidity, also the aromaticity of the ruthenacycle comprising the chelating carbene ligand has been discussed as an important factor for latency in metathesis initiators. The effect of aromaticity was observed by Grela et al.

---

[77] Szadkowska, A.; Gstrein, X.; Burtscher, D.; Jarzembska, K.; Wozniak, K.; Slugovc, C.; Grela, K.; *Organometallics,* **2010**, *29*, 117–124.

[78] Stelzer, F.; Slugovc, C.; Ruplitsch, A.; Gstrein, X.; List, E. J. W.; Mauthner, G.; Gadermaier, C.; Plank, H.; Gamerith, S.; Gaal, M. from Austrian Pat. Appl. Pre-Grant, **2008**, AT 505116 A1 20081015.

during a study on modified Hoveyda ligand design: the benzylidene ligand was extended at different positions to a naphthalene structure, which had a serious effect on the activity in the ring closing metathesis of N,N-diallyltosylamine and diethyl diallymalonate.[79] The change in reactivity was explained with aromaticity in the chelated ring according to Clar's rule.[80] Depending on the arrangement of the extended π-systems, the chelated ring can exhibit aromatic character, which results in a strengthening of the oxygen-ruthenium bond and consequently decreases activity. Regarding their performance in ROMP, these "extended **Hov** – complexes" (**extHov**) have been closely investigated within this work (*cf.* chapter 0).[81]
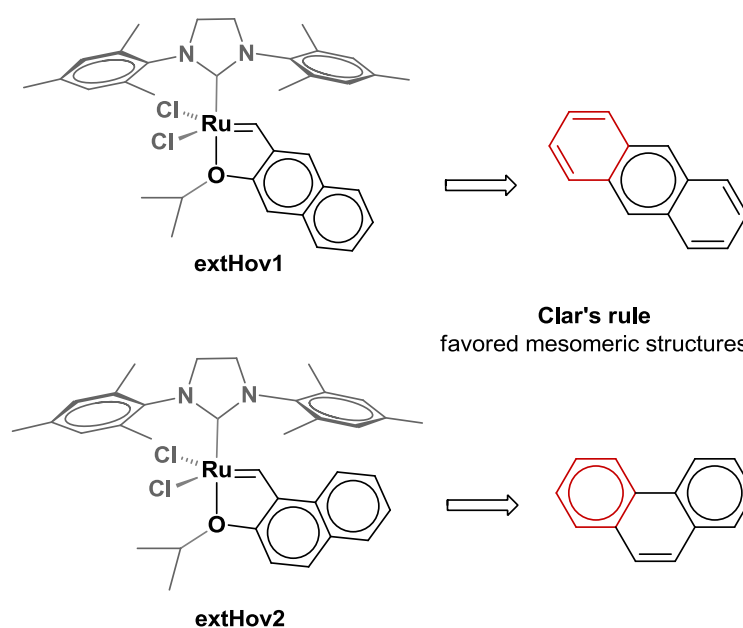

Figure 24: Clar's rule applied to π-extended Hoveyda complexes explains activity differences[79]

[79] (a) Barbasiewicz, M.; Szadkowska, A., Makal, A.; Jarzembska, K.; Woźniak, K.; Grela, K. *Chem. Eur. J.* **2008**, *14*, 9330-9337.

[80] Portella, G.; Poater, J.; Solà, M. *J. Phys. Org. Chem.* **2005**, *18*, 785-791.

[81] Leitgeb, A.; Szadkowska, A.; Michalak, M.; Barbasiewicz, M.; Grela, K.; Slugovc, C. *J. Polym. Sci. Part A: Polym. Chem.* **2011**, *49*, 3448-3454.

3   INITIATOR DESIGN and TESTING in ROMP

For all studies accomplished within this work, two commercially available ruthenium initiators **M2** and **M31** were used as reference initiators due to their extremely different initiation behavior, thus providing a reasonable benchmark for all initiators under investigation. Second generation complex **M2** is a **G2**-analogue featuring an indenylidene carbene, third generation complex **M31** constitutes the **G3**-analogue featuring an indenylidene carbene and only one pyridine. **M31** shows fast and complete initiation with most monomers (estimation for $k_i/k_p > 10$-1000 depending on the monomer) and thus every initiator molecule starts a growing chain at the same time. Therefore, polymers characterized by low M_n values and low polydispersity indices (PDIs) are obtained.[82] In contrast to that, slow and incomplete initiation is a characteristic feature of **M2** in ROMP (estimation for $k_i/k_p < 1$ - 0.01 depending on the monomer), resulting in high M_n- and high PDI values (> 2) of the corresponding polymers.[82]

Within this work, a number of different factors influencing the activity of ruthenium based olefin metathesis initiators have been studied. The following chapters will all deal with a systematical study, concentrating on a different ligand each, namely the leaving ligand, the NHC ligand and the carbene ligand involved in the metathetic cycle, respectively. Two cooperations with the group of Prof. Steven P. Nolan have been realized dealing with the neutral ligands of ruthenium initiators with an indenylidene carbene. The first treats second generation initiators exhibiting electronically modified phosphine ligands[83] (*cf.* chapter 0) , and the second examines the influence of a sterically more demanding NHC ligand SIPr (SIPr = 1,3-bis(2,6-diisopropylphenyl)-4,5-dihydro-imidazol-2-ylidene) in contrast to the conventional SIMes ligand (SIMes = N,N'-bis(2,4,6-trimethylphenyl)imidazolin-2-ylidene), in second and third generation complexes (*cf.* chapter 0).[84] The SIPr-NHC ligand has also been employed for complexes featuring chelating carbene ligands, in particular benzylidene esters. The influence on activity on the one hand, but also on the geometry of the ruthenium complexes was studied and compared to corresponding SIMes-complexes (*cf.* chapter 0). A third publication was realized as cooperation with the group of Prof. Karol Grela from the University of Warsaw. Therefore, four ruthenium initiators featuring a chelating carbene ligand, reminiscent of the Hoveyda complex (chelation via

---

[82] D. Burtscher, C. Lexer, K. Mereiter, R. Winde, R. Karch, C. Slugovc *J. Polym. Sci. Part A: Polym. Chem.* **2008**, *46*, 4630-4635.

[83] Broggi, J.; Urbina-Blanco, C. A.; Clavier, H.; Leitgeb, A.; Slugovc, C.; Slawin, A. M. Z.; Nolan, S. P. *Chem. Eur. J.* **2010**, *16*, 9215-9225.

[84] Urbina-Blanco, C. A.; Leitgeb, A.; Slugovc, C.; Bantreil, X.; Clavier, H.; Slawin, A. M. Z.; Nolan, S. P. *Chem. Eur. J.* **2011**, *17*, 5045-5053.

*iso*propylether moiety at the benzylidene ligand) were evaluated in ROMP, with a focus on thermally triggered ROMP of dicyclopentadiene (*cf.* chapter 0).[85]

NOTE: In the following part, labeling of one and the same complex may change from chapter to chapter, but will be individually adapted for the respective test series in order to enhance comprehensibility and facilitate reading of tables, figures and schemes. Structures and names of all complexes will be pointed out at the beginning of each chapter. A comprehensive overview including structure, all used labels within this work and the respective systematical name, is provided in the following.
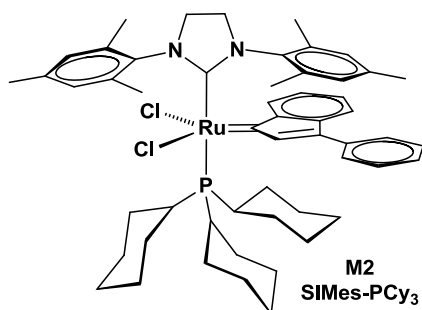
M2
SIMes-PCy₃

1,3-Bis(2,4,6-trimethylphenyl)-2-imidazolidinylidene)-dichloro-(3-phenyl-*1H*-inden-1-ylidene)(tricyclohexylphosphine)ruthenium

M31
SIMes-py
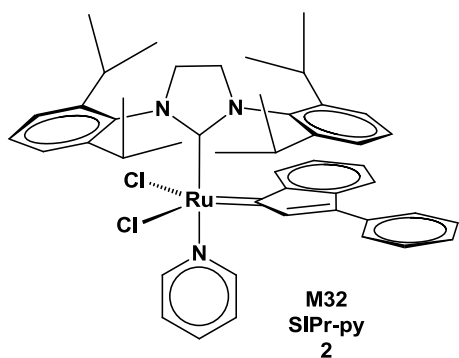**1**

(1,3-Bis(2,4,6-trimethylphenyl)-2-imidazolidinylidene)dichloro-(3-phenyl-*1H*-inden-1-ylidene)(pyridyl)ruthenium)
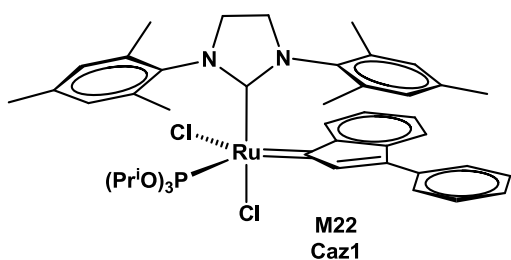

SIPr-PCy₃
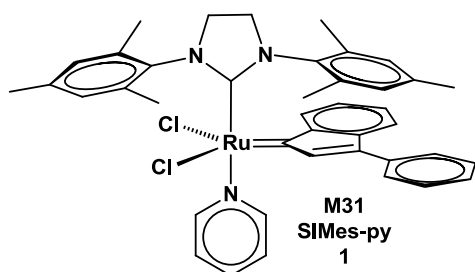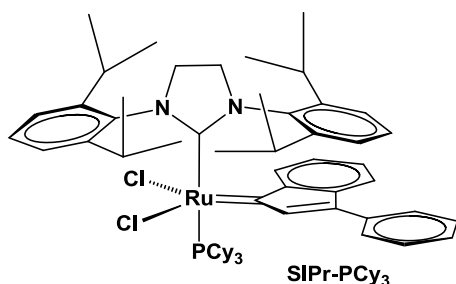
1,3-Bis(2,6-diisopropylphenyl)-2-imidazolidinylidene)-dichloro-(3-phenyl-*1H*-inden-1-ylidene)(tricyclohexyl-phosphine)ruthenium
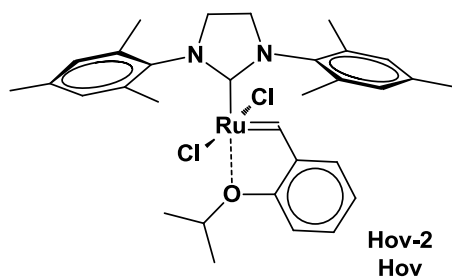
[85] Leitgeb, A.; Szadkowska, A.; Michalak, M.; Barbasiewicz, M.; Grela, K.; Slugovc, C. *J. Polym. Sci. Part A: Polym. Chem.* **2011**, *49*, 3448-3454.

(1,3-Bis(2,6-diisopropylphenyl)-2-imidazolidinylidene)-dichloro-(3-phenyl-*1H*-inden-1-ylidene)(pyridyl)ruthenium)

M32
SIPr-py
2

1,3-Bis(2,4,6-trimethylphenyl)-2-imidazolidinylidene)-dichloro-(3-phenyl-*1H*-inden-1-ylidene)(triisopropylphosphite)ruthenium

M22
Caz1

Dichloro-(κ^2(C,O)-2-isopropylether-benzylidene)-(1,3-bis(2,4,6-trimethylphenyl) 4,5-dihydroimidazol-2-ylidene)ruthenium

Hov-2
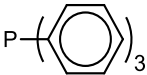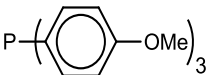**Hov**

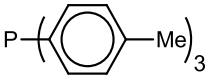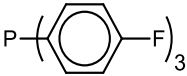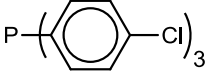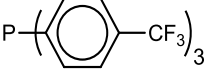## 3.1 Impact of Phosphine Tuning in Ruthenium-Indenylidene Complexes

Second generation initiators are mainly determined by the N-heterocyclic carbene ligand (NHC), that substitutes the second phosphine ligand of their first generation analogues. The NHC is bound stronger to the ruthenium centre, the dissociation and recoordination rate of the labile phosphine ligand determines the initiation and, in case of polymerizations, also the propagation of the metathesis reaction. It is therefore easily comprehensively, that any steric or electronic modification on the leaving phosphine ligand will lead to a different reactivity profile. In the course of a EUMET cooperation with the Nolan group of the University of St. Andrews, the influence of electron withdrawing and electron donating groups on the phosphine ligand was studied, regarding the potential in ring opening metathesis polymerization. The respective Hammett constant σ_p (electronic influence, negative if electron donating, positive when the substituent leads to an electron poor ligand) was taken for evaluating the complexes. Also, steric effects (cone angle of the phosphines)) have been considered, but all *para*-substituted phosphines exhibit the same angle, which is 145°, in contrast to the unsubstituted tricyclohexylphosphine (as present in **M2**) that exhibits a cone angle of 170.[86] The complexes were tested in ring closing metathesis (RCM), ring rearrangement (RRM) and cross metathesis (CM) by the Nolan group, whereas ring opening metathesis polymerization (ROMP) was carried out at Graz University of Technology.
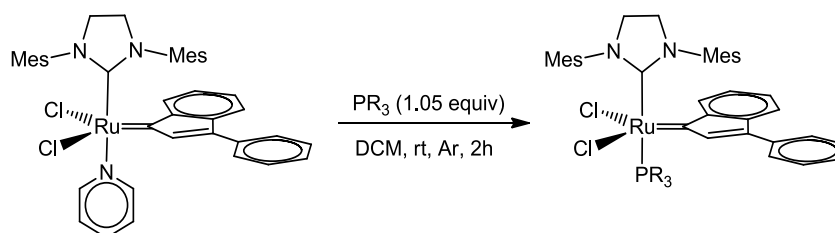
Scheme 10: Synthesis and features of 2nd generation complexes featuring different p-substituted triphenylphosphine ligands

[86] J.A. Love, M.S. Sanford, M.W. Day, R.H. Grubbs, *J. Am. Chem. Soc.* **2003**, *125*, 10103-10109.

Table 4: Yields and electronic properties of phosphine tuned complexes

Complex	PR$_3$	Yield	ρ_σ[a]	pK$_a$[a]	χ[a]
	P—(C$_6$H$_5$)$_3$	78 %	0	2.73	13.25
	P—(C$_6$H$_4$—OMe)$_3$	75 %	-0.27	4.57	10.5
	P—(C$_6$H$_4$—Me)$_3$	77 %	-0.17	3.84	11.5
	P—(C$_6$H$_4$—F)$_3$	90 %	0.06	1.97	17.5
	P—(C$_6$H$_4$—Cl)$_3$	90 %	0.23	1.03	16.8
	P—(C$_6$H$_4$—CF$_3$)$_3$	73 %	0.53	[b]	20.5

[a] Values for Hammett constant σ_p, pKa and electronegativity χ taken from reference 87.

[b] unknown

The synthesis of all phosphine-tuned complexes was accomplished by USTAN,[83] and is herein therefore not mentioned in detail.

3.1.1 Polymerization Procedures

ROMP polymerizations were conducted as follows: The corresponding initiator (1 equiv.) was weighed into a Schlenk flask with a stirring bar and dissolved in dry and degassed dichloromethane (1 mL). **EsterMon** or **EtherMon** (300 equiv.) was dissolved in the corresponding amount of solvent to reach a total concentration of 0.2 mol/L. The monomer solution was added to the initiator. The reaction mixture was stirred until polymerization was complete, which was monitored *via* thin layer chromatography (TLC) using KMnO$_4$ for staining. After completion, the polymerization reaction was quenched by addition of ethyl vinyl ether (200 μL, large excess). After 15 min of additional stirring, the solvent was reduced to approximately 1 mL in volume. The reaction mixture was then slowly added to vigorously stirred, cold methanol to precipitate the polymer which was collected and dried in vacuum. Provided yields in Table 5 refer to the amount of isolated polymer. A sample of each polymer was subjected to GPC for analysis of M$_n$ and PDI.

3.1.2 Results

Generally, and for all reactions under investigation it can be stated that **[RuCl₂(SIMes)(P(p-CF₃C₆H₄)₃)(Ind)]**, which bears the most electron-poor phosphine, is the most active initiator within the triphenylphosphine series for easy substrates. It has to be pointed out, that for sterically demanding substrates reference complex **M2** was more efficient. For CM best results were obtained with **[RuCl₂(SIMes)(P(p-ClC₆H₄)₃)(Ind)]**. As a good compromise for all examined reaction types, **[RuCl₂(SIMes)(PPh₃)(Ind)]** appeared to be a good choice.

In the following, the results for ROMP will be discussed in detail. The initiators (1 equiv.) were each reacted with 300 equiv. of two different norbornene based monomers, namely dimethylbicyclo[2.2.1]hept-5-ene-2,3-dicarboxylate (**EsterMon**) and 5,6-bis(methoxymethyl)bicyclo[2.2.1]hept-2-ene (**EtherMon**). Results are summarized in Table 5 and Figure 25. All polymerizations showed full conversion after 1 h, except for catalyst **PPh₃OMe** (2 h) and **PPh₃CF₃** (30 min). M_n values range from 102100 to 356200 g/mol and from 88700 to 302800 g/mol for polymers obtained from **EsterMon** and **EtherMon**, respectively.

Table 5: Evaluation of phosphine tuned Ru initiators in ROMP[a]

[Ru]	EsterMon			EtherMon		
	M_n[c]	PDI[c]	Yield[b]	M_n[c]	PDI[c]	Yield[b]
M2	654400	2.0	89 %	967200	2.3	87 %
M31	45400	1.1	72 %	64700	1.1	74 %
PPh₃	155000	1.4	74 %	177800	1.4	66 %
PPh₃-OMe	356200	1.5	84 %	302800	1.8	85 %
PPh₃-Me	273900	1.5	78 %	296000	1.5	86 %
PPh₃-F	151400	1.3	61 %	170200	1.4	96 %
PPh₃-Cl	129200	1.3	87 %	140000	1.4	70 %
PPh₃-CF₃	102100	1.3	67 %	88700	1.3	68 %

[a] Reaction conditions: c_{Mon} = 0.2 mol/L, monomer:initiator = 300:1, CH₂Cl₂, rt, quenching with ethyl vinyl ether. [b] Isolated yield after repeated precipitation from methanol. [c] Determined by GPC relative to polystyrene standards, THF.
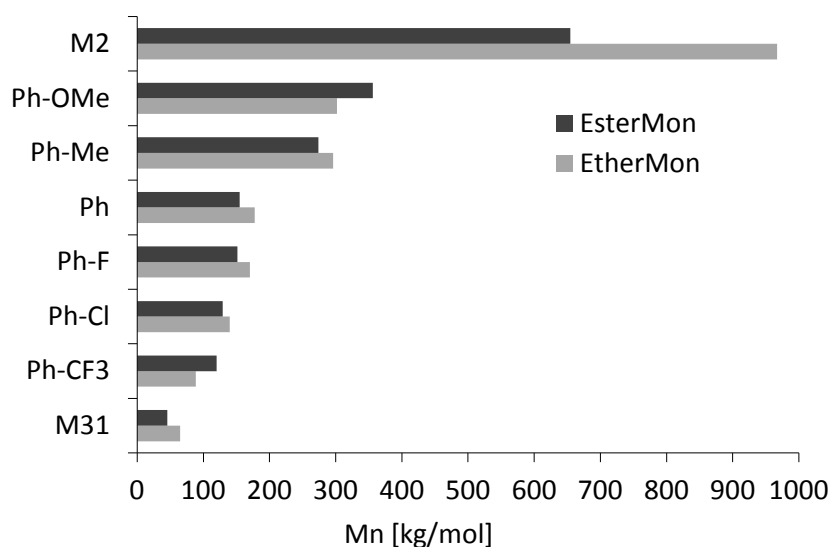
Figure 25: M_n values obtained with different triphenylphosphines as leaving ligands

The appearing correlation between donor property of the phosphine (expressed by their electronegativity χ or Hammett constant σ_p)[87][86]and the experimental M_n values is depicted in Figure 26 and Figure 27 for **EsterMon** and **EtherMon** respectively.
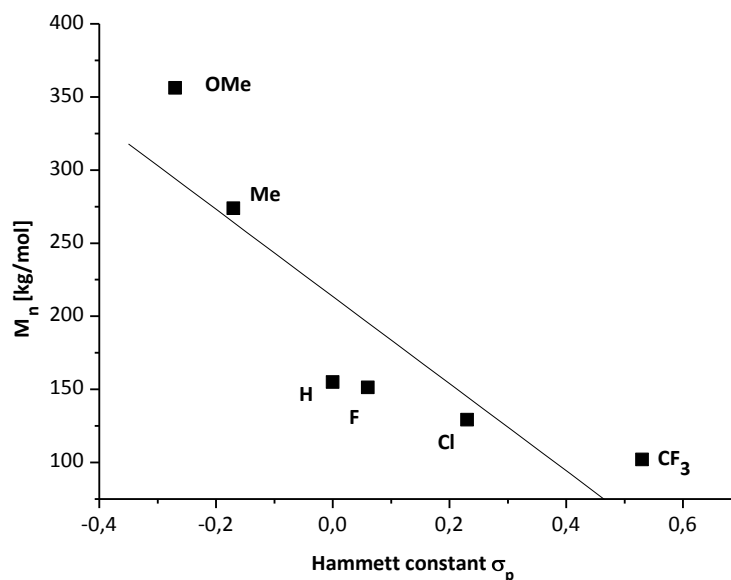

Figure 26: Correlation between Hammet constant (σ_p) of different phosphine substituents and M_n values of the polymers obtained from EsterMon.

---

[87] χ-Values from: Wilson, M. R.; Woska, D. C.; Prock, A.; Giering, W. P. *Organometallics* **1993**, *12*, 1742-1752.
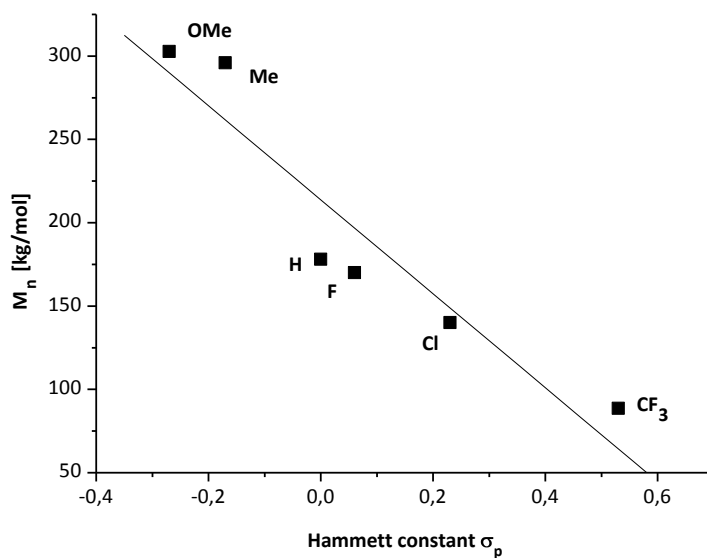
Figure 27: Correlation between Hammet constant (σ_p) of different phosphine substituents and M_n values of the polymers obtained from EtherMon.

The linear fits are not perfect but clearly confirm identical general trends for both monomers, going well along results and conclusions obtained from RCM reactions. Electron-poor PPh_3 derivatives dissociate more easily, which leads to high initiation rates while complexes bearing electron-rich phosphine ligands exhibit lower initiation rates. This fact is also illustrated by the PDI values of the polymers. These are considerably higher for the most electron-rich phosphine bearing complex **PPh₃OMe**, namely 1.5 in case of **EsterMon** and 1.8 in case of **EtherMon**, while an increasing χ of the phosphine decreases the PDI to 1.3 for both monomers in case of complex **PPh₃CF₃** (*cf*. Table 5).

3.2 Steric Impact of NHC Ligands: SI-o-Tol, SIMes and SIPr

Together with the group of Steve Nolan from University of St. Andrews, complexes featuring SIPr as NHC ligand were evaluated and compared to well-established SIMes complexes in various olefin metathesis reactions. SIPr bears sterically demanding isopropyl groups in 2- and 6-position of the phenyl groups attached to the saturated imidazolium ring. The introduction of such a ligand was aimed at facilitating the dissociation of the phosphine in *trans* position and consequently increasing the initiation rate of metathesis reactions.[88] The ligand was used in 2nd and 3rd generation indenylidene complexes, thus producing analogues to commercially available **M2** and **M31**. Moreover, the third generation complex was also tested in its bromopyridine version. For non-polymerization metathesis reactions it can be stated that especially third generation initiators with a SIPr NHC ligand are excellent choices for the synthesis of low hindered olefins by ring closing, enyne, and cross metathesis, as experiments at room temperature and low catalyst loading by the Nolan group suggest.[84]
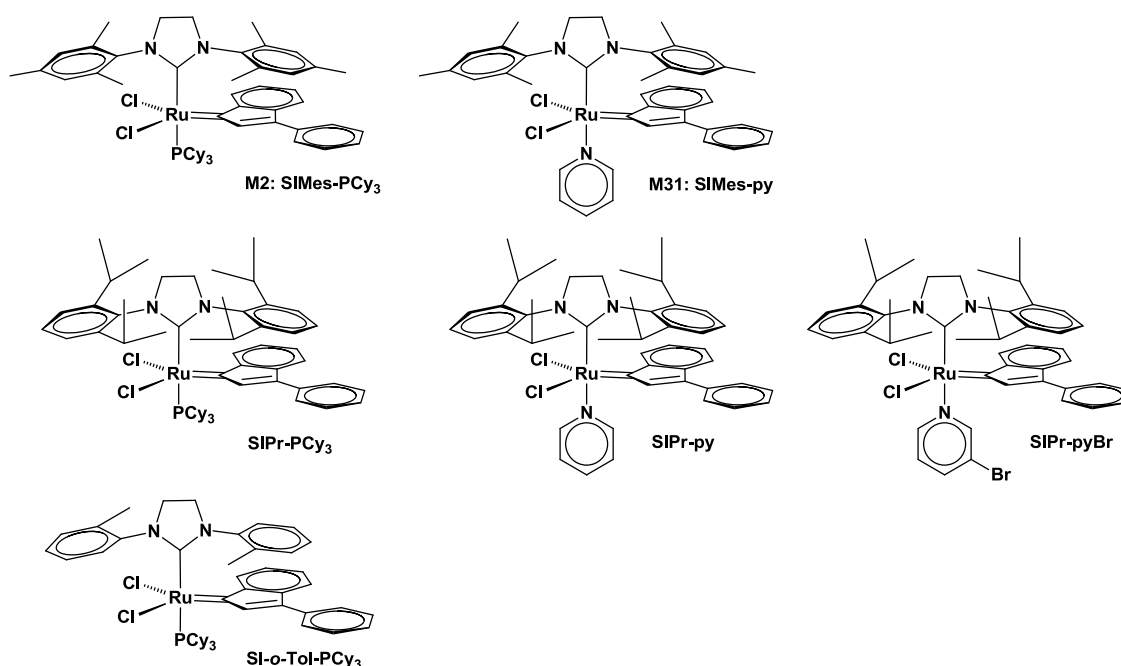

**Figure 28: Complexes under investigation for the NHC study**

As for ROMP, a systematic study on the polymerization behavior and the resulting polymers revealed some surprising aspects that call for a close, thorough examination. In course of this, a third NHC ligand was examined for 2nd generation complexes, this

---

[88] Clavier, H.; Urbina-Blanco, C. A.; Nolan, S.P, *Chem. Eur. J.* **2011**, *17*, 5045–5053.

time symmetrically equipped with *ortho*-tolyl substituents. The structures of the complexes comprised in the NHC study are depicted in Figure 28.

3.2.1 Benchmark Reactions

First, the complexes were tested in a simple standard benchmark ROMP reaction at room temperature in DCM (*cf.* Scheme 11). Two monomers, namely **EsterMon** and **KetonMon** were employed with a monomer to initiator ratio of 300:1 and a concentration of 0.1 M with respect to the monomer. For these experiments, a Schlenk flask was charged with a stirring bar, the corresponding initiator, degassed solvent and the monomer. The reaction progress was monitored by TLC. After reaction completion, excess ethylvinylether was added to quench the reaction before the polymer was precipitated and dried. Figure 29 summarizes the number molecular weight (M_n) and corresponding polydispersity indices (PDIs) obtained by GPC analysis for polymers synthesized using the abovementioned initiators.
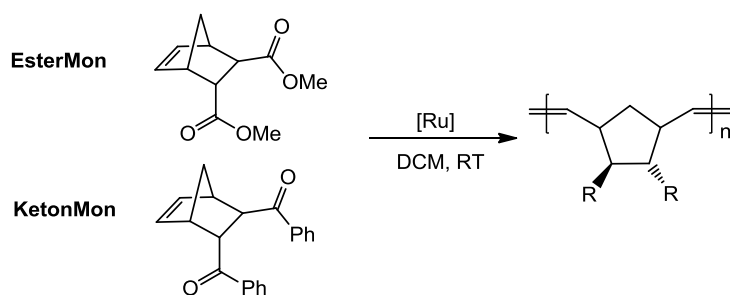
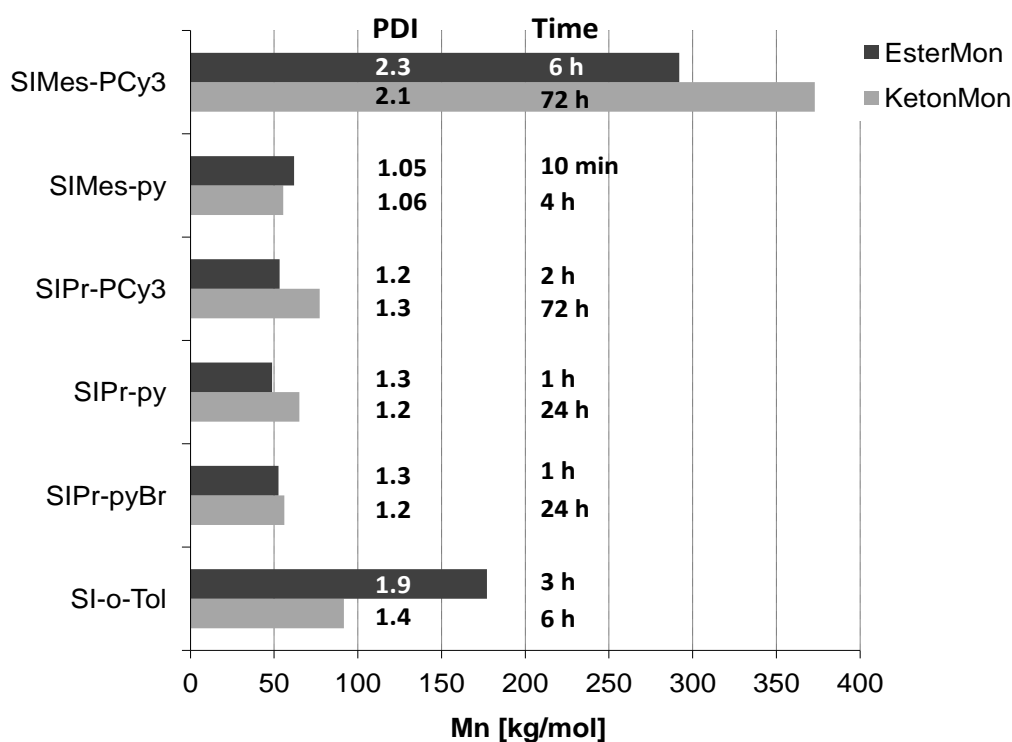**Scheme 11: Standard benchmark reaction for ROMP**

Figure 29: Benchmark ROMP reactions with various NHC complexes

The high number molecular weight (M_n) of some 300000 g/mol and a polydispersity of greater than 2 obtained from polymerizations using **M2** (SIMesPCy$_3$) are attributed to slow, non-concurrent initiation. In contrast, the "ideal" polymerization of fast-initiating pyridine adduct **M31** (SIMesPy) yields M_n values of 50000 and PDIs of lower than 1.1. Most striking, phosphine-bearing initiator **SIPr-PCy$_3$** does not fall in the same category as typical 2nd generation complex **M2** (or benzylidene analogue **G2**).[89] In contrast, the use of **SIPr-PCy$_3$** yields short polymer chains similar to **M31**, although exhibiting a broader molecular weight distribution. Pyridine adducts **SIPr-py** and **SIPr-Brpy** both conform to the expectations regarding a high initiation rate and lead to molecular weights in the same region as **M31** (and **SIPr-PCy$_3$**) with PDI values of 1.3 and 1.2 respectively. As **SIPr-py** and **SIPr-Brpy** do not show any significant reaction differences, only results using **SIPr-py** will be presented in the following section. Very interesting results were obtained with **SI-o-Tol** that obviously exhibits a higher initiation rate than the 2nd generation SIMes complex **M2**, which is displayed with the lower molecular weight of the polymers. Shorter reaction times also suggest faster propagation. The PDI values are typical for second generation initiators.

---

[89] Sanford, M. S.; Love, J. A.; Grubbs, R. H. **2001**, *J. Am. Chem. Soc. 123*, 6543-6554.

3.2.2 Reaction Profiling

In order to better illustrate the NHCs' influence on initiation and propagation, **KetonMon** was employed for reaction profiling followed by ^{1}H-NMR spectroscopy. The reaction progress was determined at distinct intervals during polymerization. A ratio of initiator to monomer of 1:50 was used in a concentration of 0.1 M with respect to monomer. Conversion was then determined by integration of the olefinic monomer and polymer peaks (5.95 ppm, dd, 1H; 5.62-4.62 ppm, mult, 2H) respectively. Such time/conversion plots are presented in Figure 30 and results are summarized in Table 6.
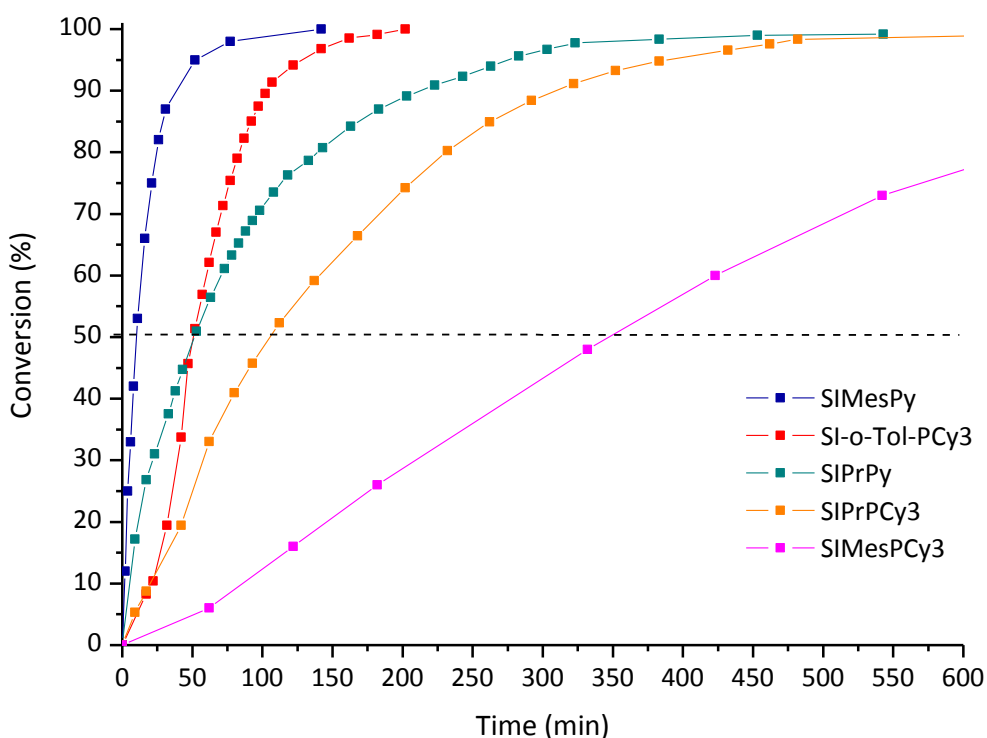

Figure 30: Conversion plot of KetonMon followed by ^{1}H-NMR spectroscopy (500MHz, CDCl₃, 25°C)

The results obtained in the above described experiments can be summarized in the following principal points:

1) **SIPr-PCy₃** is distinctly faster than the SIMes analogue **M2**, reaching 50% conversion in approximately half the time. These results are in line with recent RCM studies.[90] Increased steric bulk of the NHC is held responsible for enhanced phosphine dissociation and thus faster initiation of the metathesis catalytic cycle, accompanied by

---

[90] H. Clavier, C. A. Urbina-Blanco, S. P. Nolan, *Organometallics* **2009**, *28*, 2848-2854;

a less pronounced tendency of the PCy_3 ligand to re-coordinate during propagation in the case of **SIPr-PCy_3**. Polymerization experiments presented in Figure 29 support these observations. The low polymer molecular weight obtained with **EsterMon** and initiator **SIPr-PCy_3** can be attributed to a considerably higher value for k_i/k_p (ratio of initiation rate to propagation rate) in this system compared to that found for **EsterMon** and **M2** - provided that no backbiting occurs. 2) Pyridine adduct **SIPr-py** reacts faster than the PCy_3 as could be anticipated from the comparison of **G2** with **G3** and **M2** with **M31**, respectively. Still the effect is less distinct for the SIPr complexes. Because initiation rates for 2nd and 3rd generation SIPr complexes are similar as retrieved from interpretation of the M_n values obtained with **EsterMon** (see Figure 29), the acceleration has to be essentially related to the reluctance of pyridine to compete for the vacant coordination site during propagation.[91] 3) SIMes bearing pyridine complex **M31** is distinctly faster than its 3rd generation SIPr analogue. Comparing the polymerization half-lives (time for 50% conversion), we found a 10 fold decrease in the behaviour of **SIPr-py** compared to that of **M31**. Apparently, steric hindrance induced by the NHC ligand severely decreases the propagation rate during the course of the ROMP reaction. 4) The SI-o-Tol NHC ligand is featuring less steric impact compared to both, SIMes and SIPr. In the initial phase, the 2nd generation complex shows typical behaviour, and shows an induction phase due to slow phosphine dissociation. The first 20 min proceed identical to the reaction with **SIPr-PCy_3**. Then, obviously the reduced steric impact leads to very fast propagation, resulting in a half live equal to 3rd generation **SIPr-py**, namely 75 min for the reaction under investigation. In the end, full conversion is reached after 3.5 hours, which means that **SI-o-Tol-PCy_3** is more than three times faster than **SIPr-py**.

A third generation derivative featuring the o-Tol NHC would definitely be very interesting to be included in the study, but successful synthesis of the compound (**SI-o-Tol-py**) could not yet be accomplished.

Table 6: Conversion times for initiators featuring different NHC ligands in ROMP of KetonMon

Initiator	t 50% conv. (min)	t >99% conv. (h)
M2: SIMes-PCy_3	348	28
SIPr-PCy_3	168	19
M31: SIMes-py	8	2.25
SIPr-py	75	12
SI-o-Tol-PCy_3	75	3.5

[91] (a) Burtscher, D.; Lexer, C.; Mereiter, K.; Winde, R.; Karch, R.; Slugovc, C. *J. Polym. Sci., Part A: Polym. Chem.* **2008**, *46*, 4630; (b) Dunbar, M. A.; Balof, S. L.; LaBeaud, J.; Yu, B.; Lowe, A. B.; Valente, E. J.; Schanz, H.-J. *Chem. Eur. J.* **2009**, *15*, 12435-12446.

3.2.3 Scope Regarding Controlled Polymerization

Comparison of the molecular weights of polymers resulting from different ratios of monomer to initiator will give information about the controlled nature of the polymerization. In case of a linear correlation between the applied ratio of monomer to initiator and the resulting molecular weight and at the same time constantly low PDI values, the respective initiator does promote polymerization in a living (i.e. controlled) manner. The corresponding experiments were carried out under standard ROMP conditions (see above) with the required amount of monomer to achieve theoretical chain lengths of 200, 300, 450, 600 and 900 monomer units respectively. **M2** and **M31** served as reference initiators (**M2** as a typical representative for non-controlled ROMP, and **M31** representing ideal controlled-living behavior) for the testing of the SIPr derivatives. Second generation o-Tol complex was not included for obvious reasons (*cf*. benchmark results in Figure 29). The isolated polymers were analyzed by GPC. Results are displayed in Figure 31. **SIPr-Py** yields polymers with linearly increasing molecular weights for **EsterMon**, controlled ROMP can therefore be accomplished. The same can be reported for **KetonMon**, which was employed for further detailed investigations that are described below. In contrast, controlled polymerization is definitely not achieved by 2nd generation complex **SIPr-PCy$_3$**, where no linear correlation can be found within the investigated range. Additional information can be drawn from a closer look at the obtained weight distributions and PDI values respectively, depicted in Figure 32.
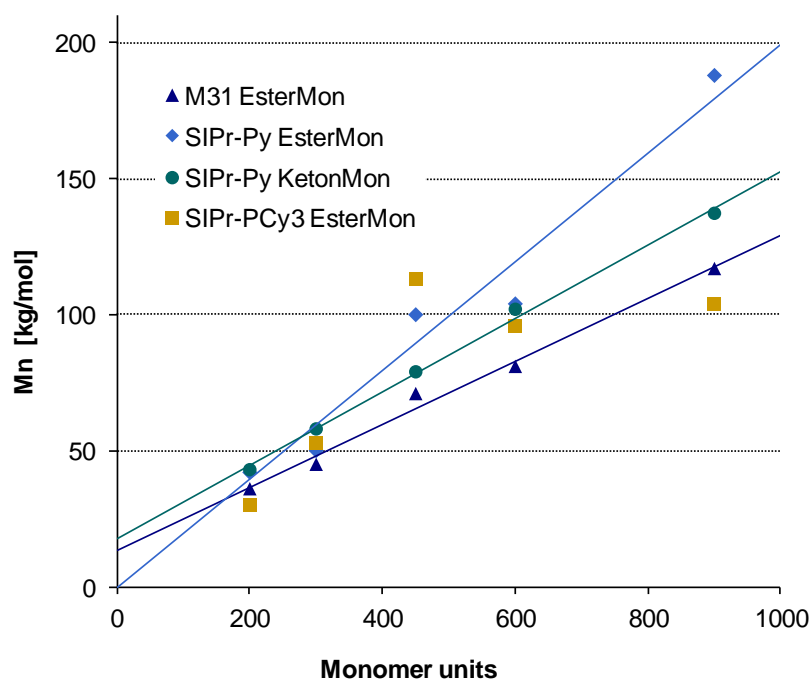

Figure 31: Number molecular weight M$_n$ of polymers with increasing monomer : initiator ratio
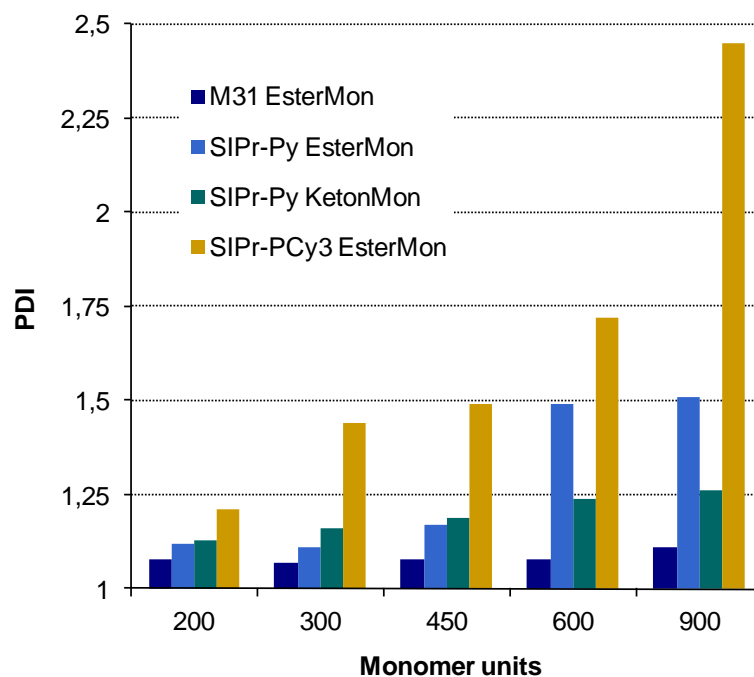
Figure 32: and PDI values (below) of polymers with increasing monomer : initiator ratio

Within polymerizations with ideal reference initiator **M31**, the PDI does not substantially increase with growing polymer weight. This is not the case for **SIPr-PCy₃** that exhibits typical behavior for non-controlled polymerization with PDIs higher than 2, comparable to **M2**.[92] But also 3rd generation complex **SIPr-Py** yielded relatively high PDIs up to 1.5 in case of **EsterMon** for high monomer : initiator ratios. Interestingly, these values result from a persistent bimodality that was observed in the molecular weight distribution when using SIPr-bearing ROMP initiators. For their SIMes analogues, bimodality was never observed as shown in exemplary GPC elugrams from benchmark reactions with **KetonMon** (Figure 33).

---

[92] (a) T.-L. Choi, R. H. Grubbs, *Angew. Chem., Int. Ed.* **2003**, *42*, 1743. (b) C. W. Bielawski, R. H. Grubbs, *Angew. Chem., Int. Ed.* **2000**, *39*, 2903.
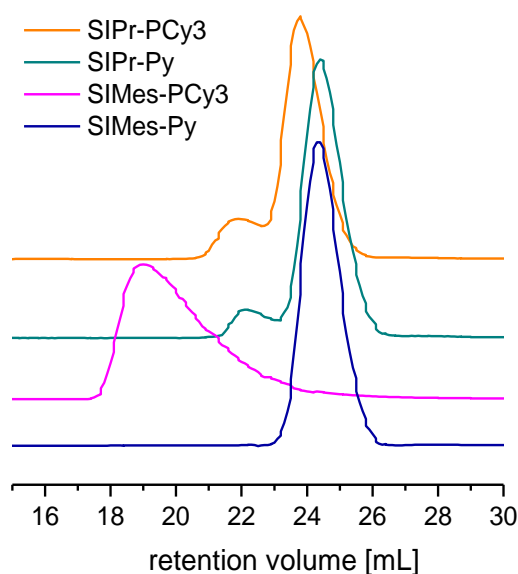
Figure 33: GPC chromatographs for poly(KetonMon) from benchmark reactions (*cf*. Figure 29)

3.2.4 Bimodality

The occurrence of bimodality is an undesired polymerization feature contradicting control over the molecular weight distribution. Hence, we investigated possible causes for this unexpected phenomenon. Generally, a bimodal distribution originates from mixed active species e.g. an (undiscovered) impurity. However, impurities of all kinds have been excluded by thorough analysis of the complexes employed. Another reason for the bimodality could be partial degradation of the polymer by backbiting during the course of polymerization. Regarding the well-shaped GPC graphs this was thought unlikely. To be sure, a standard polymerization procedure was carried out using **KetonMon** and **M31**, yielding a perfectly narrow, mono-modal distributed polymer. The polymer was re-dissolved in DCM and fresh initiator **SIPr-Py** was added. After a reaction time of 24 h, the polymer exhibited the same previously observed distribution, as depicted in Figure 34. Thus, backbiting was definitely excluded.
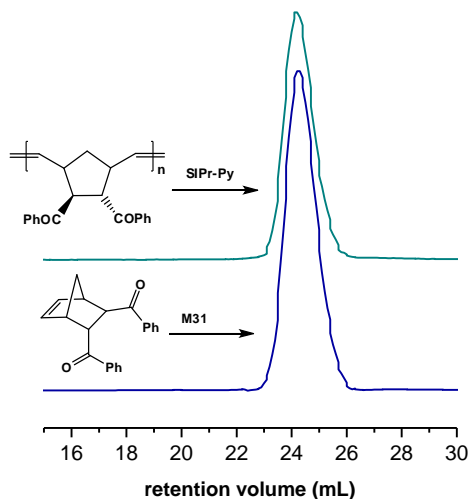
Figure 34: GPC chromatographs from backbiting experiment

Next, the correlation between polymerization progress with time and the occurrence of bimodality was investigated. Therefore "slow" monomer **KetonMon** was employed, knowing that a 300-unit-chain would take some hours to be completed with **SIPr-Py**. One third of the reaction mixture was removed after 90 min and quenched with excess ethyl vinyl ether. The polymer was precipitated in MeOH, dried in vacuum and subjected to GPC analysis. The residual reaction was allowed to proceed to completion, and again, GPC analysis performed after analogous workup.
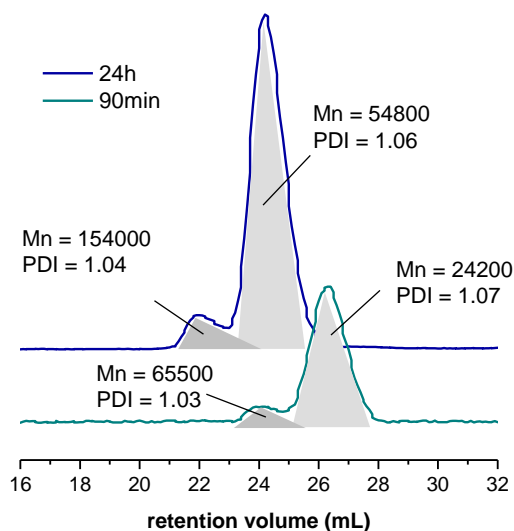
Figure 35: Bimodality as a function of time

It becomes clear, that the weight distribution is already bimodal after 90 min, showing the same ratio of the M_n values within the two fractions as the final polymer after 24 h (roughly 1:3). Moreover, it is obvious that both fractions keep growing until

52

completion of the polymerization. It is noteworthy that also for higher monomer : initiator ratios each fraction exhibits an ideally narrow weight distribution with a PDI smaller than 1.1 (Figure 36, Table 7). This again implies two different active species of the initiator operating at the same time at different speeds, whereas the fractions exhibiting a higher molecular weight (corresponding to lower retention volume in size exclusion chromatography) originate from a species faster than **SIPr-Py**. At the moment we can only speculate about the nature and the origin of a second active species. We believe, that a fast decomposition of initiator leads to a yet unknown but highly active initiator species. As a working hypothesis we assumed initiation via the NHC ligand, leading to a bis(Schrock-type) carbene complex.

Table 7: GPC data of polymers from KetonMon and SIPr-Py in different ratios

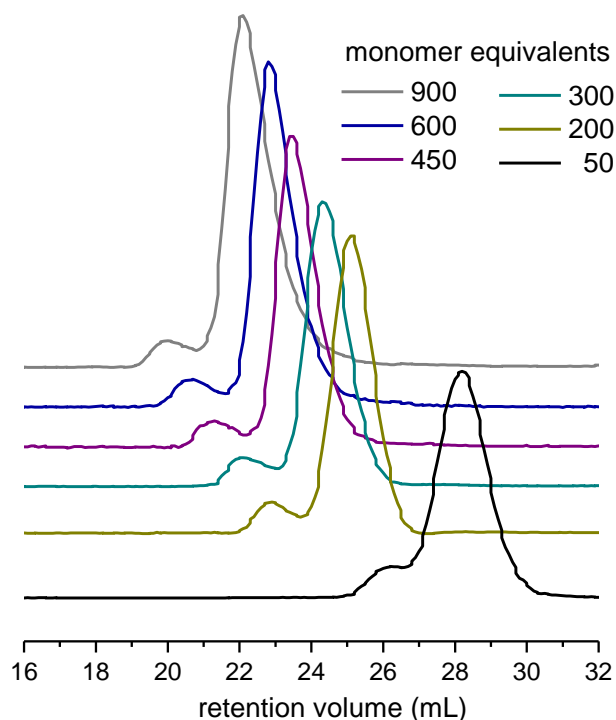| ratio	M_n (g*mol^{-1})			PDI (M_n/M_w)	
KetonMon : SIPr-Py	overall	/	main peak	overall / main peak	
50	10400	/	9800	1.2 / 1.12	
200	43000	/	41000	1.13 / 1.05	
300	58000	/	54000	1.16 / 1.07	
450	79000	/	75000	1.19 / 1.09	
600	102000	/	96000	1.24 / 1.11	
900	137300	/	130400	1.26 / 1.14	

Figure 36: GPC elugrams of polymers from KetonMon and SIPr-Py

### 3.2.5 Alternative Activation of SIPr-Complexes?

One attempt to prove the abovementioned theory was accomplished by directed synthesis of a SIPr-complex bearing a strongly coordinating chelating benzylidene carbene ligand, namely 10-vinylbenzo[h]quinoline (**L-1**). In analogy to a complex **SIMes-benzoquinoline** that had previously been synthesized and tested in our group[93], **SIPr-benzoquinoline** was prepared according to Scheme 12. The synthesis was straight forward and furnished the desired product as a light green powder in 81% yield. Elemental analysis and NMR-spectroscopy confirmed the structure and the *trans*-dichloro configuration (*cf.* chapter 7.1).
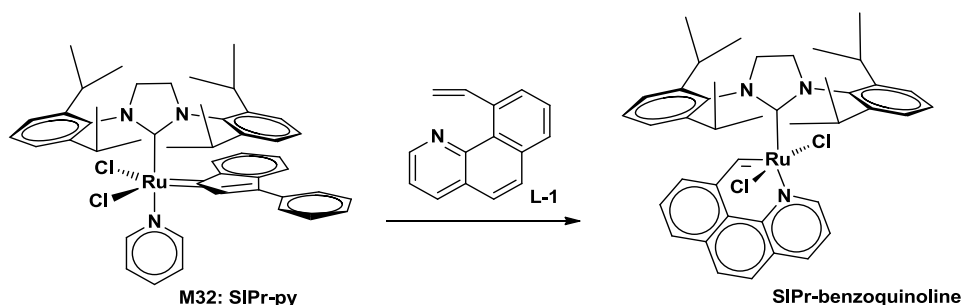
Scheme 12: Synthesis of complex SIPr-benzoqinoline for mechanistic studies

The idea was to reduce probability of the classical well known activation mechanisms (coordination of olefin *trans* to the NHC ligand after dissociation of chelating bond) and force the complex to get active via the SIPr ligand. A hypothetic initiation mechanism is depicted in the following Scheme 13 (b).

---

[93] Szadkowska, A.; Gstrein, X.; Burtscher, D.; Jarzembska, K.; Woźniak, K.; Slugovc C.; Grela, K. *Organometallics* **2010**, *29*, 117-124.
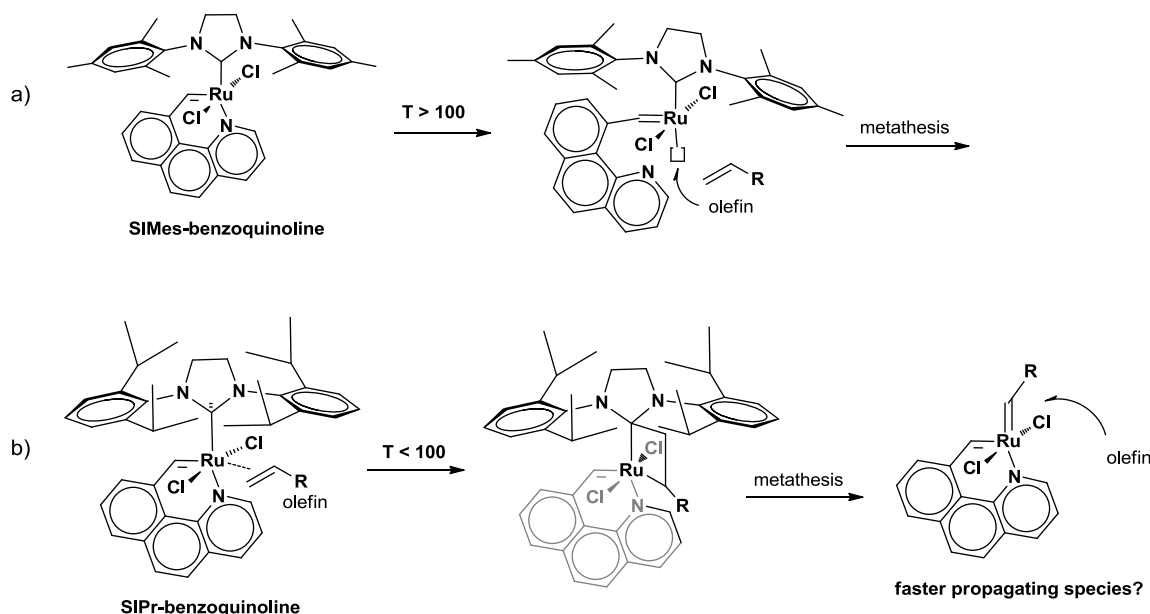
Scheme 13: a): Initiation mechanism described in literature for latent reference initiator SIMes-benzoquinoline; b): hypothetic alternative mechanism for SIPr-complexes yielding fast propagating species

The complex was tested in ROMP employing **EsterMon** with a monomer to initiator ratio of 300 and a concentration of 0.1 M in dichloromethane with respect to the monomer. The test was started at room temperature and polymerization progress was monitored by TLC. Temperature was increased several times during the test, when no polymerization could be detected. Accordingly, solvents were altered. The reaction was started in a Schlenk flask under nitrogen conditions at room temperature. After 3h, no polymerization could be detected via TLC, so temperature was raised to 40°C. After 1h, no polymerization was detected. Dichloromethane was removed in vacuo and toluene was added instead, again maintaining a concentration of 0.1 M with respect to the monomer. Even after 72 h at 80°C, TLC proved the absence of any polymer. Yet, the reaction mixture was of bright green colour, indicating the initiator being still unspoiled. Temperature was now increased to 110°C, which did not lead to polymerization. Now, toluene was removed in vacuo, the monomer-initiator mixture was transferred to an open vial with a stirring bar and heated to 140°C in order to perform bulk polymerization. Indeed, after 5 h the mixture solidified (maintaining the green colour of the unspoiled initiator). The mixture was investigated by NMR spectroscopy which revealed a conversion of 85% from monomer to polymer (*cf.* Figure 37).
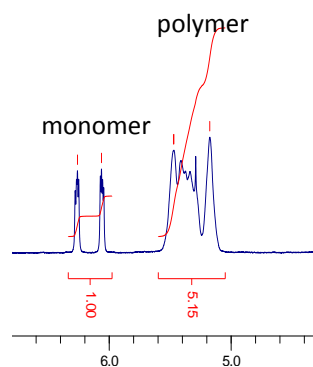
Figure 37: ^{1}H-NMR spectrum (CDCl₃, 300 MHz) of bulk polymerization after 5h at 140°C (olefinic peaks)

The resulting polymer was then re-dissolved in dichloromethane, precipitated in methanol, dried and subjected to GPC. A number molecular weight of M_n = 172800 and a polydispersity of PDI = 2.2 were determined. The weight distribution is too broad to decide whether it is bimodal or not. Also, the relatively high average molecular weight confirms a low initiation rate that had been anticipated due to the green color of the polymer stemming from the initiator. Summarizing it can be concluded from this test that for this specific SIPr complex no alternative initiation occurs. In contrast, **SIPr-benzoquinoline** turned out to be ultra-latent, in ROMP, even more latent than **SIMes-benzoquinoline** that is clearly active above 100°C.93 **SIPr-benzoquinoline** was also tested in several RCM experiments at 110°C in toluene, however, all reactions had to be cancelled without yielding any conversion. So again, the reason for bimodality in ROMP polymers from SIPr-complexes remains subject of speculations and will be further investigated in order to elucidate this phenomenon. Yet, the above described experiment impressively illustrates the influence of the NHC ligand for ruthenium olefin metathesis initiators. The interaction of the various ligands is illustrated when comparing the effects on complexes with an indenylidene ligand (enhanced initiation for 2nd generation complexes, decreased propagation fo 3rd generation complex) and the latter complex with a chelating carbene ligand that shows barely any activity. It is therefore logical to employ the SIPr ligand also in other initiators (chapter 0)

3.2.6 The Influence of the NHC Ligand on the Configuration of Polymeric Double Bonds

The steric impact of the NHC ligand on the propagation during ROMP has been discussed (*cf*. chapter 3.2.3). During the formation of a new double bond the steric bulk in vicinity of the bond to be formed obviously plays a major role. It is therefore only logical, that complexes with a different steric impact yield different polymers regarding the *cis*/*trans* ratio of double bonds. By means of NMR spectroscopy this ratio

can be determined. Symmetrically 2,3-disubstituted norbornadiene derivatives are very well suited for this kind of investigation. As described in detail by Delaude et al., ROMP polymers from this class of monomer yield rather simple NMR spectra due to the lack of *exo*- and *endo* isomers. Still, four possible structures are to be expected, namely *cis* and *trans* configuration in their respective isotactic or syndiotactic form (*cf.* Figure 38).[94]
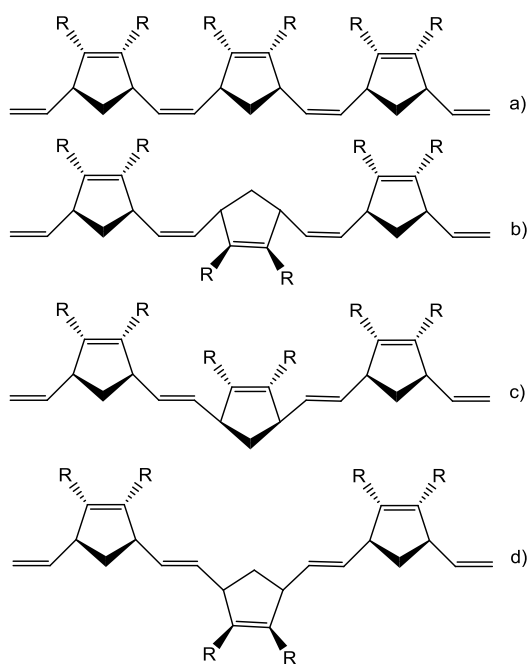

Figure 38: Possible configurations of 2,3-disubstituted polynorbornadienes from ROMP: (a) *cis*, **isotactic; (b)** *cis*, **syndiotactic; (c)** *trans*, **syndiotactic; and (d)** *trans*, **isotactic**

The nature of substituent R at 2- and 3-position of the monomer will also influence which configuration will predominantly occur. Also, R will determine whether backbiting of the initiator is feasible or not, which can be seen from the molecular weight distribution of the resulting polymer. Therefore more than one monomer has to be tested and compared to reasonably judge the influence of the initiator. **EsterDieneMon** ((bicyclo[2.2.1]hepta-2,5-diene-2,3-dicarboxylic acid dimethyl ester) and **OxaDieneMon** (7-oxabenzonorbornadiene) were employed in a systematic study of the NHC ligand's influence on the *cis/trans* ratio in ROMP polymers. **EsterDieneMon** was chosen because of its similarity to **EsterMon** and the subsequent analogies that can be drawn. **OxaDieneMon** was chosen as second monomer because of its lower steric encumbrance and different polymerization behavior resulting therefrom. The

---

[94] Delaude, L.; Demonceau, A.; Noels, A. F.; *Macromolecules* **1999**, 32, 2091-2103.

polymerizations were carried out in dichloromethane at room temperature employing a concentration of 0.1 M with respect to the monomer and 100 equivalents of monomer with respect to the initiator. After full consumption of the monomer according to TLC, a standard work-up procedure followed and the resulting polymers were analyzed by GPC and NMR spectroscopy. For simplicity reasons, only *cis* and *trans* isomers were differentiated in the spectra, but not their iso- or syndiotactic structure. In case of **EsterDieneMon** it was found most reliable to compare the methyl peaks in the ^{13}C-NMR spectra of the polymers (52.1 ppm for the *trans* isomer and 48.6 ppm for the *cis* isomer; *cf*. Figure 39), as peaks are largely overlapping in the ^{1}H NMR spectra.
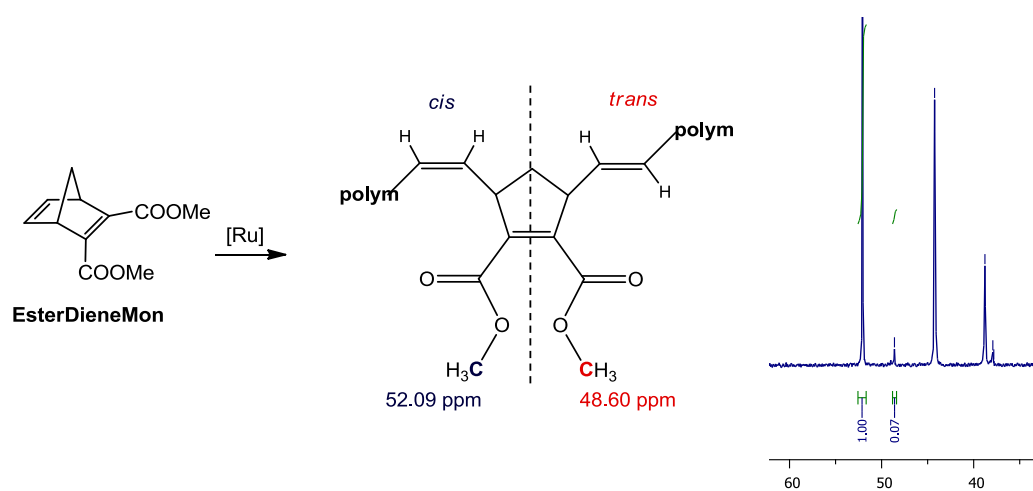
Figure 39: EsterDieneMon and characteristic part of ^{13}C NMR spectrum to determine the *cis*/*trans* ratio
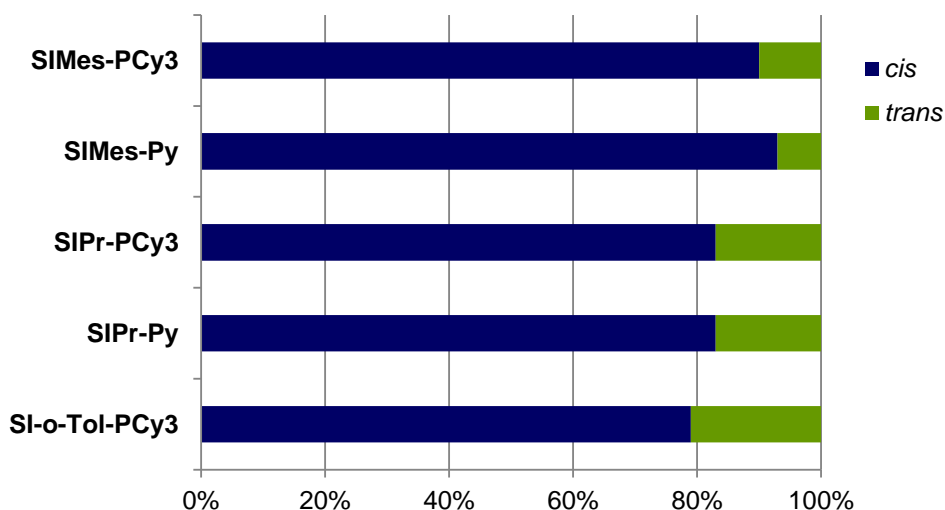
Figure 40: *cis*/*trans* ratio in poly(EsterDieneMon)

For polymers from **OxaDieneMon** two signals in the ^{1}H-NMR spectra were well suited for determination of the *cis/trans* ratio, namely the olefinic peaks at 6.16 ppm and 6.02 ppm, and peaks from the chiral allylic hydrogens at 5.79 ppm and 5.65 ppm for *cis* and *trans* isomers respectively (*cf.* Figure 41). Results from NMR and GPC analysis are summarized in Table 8.
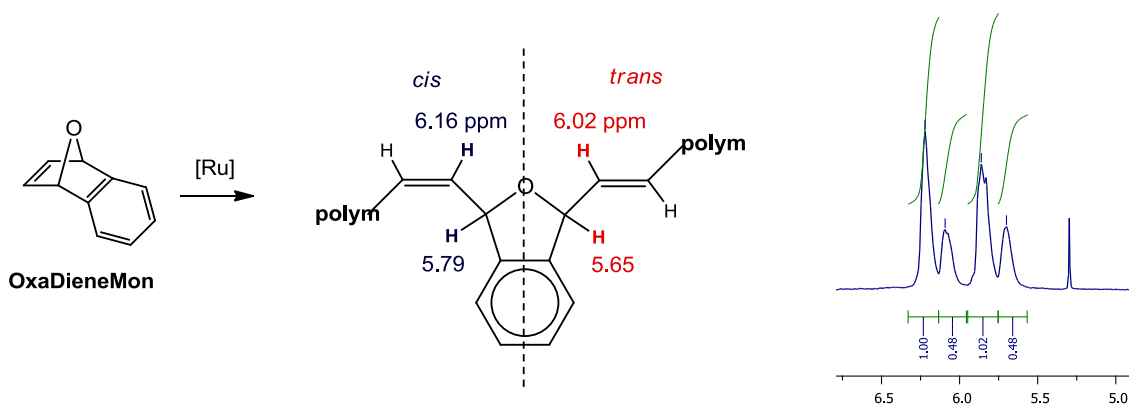
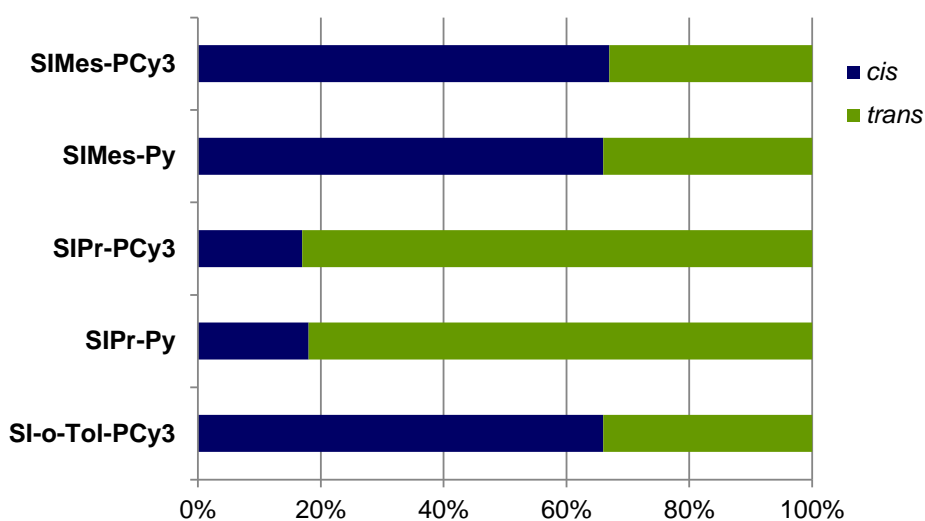**Figure 41: OxaDieneMon and characteristic part of ^{1}H NMR spectrum to determine the *cis/trans* ratio**

Figure 42: *cis/trans* ratio in poly(OxaDieneMon)

The two monomers under investigation show large differences regarding both, GPC and NMR analysis (Table 8). Analogously to **EsterMon**, **EsterDieneMon** is not degraded by backbiting, indicated by comparatively low number molecular weights M_n and PDI values. Also, the achieved molecular weights with 100 equivalents **EsterDieneMon** roughly correspond to one third of the molecular weights achieved with the respective

initiators and 300 equivalents of **EsterMon** (*cf*. Figure 29). In contrast, polymer chains from **OxaDieneMon** obviously suffer from backbiting. The molecular weights are between 4 and 40 times lower compared to **EsterDieneMon** and PDI values range from 2.6 (**SIPr-Py**) to 4.1 (**SIPr-PCy₃**), a clear sign for polymer degradation. Regarding the *cis/trans* ratios determined by NMR spectroscopy it could be shown that the NHC ligand does have an influence for both monomers. However, for **EsterDieneMon** the differences are rather small and a clear trend is difficult to be stated. The SIPr-NHC ligand seems to rather promote *trans* configuration compared to SIMes. The performance of SI-o-Tol (21 % of *trans* polymer) cannot be properly assessed due the lack of the 3rd generation derivative. Anyway, the situation is much clearer with **OxaDieneMon**. Whereas SIMes complexes **M2** and **M31** yielded two thirds of *cis* configurated double bonds, SIPr complexes produced more than 80 % of *trans* polymer. There is no significant difference between 2nd and 3rd generation complexes. **SI-o-Tol-PCy₃** behaved similar to the SIMes complexes. A possible explanation for generally higher *trans* ratio is the degradation of polymer by secondary metathesis. Possibly, this concurrent degradation and rebuilding process shifts the *cis/trans* ratio towards *trans*, assuming that for steric reasons an attack is more likely in case of *cis* configuration. The newly formed bond can then be either *cis* again, but also t*rans*. Thus the *cis* ratio is decreased with time. Obviously, the bulky SIPr ligand promotes the formation of *trans* bonds.

Table 8: Molecular weight distribution and *cis/trans* ratio of polymers from EsterDieneMon and OxaDieneMon

| Initiator	poly(EsterDieneMon)				poly(OxaDieneMon)			
	GPC		^{13}C-NMR		GPC		^{1}H-NMR	
	M_n (g/mol)	PDI	*cis*	*trans*	M_n (g/mol)	PDI	*cis*	*trans*
M2: SIMes-PCy₃	64388	2.2	90 %	10 %	1690	3.9	67 %	33 %
M31: SIMes-Py	18477	1.3	93 %	7 %	1240	2.9	66 %	34 %
SIPr-PCy₃	21305	1.2	83 %	17 %	3070	4.1	17 %	83 %
SIPr-Py	21910	1.3	83 %	17 %	5860	2.6	18 %	82 %
SI-o-Tol-PCy₃	52955	1.6	79 %	21 %	2280	2.8	66 %	34 %

3.3 Tuning the Geometry in Olefin Metathesis Initiators Featuring Chelating Carbene Ligands

The influence of the NHC ligand on the activity of olefin metathesis initiators has been made clear in the previous chapter. It is now logical to extend the application of the SIPr ligand to ruthenium complexes featuring chelating carbene ligands, one of the main investigation fields within the group. In the following study, four ruthenium complexes featuring chelating ester ligands are presented. Their respective configuration of the chloride ligands was found to be strongly depending on the steric bulk of the NHC ligand on the one hand, but on the other hand also on the electrophilicity of the functional group attached *trans* to the chelating ester (methoxy or nitro group). As parent complexes, two third generation ruthenium initiators for olefin metathesis, namely **1** (= **M31**) and **2** (= **M32**), featuring either SIMes or SIPr as NHC ligand respectively, were used. Upon metathetic ligand exchange, they have been equipped with two different ester based carbene ligands each, namely 1-isopropoxy-4-methoxy-2-vinylbenzene (**L-3**) and 1-isopropoxy-4-nitro-2-vinylbenzene (**L-4**). Four main products were isolated (*cf*. Scheme 14) and studied regarding the differences in their respective structure and activity. Both turned out to be considerably diverging.

3.3.1 Syntheses of OMe-SIMes, OMe-SIPr, NO$_2$-SIMes and NO$_2$-SIPr

The syntheses of the abovementioned complexes were carried out in Schlenk flasks under nitrogen conditions, using degassed DCM as solvent. The parent complexes were dissolved together with a slight excess of the corresponding ligand (1.3 to 1.5 equivalents) and stirred for 24 to 48 hours at room temperature. After full conversion according to TLC, the new complexes were isolated either by precipitation with n-pentane or by column chromatography (details *cf*. experimental part). With the SIMes complex **M31**, different complex isomers occurred during the synthesis. As it had previously been disclosed by our group, methoxy substituted ligand **L-3** mainly yielded a complex exhibiting the *cis* dichloro configuration (**5a: OMe-SIMes**, 77%), together with 21% of a cationic species (**5b**) and minor amounts of the respective *trans* dichloro product **5c**.[72b] In contrast, nitro substituted ligand **L-4** furnished the *trans* dichloro complex **8a: NO$_2$-SIMes** as main product, that is in equilibrium with its pyridine adduct **8b**, as long as pyridine is not removed by column chromatography. Also, a small amount of the *cis* dichloro compound **8c** was identified in the product mixture by means of NMR spectroscopy. The SIPr complex **M32** exclusively yielded the respective *trans* compounds **6: OMe-SIPr** and **7: NO$_2$-SIPr**, with both ligands **L-3** and **L-4**. The two "methoxy-complexes" **5a** and **6** are of bright green color and exhibit high stability at

ambient conditions and in solution at room temperature. The nitro compounds **7** and **8a** are of brownish color, less stable in solution and more difficult to obtain in pure form.
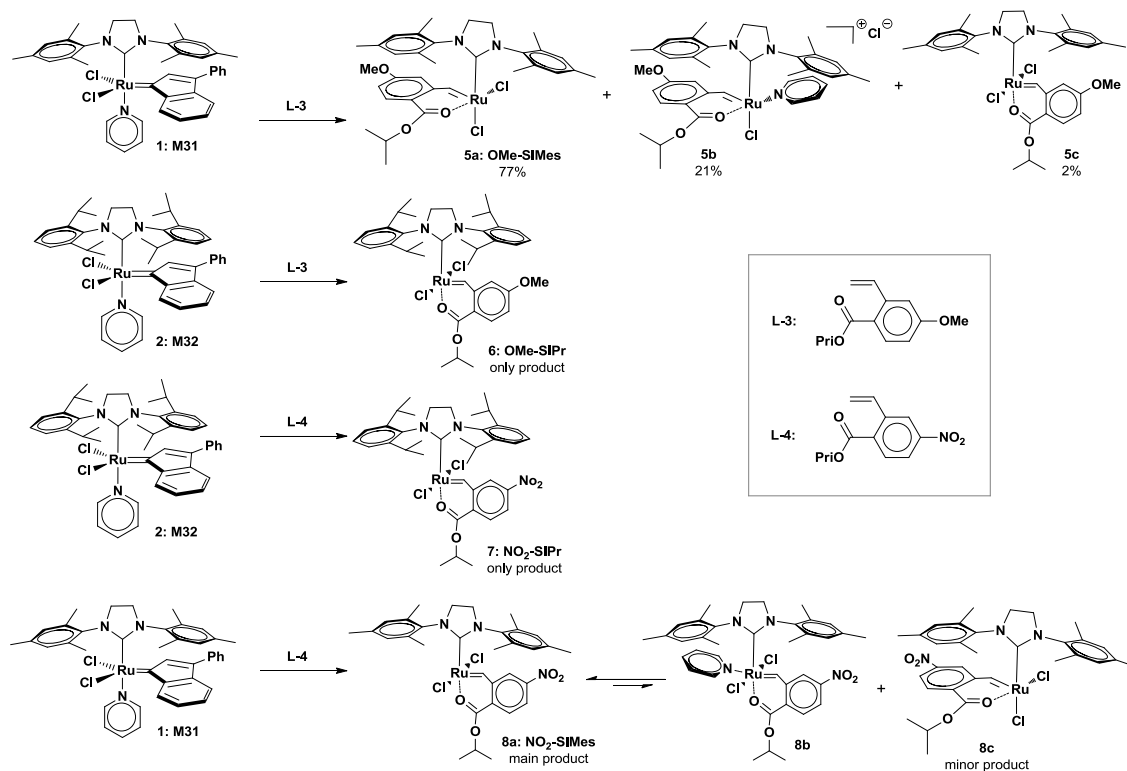
Scheme 14: Synthesis of various ruthenium complexes with chelating carbene ligands

3.3.2 Structural Comparison of OMe-Complexes 5a and 6

It was possible to obtain crystal structures from the complexes featuring a methoxy substituted ligand (Figure 43). The opposite chloride configuration within the two structures (SPY-5-34 *cis* dichloro for **5a** and SPY-5-31 *trans* dichloro for **6**) that had been suggested due two ^{1}H-NMR spectra (cf. Figure 44, Figure 46) was confirmed. Hence, the corresponding structures for the two nitro complexes **7** and **8a** could be reliably deduced from the corresponding NMR spectra.
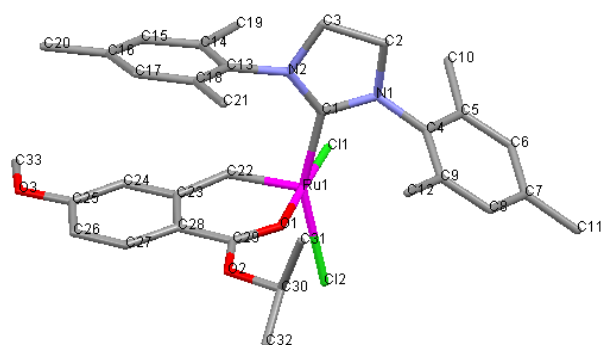
Figure 43: Crystal structure of 5a: *cis*-dichloro configuration
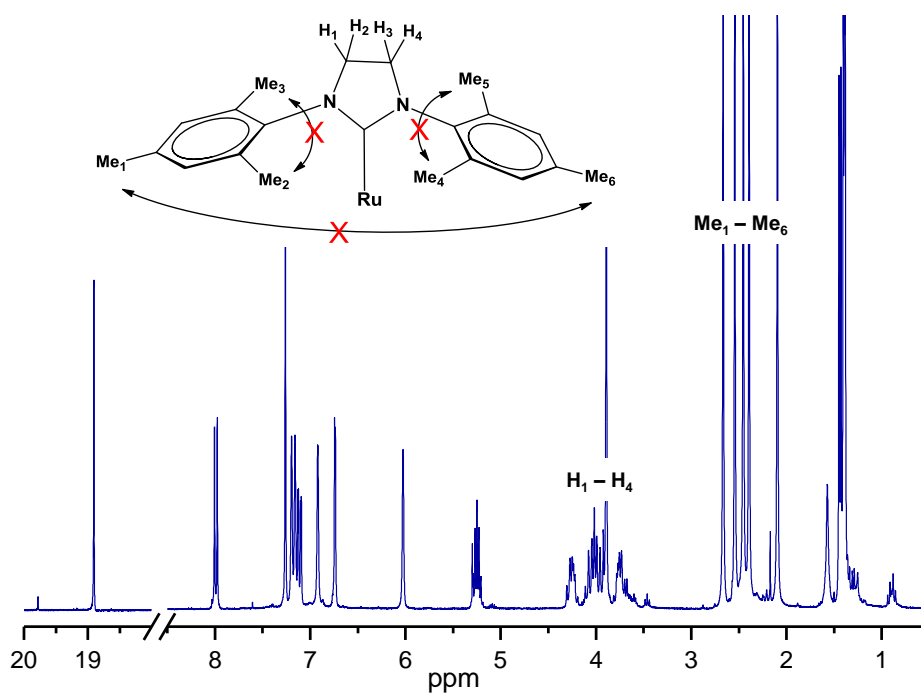
Figure 44: ^{1}H-NMR spectrum of *cis* dichloro structure 5a: OMe-SIMes (CDCl$_3$, 300 MHz): rotation of NHC ligand inhibited, diastereotopic splitting due to unsymmetric environment (*cf*.Figure 43)
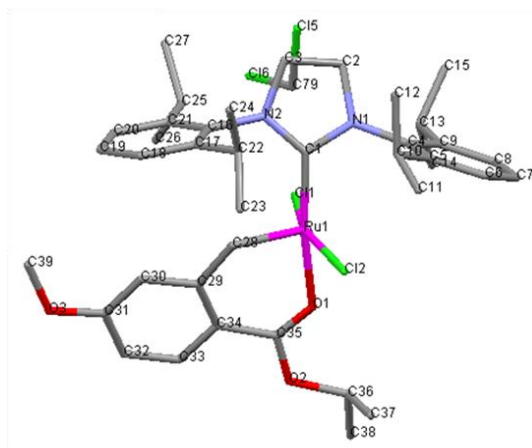
Figure 45: Crystal structure of 6: *trans*-dichloro configuration
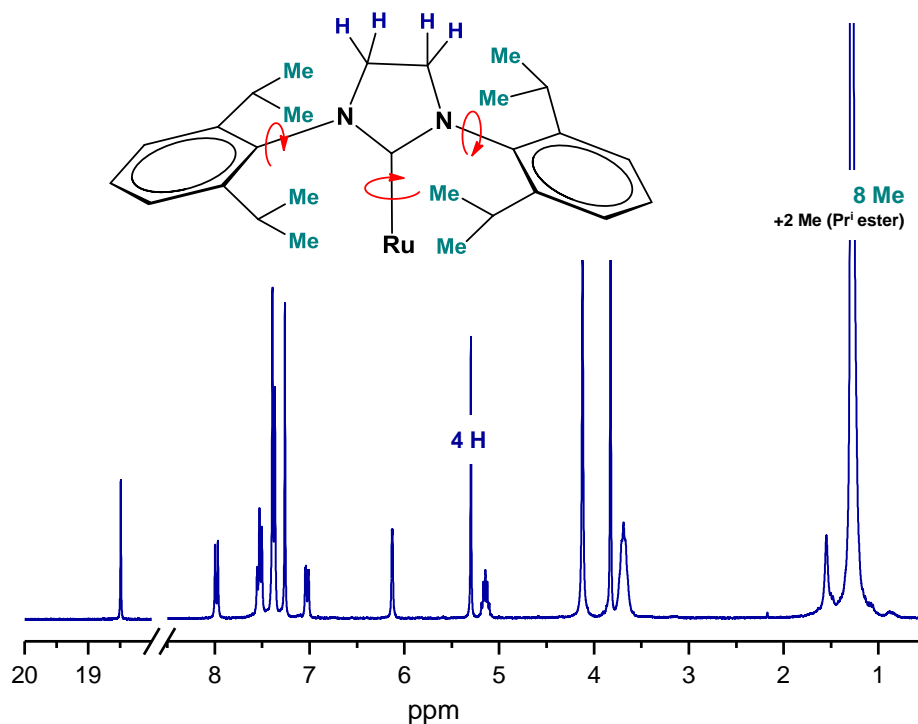
Figure 46: ^{1}H-NMR spectrum of *trans* dichloro complex 6: OMe-SIPr (CDCl$_3$, 300 MHz): NHC ligand can rotate freely: no pi-stacking of benzylidene cabene ligand, symmetric environment (Figure 43)

In the following tables, structure determining bond features of the two complexes **5a** ((SPY-5-34)-dichloro-(κ^2(C,O)-(2-isopropylester-5-methoxy benzylidene)-(1,3-bis(2,4,6-trimethylphenyl)-4,5-dihydroimidazol-2-ylidene)ruthenium and **6** ((SPY-5-31)-dichloro-(κ^2(C,O)-(2-isopropylester-5-methoxy benzylidene)-(1,3-bis(2,6-diisopropylphenyl)-4,5-dihydroimidazol-2-ylidene)ruthenium are summarized.

64

Table 9: Selected bond lengths

Atom 1	Atom 2	Length (Å)	Atom 1	Atom 2	Length (Å)
5a: OMe-SIMes			**6: OMe-SIPr**		
Ru1	Cl1	2.3708(5)	Ru1	Cl1	2.3401(5)
Ru1	Cl2	2.3643(5)	Ru1	Cl2	2.3461(5)
Ru1	C1	2.020(2)	Ru1	C1	1.998(2)
Ru1	C22	1.811(2)	Ru1	C28	1.820(2)
Ru1	O1	2.092(1)	Ru1	O1	2.132(1)
N2	C1	1.345(2)	N2	C1	1.359(2)
N2	C3	1.481(2)	N2	C3	1.481(3)
N1	C1	1.346(2)	N1	C1	1.361(2)
N1	C2	1.481(2)	N1	C2	1.477(3)
C3	C2	1.524(3)	C3	C2	1.517(3)

Table 10: Selected bond angles

Atom 1	Atom 2	Atom 3	Angle (°)	Atom 1	Atom 2	Atom 3	Angle (°)
5a: OMe-SIMes				**6: OMe-SIPr**			
Cl1	Ru1	Cl2	91.48(2)	Cl1	Ru1	Cl2	159.05(2)
Cl1	Ru1	C1	90.30(5)	Cl1	Ru1	C1	88.53(5)
Cl1	Ru1	C22	90.16(6)	Cl1	Ru1	C28	98.47(6)
Cl1	Ru1	O1	177.64(4)	Cl1	Ru1	O1	84.73(4)
Cl2	Ru1	O1	86.23(4)	Cl2	Ru1	O1	85.51(4)
C1	Ru1	O1	169.99(7)	C1	Ru1	O1	92.00 (6)
C1	Ru1	C22	98.14(8)	C1	Ru1	C28	99.56(8)
C22	Ru1	O1	90.04(7)	C28	Ru1	O1	88.76(7)
C1	N1	C2	113.1(2)	C1	N1	C2	111.8(2)

Table 11: Distortion of NHC ligand

	Atom 1	Atom 2	Atom 3	Atom 4	Torsion (°)
5a: OMe-SIMes	N1	C2	C3	N2	6.8 (2)
6: OMe-SIPr	N1	C2	C3	N2	23.2 (2)

Table 12: Burried volume of NHC

	V_{bur}[a]
5a: OMe-SIMes	32.8%
6: OMe-SIPr	33.6%

[a] (sambVca web application https://www.molnac.unisa.it/OMtools/sambvca.php)[95]

The respective configuration of the complexes can be best deduced from the corresponding bond angles (Table 10). Whereas in SIMes complex **5a** the two chloride-ruthenium bonds are almost vertical to each other (Cl1-Ru-Cl2 = 91.48°) and Cl1, the ruthenium center Ru and chelating oxygen O1 are more or less in a straight line (Cl1-Ru-C1 = 177.64°), the situation is diametrically opposite in the SIPr complex **6**, where the corresponding angles are 159.05° and 84.73° respectively. The different relative position of the ligands towards each other is also clearly indicated by the NHC ligand's position relative to benzylidene carbene. For SPY 5-34 configured complex **5a** this corresponds to C1-Ru-O1 (169.99°), for SPY 5-31 configured complex **6** this is C1-Ru-O1 (92.00°). Apart from the chloride configuration, the crystal structures are rather similar regarding bond lengths and bond angles. The most striking difference not correlated to *cis* or *trans* configuration, is the distortion of the imidazolium ring in the NHC ligand (Table 11). A moderate torsion in SIMes complex **5a** of 6.8° is in clear contrast to a heavily distorted ring in complex **6** (23.2°). On the other hand, the buried volumes %V_{bur} of the two different NHC ligands that give information about the space occupied by an organometallic ligand in the first coordination sphere of the metal center, and thus provides an estimation of the accessibility to the chelating carbene ligand for an approaching olefin, are in the same range (32.8 and 33.6 %). This again suggests that reactivity differences between these two complexes be mainly determined by the chloride configuration and stability of the complexes.

Unfortunately, crystallization of the nitro complexes **7: NO$_2$-SIPr** and **8a: NO$_2$-SIMes** was not successful. Nevertheless, upon comparison of the NMR spectra of the isolated complexes to those of fully characterized complexes **5a** and **6**, their respective configuration can easily be extrapolated, and it was concluded that both nitro complexes are *trans* dichloro configurated.

---

[95]Poater, A.; Cosenza, B.; Correa, A.; Giudice, S.; Ragone, F.; Scarano, V.; Cavallo L, *Eur. J. Inorg. Chem.* **2009**, *13*, 1759-1766.
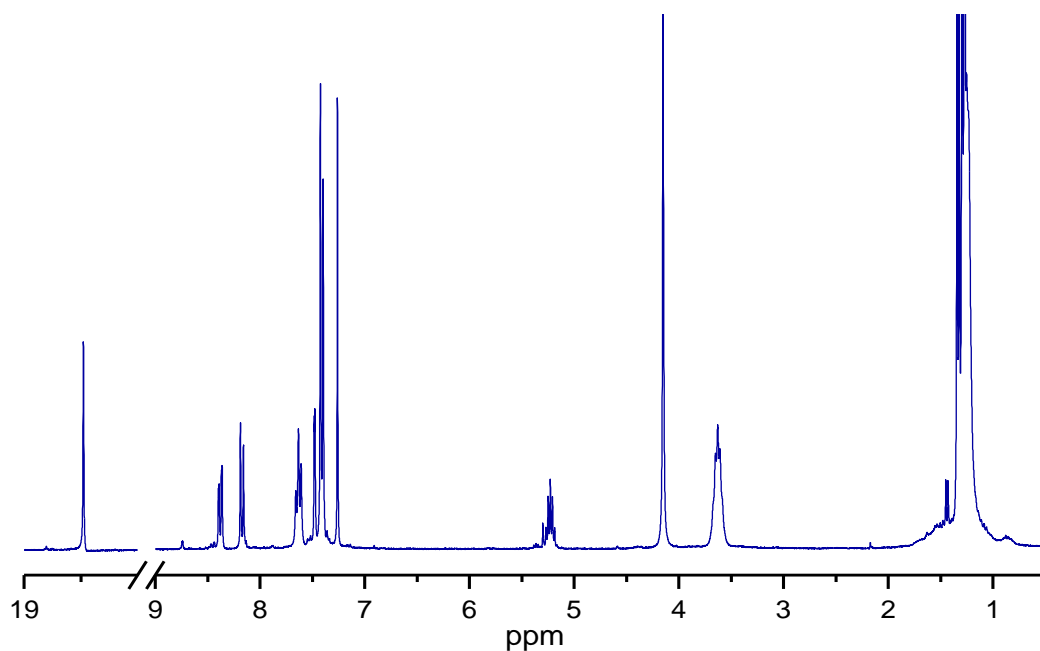
Figure 47: ^{1}H-NMR spectrum of *trans* dichloro complex 7: NO$_2$-SIPr (CDCl$_3$, 300 MHz): signal splitting similar to OMe-SIPr-complex 6 – freely rotating NHC ligand

The ^{1}H-NMR spectrum of complex **7: NO$_2$-SIPr** is characterized by a carbene peak at 18.48 ppm, all aromatic signals in the expected region, a sharp singlet peak at 4.15 ppm corresponding to four identical hydrogens on the NHC backbone. In contrast to the methoxy substituted complex **6**, the orientation of the SIPr ligand's isopropyl groups in **7** are obviously slightly deviated from perfect symmetry which leads to one rather sharp duplett (1.30-1.27 ppm) and a very broad duplett (1.25 - 1.23 ppm) each counting for 12 hydrogen atoms (Figure 47).

The isolation of the corresponding SIMes complex was far more challenging, as several isomers are being formed during synthesis. The raw product (after precipitation with n-pentane) consists of two isomers that give their carbene signals in the ^{1}H-NMR spectrum at 19.09 ppm (accounting for 26 %) and 18.78 ppm (74 %) respectively.
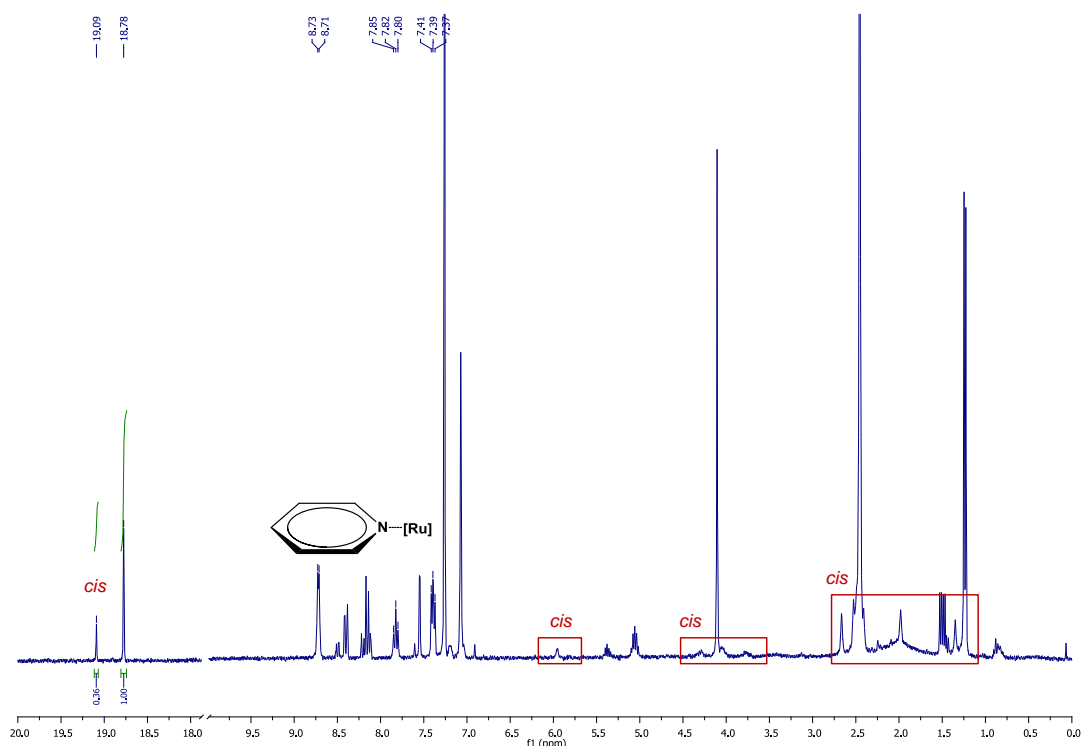
Figure 48: ^{1}H-NMR spectrum of raw product 8, two isomers; Main product 8b (carbene signal at 18.78 ppm with coordinated pyridine (peaks picked), minor product 8c (*cis* dichloro configuration similar to 5a, *cf*. Figure 44)

Minor product **8c** (carbene at 19.09 ppm) was identified as a *cis* dichloro complex because of its characteristic diastereotopic signal pattern. Typical features therefore can be detected in the spectrum depicted in Figure 48. They are: firstly the widely spread aromatic mesityl signals (whereof one signal is far high-field shifted, in this case to 5.95 ppm), secondly the diastereotopic NHC backbone hydrogen atoms (signals from 4.4 ppm to 3.6 ppm) and thirdly, the mesityl methyl groups that give an unsymmetric pattern (singlet peaks in the range of 2.7 ppm to 1.2 ppm, in this case superimposed by solvent peaks and signals from main product **8b**). Regarding typical symmetry features, **8b** yields a very similar spectrum as SIPr complexes **6** and **7** (see above). The additional aromatic peaks in the spectrum (corresponding peaks are picked in Figure 48) were assigned to coordinated pyridine that originates from **M31**, the parent complex. This assumption was confirmed by a crystal structure of **8b** that could luckily be obtained from the raw product (Figure 50).

In order to get pure complexes, the mixture of isomers was subjected to column chromatography employing a solvent gradient with dichloromethane and methanol (details in experimental part, chapter 7.1). Thus, one clean complex could be isolated that surprisingly turned out to be neither of the isomers present in the raw product, but pyridine-free *trans* dichloro complex **8a: NO₂-SIMes**. The corresponding NMR spectrum is depicted in Figure 49.
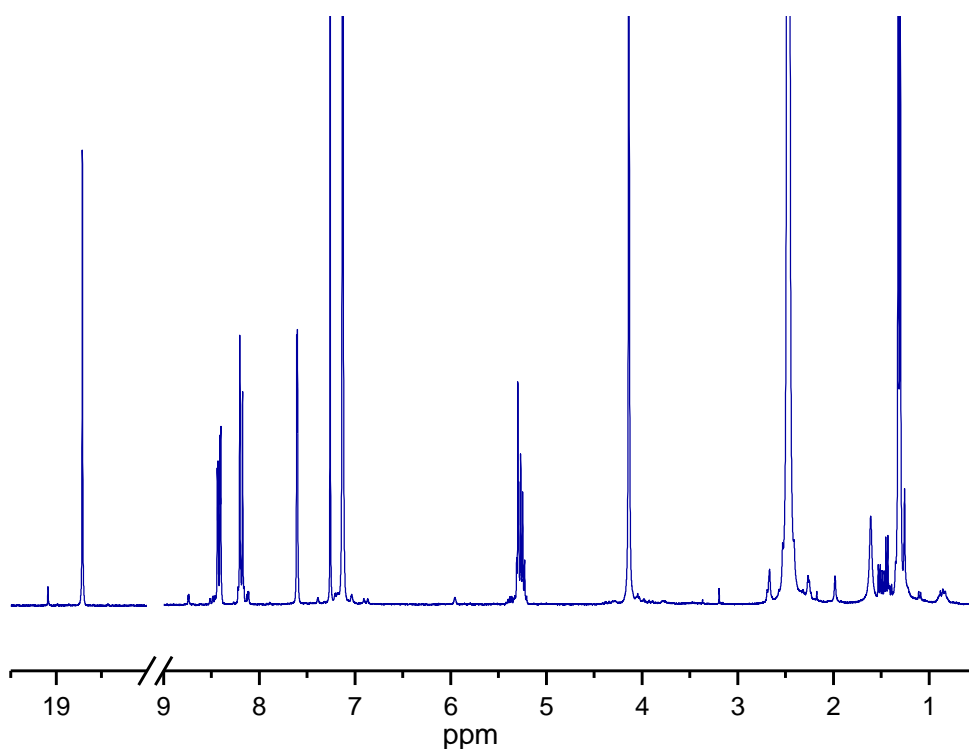
Figure 49: ^{1}H-NMR spectrum of *trans* dichloro complex 8a: NO$_2$-SIMes (CDCl$_3$, 300 MHz): signal splitting similar to SIPr-complex 6 – freely rotating NHC ligand

The ^{1}H-NMR spectrum of complex **8a: NO$_2$-SIMes** is characterized by a carbene peak at 18.71 ppm. A tiny amount (4%) of the *cis* dichloro compound **8c** is indicated by the small carbene peak at 19.09 ppm and the corresponding signals throughout the spectrum. Again, the NHC ligand rotates freely shown by two sharp singlet peaks in the aromatic region at 7.13 ppm, corresponding to position 3 and 5 of the mesityl group, and at 4.14 ppm, stemming from the saturated imidazole backbone. The methyl groups of the mesityl ligands are represented by two singlets at 2.48 and 2.46 ppm which correspond to 6 H (Mes^4) and 12 H (Mes^{2,6}) respectively.

Obviously, **8b** could not be isolated due to the lability of the pyridine ligand. Nevertheless the crystal structure of **8b** gave additional evidence about previously stated assumptions regarding possible configurations of dichloro ruthenium complexes featuring a chelating carbene ligand. Some details are described in the following. Also, the structure will be compared to the above described methoxy complexes.
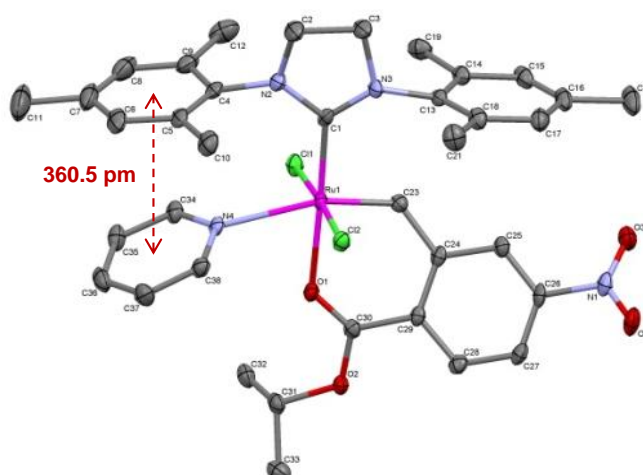
Figure 50: Crystal structure of 8b: NO$_2$-SIMes-Py (Full characterization in Appendix)

Table 13: Selected bond lengths, bond angles, torsion and V$_{bur}$[a] of pyridine adduct 8b

Atom 1	Atom 2	lengths (Å)	Atom 1	Atom 2	Atom 3	Angle (°)
Ru1	C23	1.849(3)	C23	Ru1	C1	95.97(12)
Ru1	C1	2.021(3)	C23	Ru1	O1	87.18(11)
Ru1	O1	2.150(2)	C23	Ru1	N4	159.19(11)
Ru1	N4	2.373(2)	C1	Ru1	O1	175.38(10)
Ru1	Cl2	2.3792(8)	C1	Ru1	N4	103.75(10)
Ru1	Cl1	2.4084(8)	Cl2	Ru1	Cl1	176.36(3)
Torsion NHC (°)			O1	Ru1	N4	73.56(8)
N2	C2	C3	N3	O1	Ru1	Cl2	86.87(6)
16.6 (3)				O1	Ru1	Cl1	89.99(6)
V$_{bur}$[a]			N4	Ru1	Cl2	90.38(6)
29.73%			N4	Ru1	Cl1	89.96(6)

[a] (sambVca web application https://www.molnac.unisa.it/OMtools/sambvca.php)[95]

The crystal structure reveals an almost perfectly shaped square-pyramidal octahedron, with ruthenium in the center. The chloride ligands are *trans* configurated and positioned on a fairly straight line (Cl2-Ru1-Cl1 = 176.4°), equal to the NHC ligand and the chelating ester (C1-Ru1-O1 = 175.4°). The pyridine is coordinated diametrically opposite to the benzylidene carbene, yet slightly distorted (C23-Ru1-N4 = 159.2°). Also, on this axis the strongest ligand opposes a very labile ligand, which is clearly demonstrated by a bond lengths' difference of 0.5 Å (Ru1-C23 = 1.85 Å, Ru12-N4 = 2.37 Å). It can be assumed, that the pyridine is only coordinated to the ruthenium centre due to π-π-interaction with the mesityl group positioned only 360.5 picometer above. Obviously, the coordinated pyridine also influences the buried volume V$_{Bur}$ of

the complex, that with 29.7% is considerably lower than in complexes **5a** and **6** (32.8 and 33.6 % respectively). Distortion of the NHC ligand of **8b** (16.6°) lies in between those of **5a** and **6** (*cf*. Table 11).

3.3.3 Reactivity in Various Metathesis Reactions

With the four different, yet strongly related complexes in hand (complexes **5a: OMe-SIMes**, **6: OMe-SIPr**, **7: NO₂-SIPr**, and **8a: NO₂-SIMes**), comparative activity studies in various olefin metathesis reactions have been accomplished.

3.3.3.1 ROM Polymerization

In order to disclose the activity of the complexes in metathesis polymerization, they were employed in standard benchmark reactions for ROMP with **EsterMon**. The reactions were carried out in dichloromethane at 40°C and secondly in toluene at 80°C. As reference initiators both 3rd generation starting complexes **M31** and **M32** as well as 2nd generation complex **M2** were included in the study, each at a respective reasonable temperature (Table 14). A monomer to initiator ratio of 300, and a concentration of 0.1 M with respect to the monomer was maintained in all cases. The experiments were performed in a Schlenk flask in degassed solvents. The reaction progress was monitored by thin layer chromatography (TLC). After reaction completion, excess ethylvinylether was added to quench the reaction before the polymer was precipitated in methanol and dried in vacuum. Scheme 15Scheme 15 displays the general reaction conditions.
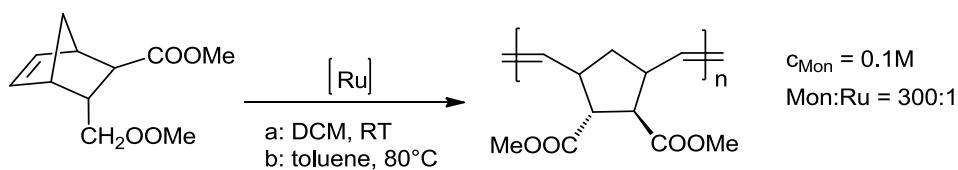
Scheme 15: Benchmark reactions for ROMP

Table 14 summarizes the number molecular weight (M_n), corresponding polydispersity indices (PDIs) obtained by GPC analysis and reaction times for full conversion for polymers synthesized using the abovementioned initiators.

Table 14: GPC results of benchmark polymerizations (full conversion)

initiator	DCM				Toluene, 80 °C		
	M_n (g/mol)	PDI	time	T (°C)	M_n (g/mol)	PDI	time
1: M31	45000	1.07	10 min	RT	n.d.	n.d.	n.d.[a]
2: M32	48800	1.2	2 h	RT	n.d.	n.d.	n.d.[a]
M2	292000	2.3	4 h	RT	72400	2.7	1h
5a: OMe-SIMes	442700	2.2	5 h	40°C	114300	2.4	10 min
6: OMe-SIPr	264200	1.7	5 h	40°C	214400	1.5	10 min
7: NO$_2$-SIPr	142900	1.4	2.5 h	40°C	145400	1.4	10 min
8a: NO$_2$-SIMes	110700	1.5	1 h	40°C	143200	1.4	10 min

Reaction conditions: c_{Mon} =0.1 mol/L, monomer:initiator = 300:1, quenching with ethyl vinyl ether. [a] **M31** and **M32** were not tested in the high temperature experiment as they are highly active already at room temperature.
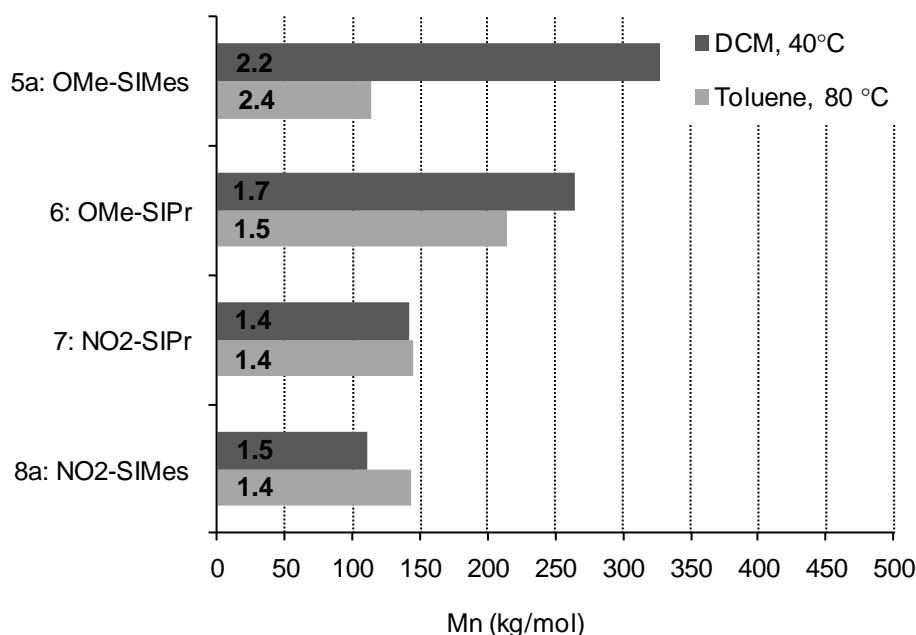
Figure 51: Number molecular weights and PDI values of polymers obtained with the new complexes

The results obtained by GPC analysis allow conclusions regarding initiation and propagation behavior of the tested complexes. Data of the reference complexes have been published before[96] and were described in detail in the previous chapter. As anticipated, the activity of the new complexes lies far beneath the activity of their parent complexes **M31** and **M32**. The nitro complexes **7** (SIPr) and **8a** (SIMes) exhibit rather high activity already at 40°C and completed the test polymerization in 2.5h and

---

[96] Urbina-Blanco, C. A.; Leitgeb, A.; Slugovc, C.; Bantreil, X.; Clavier, H.; Slawin, A. M. Z.; Nolan, S. P. *Chem. Eur. J.* **2011**, *17*, 5045-5053.

1h respectively. Yet, the average molecular weight is more than doubled with respect to **M31** (*cf*. Table 14), meaning that their initiation rate is much lower. The "methoxy-complexes" **5a** (SIMes) and **7** (SIPr) yield polymers with clearly higher molecular weights and PDI values and also take longer for completion, namely 5 hours. This obvious decrease in activity impressively demonstrates the strengthening influence on the chelate by the electron donating methoxy substituent. At 80°C, all four chelating-carbene-complexes complete polymerization within 10 minutes. Only **5a**, the methoxy SIMes complex produces a broader weight distribution, which might be best explained by progressing decomposition of the active species during polymerization.

3.3.3.2 Ring Closing Metathesis

For ring closing metathesis (RCM), a challenging substrate (4-methyl-N,N-bis(2-methylallyl)benzenesulfonamide) was chosen that yields a tetra substituted cyclic olefin. For easy substrates it is not reasonable to use the herein described catalysts, as many other already known catalysts are superior in activity. Nevertheless, the increased stability in solution at high temperature due to the strong chelating carbene ligand (strong compared to e.g. the Grubbs Hoveyda catalyst **Hov**), in combination with low initiation rates will prolong the presence of an active species in the reaction and hence conversion to the ring-closed target molecule can be increased.
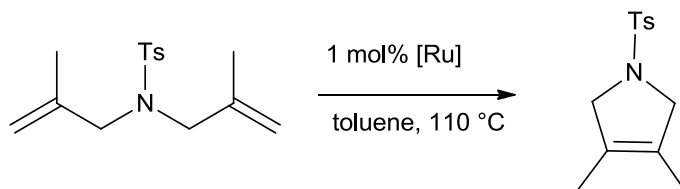
Scheme 16: RCM reaction with challenging substrate [substrate] = 0.1 M

The RCM reaction was carried out in degassed puresolv toluene under nitrogen conditions in small glass vials with sealed screw caps, heated in an alumina mold. In order to minimize weighing mistakes, stock solutions of the complexes were prepared. The solutions (toluene) had to be heated to 40°C to provide full solubility of the complexes. Reproducibility turned out to be a main issue for both complexes, so that 10 experiments under the same conditions were performed each. Conversion was determined by NMR spectroscopy after 1 hour and 4 hours, and in case of increased conversion after that time, also after 24 hours. Therefore, a small amount (approximately 15 µL) of the reaction mixture was directly put into an NMR tube

without any workup or purification, diluted in $CDCl_3$ and measured. All reactions were stopped after 24 hours. The final conversions are summarized in Table 15 and shown in Figure 52.

Table 15: conversions of RCM experiments with complexes 5a and 6

experiment Nr.	5a: OMe-SIMes conv (%)	6: OMe-SIPr conv. (%)
1	65	66
2	59	66
3	65	66
4	93	82
5	50	87
6	50	88
7	58	65
8	58	73
9	89	67
10	60	78
mean	64,7	73,8
standard deviation	14,8	9,2
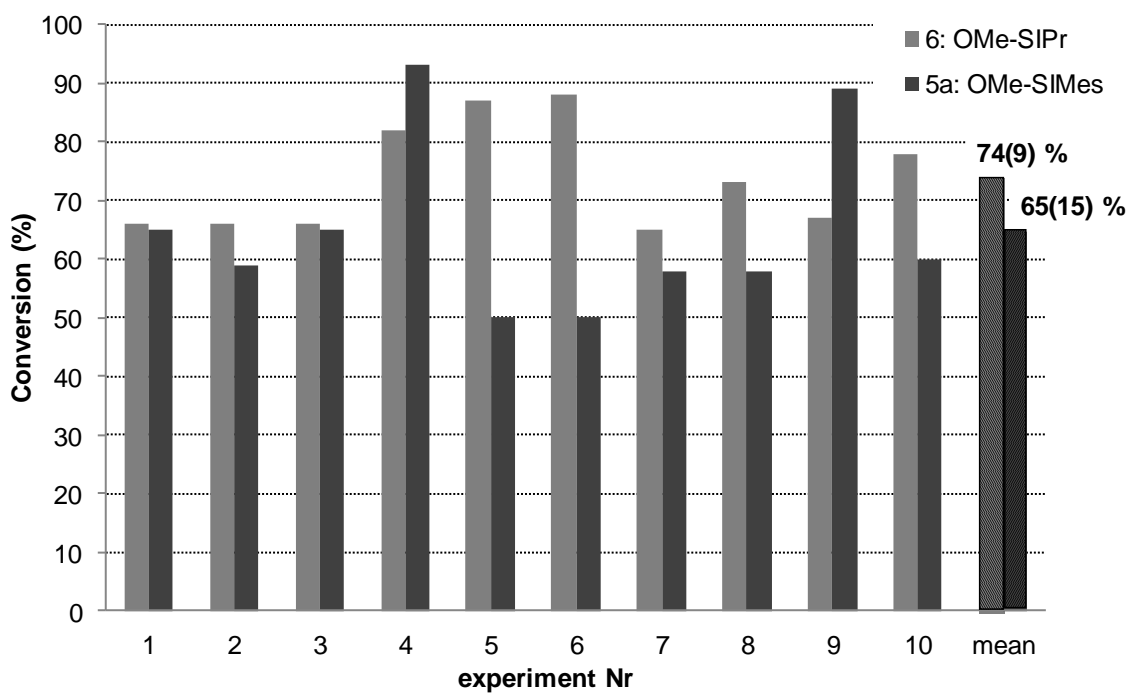
Figure 52: Conversion of 4-methyl-N,N-bis(2-methylallyl)benzenesulfonamide) to 3,4-dimethyl-1-tosyl-2,5-dihydro-1H-pyrrole by RCM, performed with 5a: OMe-SIMes and 6: OMe-SIPr

Comparing the average results, complex **6** featuring the SIPr NHC ligand yielded roughly 10% more product compared to its SIMes counterpart **5a** (Figure 52). This result is supported by the observation of longer stability of the complex in toluene at reflux temperature: reactions with complex **6** maintained the bright green color stemming from the complex (before initiation) for more than 4h, whereas reaction solutions with **5a** had all turned brownish after 30 min.

3.3.3.3 Cross Metathesis

Complexes **5a** and **6** have also been tested in cross metathesis (CM) within our group by M. Abbas. As a reference catalyst, **Hov** was employed, which was until now the best commercially available catalyst for that purpose. SIPr-bearing complex **6** yielded impressive results at minimal loadings, proving once more that initiator design in olefin metathesis for specific reactions is worth the effort and has not yet reached its climax.[97]

---

[97] Abbas, M. Slugovc C. *unpublished*

3.4 Unequal Siblings: Adverse Characteristics of Naphtalene-Based Hoveyda-Type Second Generation Initiators in ROMP

The following study evaluates a family of π-extended Hoveyda-type complexes , namely **extHov1 – extHov4**, in ROMP and compares their performance to the commercially available initiators 2nd generation Hoveyda (**Hov**), the indenylidene bearing analogues of Grubbs' 2nd and 3rd generation catalysts, **M2** and **M31**, respectively. The modified Hoveyda complexes were synthesized by the group of Karol Grela from University of Warsaw, the collaboration partners in this study. The complexes all bear a so-called π-extended carbene ligand, where the aromatic π-system of the original "**Hov** benzylidene ligand" (2-isopropoxystyrene) has been extended to a naphthalene system in various positions (**extHov1**, **extHov2** and **extHov3**), or even a phenantrene system as in **extHov4** (*cf*. Figure 53). The four different monomers that have been employed in this study are **EsterMon**, **KetonMon**, **EtherMon** and dicyclopentadiene **DCPD**, which each exhibit a specific feature necessary for the respective test series. All of them are norbornene derivatives which are favorable due to their high ring strain, and have proved useful for the synthesis of specialty polymers.[98] The complexes' initiation characteristics in ROMP strongly vary within different monomers. Each monomer has a different affinity to binding to the ruthenium center and, depending on the ring strain and other coordinating functionalities, the propagation rate will also be influenced by the monomer.[99]

---

[98] (a) Handbook of Metathesis (Ed.: R. H. Grubbs), Wiley-VCH, Weinheim, 2003. (b) Bielawski, C. W.; Grubbs, R. H. *Prog. Polym. Sci.* **2007**, *32*, 1-29. (c) Slugovc, C. *Macromol. Rapid. Commun*. **2004**, *25*, 1283-1297. (d) Leitgeb, A.; Wappel, J.; Slugovc, C.; *Polymer* **2010**, *51*, 2927 – 2946.

[99] Slugovc, C.; Demel, S.; Riegler, S.; Hobisch. J.; Stelzer, F. *Macromol. Rapid. Commun.* **2004**, *25*, 475–480.
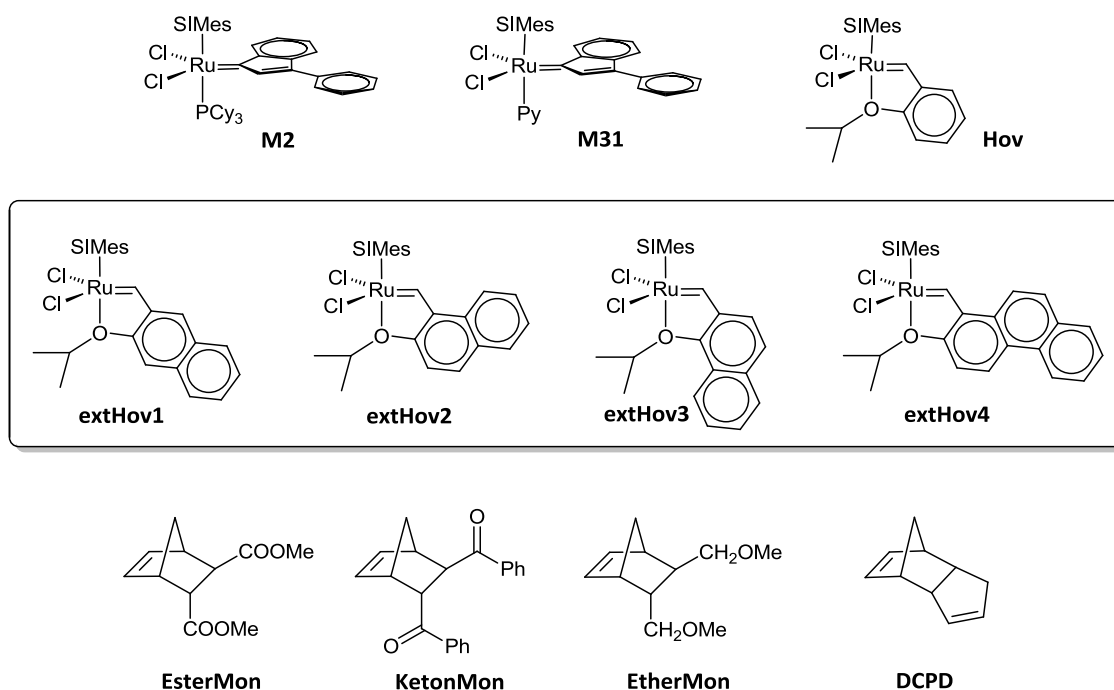
Figure 53: Initiators and monomers used in the study (SIMes = 1,3-bis(2,4,6-trimethylphenyl)-4,5-dihydro-imidazol-2-ylidene)

Ring opening metathesis polymerization was used as a sort of amplifier for studying the effects of bond-strengths-variations of the ruthenium-oxygen chelate, on the catalytic performance of the initiators. For that purpose ROMP is particularly suited because only the initiation step will be affected by the chelating carbene ligand's nature, while propagation is not (*cf.* Scheme 9). Hence, quantities like polymerization rate, molecular weight and molecular weight distribution are, in a first approximation, directly related to the chelating carbene moiety. However, exact determination of these numbers is hampered by potential secondary metathesis reactions such as back-biting, which could influence molecular weight and molecular weight distribution.
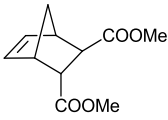
3.4.1 Benchmark Reactions

For a first estimation of their activity, the initiators were compared to well established olefin metathesis initiators **M31**, **M2** and **Hov** using (±)-*endo,exo*-bicyclo-[2.2.1]hept-5-ene-2,3-dicarboxylic acid dimethyl ester (**EsterMon**). This easily accessible monomer is used for standard benchmark reactions in ROMP because the formed polymer will not be degraded by the active initiator.[83,100] Thus determination of the polymer's number molecular weight (M_n) allows for an estimation of the initiation behavior of the

---

[100] (a) Demel, S.; Schoefberger, W.; Slugovc, C.; Stelzer, F. *J. Mol. Catal. A* **2003**, *200*, 11-19.
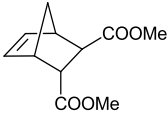
corresponding complex. The reactions were carried out in dichloromethane at room temperature using Schlenk technique. The ratio of monomer to initiator was 300, maintaining a concentration of 0.1 M with respect to the monomer. After completion (monitored by TLC) the polymerizations were quenched with excess ethyl vinylether before the polymers were precipitated in cold methanol, dried and analyzed by means of GPC.

Table 16: Standard benchmark: CH₂Cl₂; [Mon1] = 0,1M; ratio initiator:monomer = 1:300

initiator	time	conversion	M_n (g/mol)	PDI
M31	<<1 h	100 %	62000	<1.1
M2	6 h	100 %	292000	2.3
Hov	<1 h	100 %	89000	1.3
extHov1	2 h	100 %	102000	1.5
extHov 2	20 h	< 5%	n.d.	n.d.
extHov 3	20 h	none	n.d.	n.d.
extHov 4	20 h	none	n.d.	n.d.
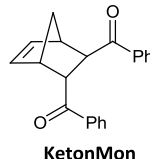
At room temperature, initiator **extHov1** turned out to be the only active initiator bearing a π-extended carbene ligand. The polymerization was completed after 2 hours, slightly slower than with **Hov**, yielding a polymer with a higher molecular weight and a broader weight distribution (*cf*. Table 16). After 20 hours initiator **extHov2** yielded only traces of polymer (according to ^{1}H-NMR), whereas **extHov3** and **extHov4** did not get active at all. Therefore, the latent initiators **extHov2 – extHov4** were tested at elevated temperatures, using dichloromethane and toluene at 40°C and 80 °C respectively. After 24h the polymerizations were stopped and the reached conversion was determined by ^{1}H- NMR (*cf*. Table 17).

Table 17: ROMP with latent initiators: [Mon1] = 0,1M; ratio initiator:monomer = 1:300

initiator	DCM, 40°C		Toluene, 80 °C	
	time	conversion	time	conversion
extHov2	24h	< 5%	24h	69 %
extHov3	24h	< 5%	24h	24 %
extHov4	24h	none	24h	none

Reactions at 40°C did not yield considerable amounts of polymer in any case. At 80°C, 69% conversion was observed with **extHov2**, the most active initiator in that series. **extHov3** was considerably slower and yielded 24% conversion. With **extHov4**, no measurable amount of polymer was formed even at 80 °C. These results can be rationalized by a drastically slower initiation of initiators **extHov2 – extHov4** compared to **extHov1** or **Hov**. The differences in activity between **extHov1** which is quite active at room temperature and its siblings **extHov2**, **extHov3** and **extHov4**, which all three exhibit a pronounced latency even at elevated temperatures, are remarkable. Therefore, different ways were used to further elucidate the activity of these two compound classes. **KetonMon** bicyclo-[2.2.1]hept-5-ene-2,3-diphenylketon was chosen as test monomer for the closer evaluation of **extHov1** (benchmark reaction *cf*. Table 18).

Table 18: Polymerization results CH$_2$Cl$_2$; [Mon2] = 0,1M; ratio initiator : monomer = 1:300

initiator	time	conversion	M$_n$ (g/mol)	PDI
M31	4h	100 %	55000	<1.1
M2	72h	100 %	373000	2.1
Hov	5h	100 %	52000	1.1
extHov1	5h	100 %	48800	1.1

3.4.2 Scope of extHov1 Regarding Controlled ROMP

KetonMon strongly coordinates towards the active ruthenium center of the initiator and consequently causes a very slow propagation rate relative to **EsterMon**.[99] Therefore, polymerization progress can be conveniently followed by NMR spectroscopy. The monomer was employed in a ratio of 50 with respect to the initiators, the concentration was kept constant at 0.1 mol/L in CDCl$_3$. Time/conversion plots of the polymerization of **KetonMon** are shown in Figure 54.
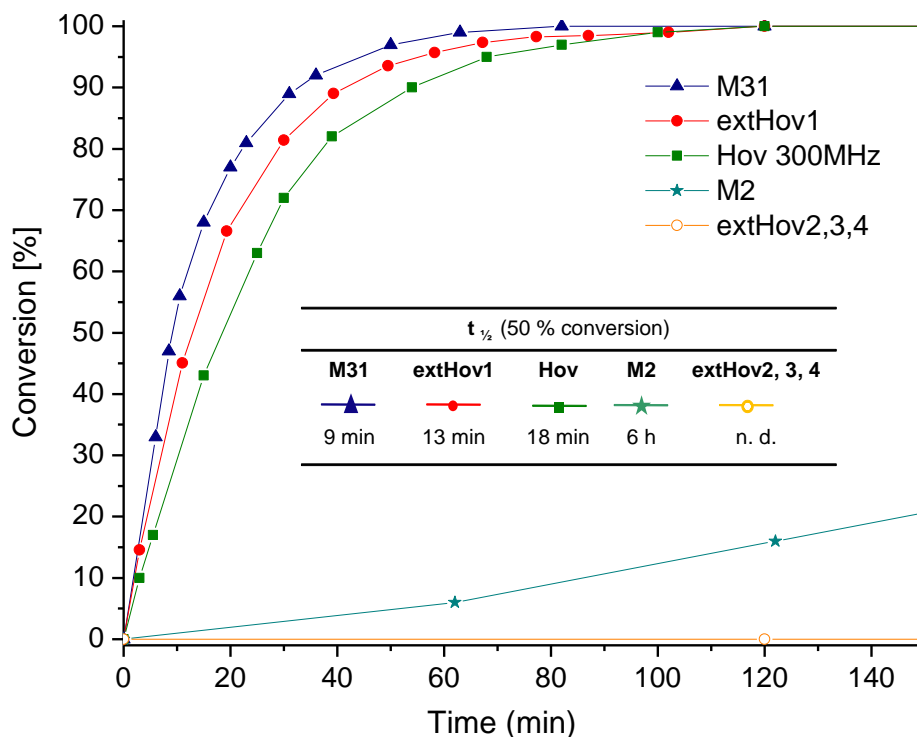
Figure 54: Conversion plot: rt; CDCl$_3$; [KetonMon] = 0.1 mol/L; ratio initiator:monomer = 1:50

As can be seen upon comparison of the data **extHov1** definitely belongs to the same category as **M31** and **Hov** and clearly outperforms **M2**. The half-life (time for 50% conversion) was determined to be 9 min, 13 min and 18 min for **M31**, **extHov1**, and **Hov**, respectively. In the same setup, initiators **extHov2**, **extHov3** and **extHov4** gave no conversion after 10h. Interestingly, **extHov1** is a more active initiator for the polymerization of **KetonMon** than **Hov**, which can only be explained by a faster initiation of **extHov1** in this case. Having in mind that the polymerization of **EsterMon** is slower with **extHov1** than with **Hov** it has to be emphasized, that the monomer's nature not only determines the propagation rate (k_p) but also the initiation rate (k_i) and consequently the ratio k_i/k_p. This fact is reflected in the ability of an initiator to provide controlled polymerization with a certain monomer. While **EsterMon** is not suited for being polymerized in a controlled manner by **extHov1** as molecular weights and PDI values are distinctly higher than with **M31**, **KetonMon** can be polymerized in a controlled fashion. This was proven by the preparation of a series of polymers using increasing ratios of **KetonMon** with respect to **extHov1**, ranging from 100 to 900 equivalents. The evaluation of the corresponding average number molecular weights (M_n) revealed a linear correlation with the employed monomer amount, and narrow weight distributions featuring PDis below 1.2 in all cases. For comparison, the same test series was accomplished with reference initiators **M31** and **Hov**. The results are summarized in Figure 55 and Table 19.
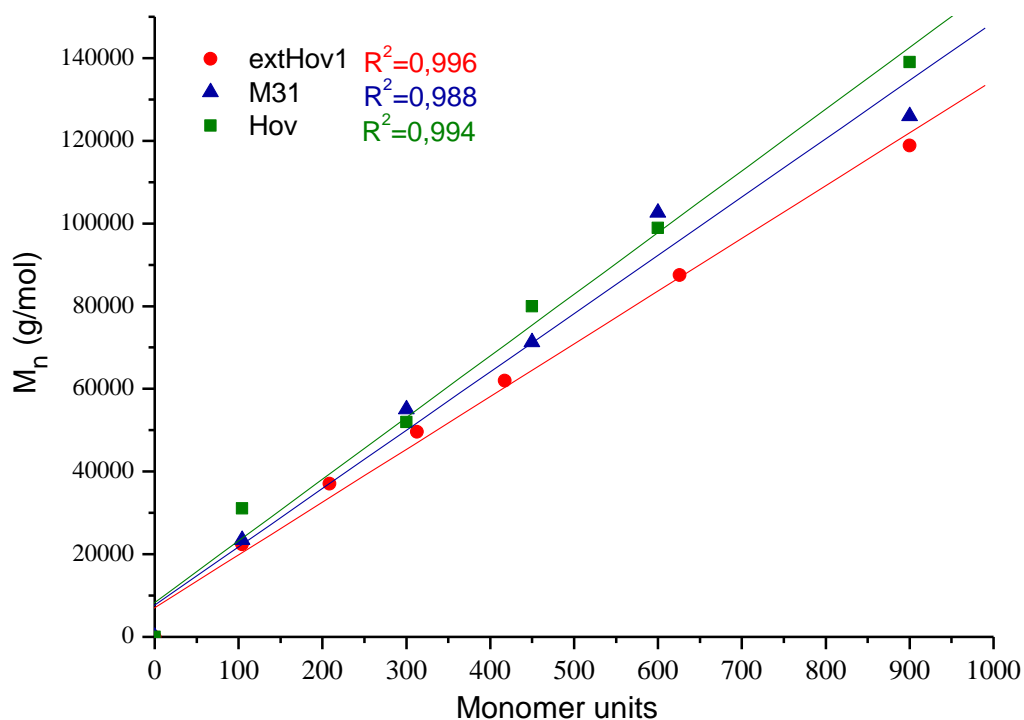
Figure 55: Controlled polymerization of KetonMon: rt; DCM, 0.1M

All three initiators under investigation are capable of polymerizing **KetonMon** in a perfectly controlled fashion as can be easily deduced from the R^2 values approximating 1.0. The slightly different slopes of the straight lines are attributed to weighing errors.

Table 19: GPC results of ROMP with [KetonMon] = 0.1M, rt

KetonMon	extHov1		Hov		M31	
Equivalents	M_n (g/mol)	PDI	M_n (g/mol)	PDI	M_n (g/mol)	PDI
104	22400	1.15				
150			31100	1.19	23400	1.06
209	37100	1.13				
300			52000	1.10	55000	1.06
313	49600	1.10				
417	62000	1.11				
450			80000	1.08	71300	1.11
600			99000	1.10	102600	1.16
626	87500	1.12				
900	118900	1.14	139100	1.14	125900	1.20

Complex **extHov1** was then tested for the synthesis of block-co-polymers. Either, fast polymerizing **EsterMon** was added first to be then followed by slowly polymerizing **KetonMon** after full conversion, or vice versa (cf. Figure 56). 150 equivalents of each monomer were used with respect to the initiator. After full consumption of the second monomer, the resulting polymer was isolated in the usual manner and subsequently characterized by GPC. In both cases, bimodal weight distributions were obtained, exhibiting PDI values between 1.3 and 1.4. Results clearly reveal **extHov1** less suited for living polymerization in comparison to **M31** that yields narrow, monomodal molecular weight distributions in any case.
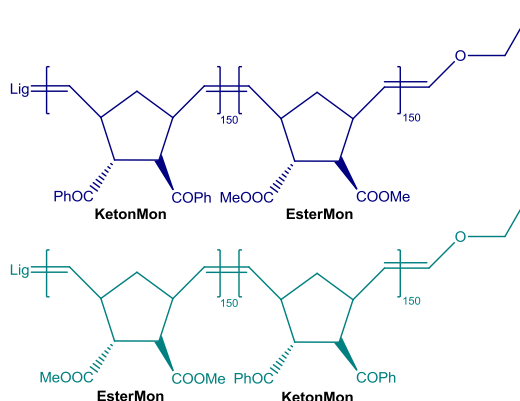
Figure 56: Block-co-polymers from EsterMon and KetonMon
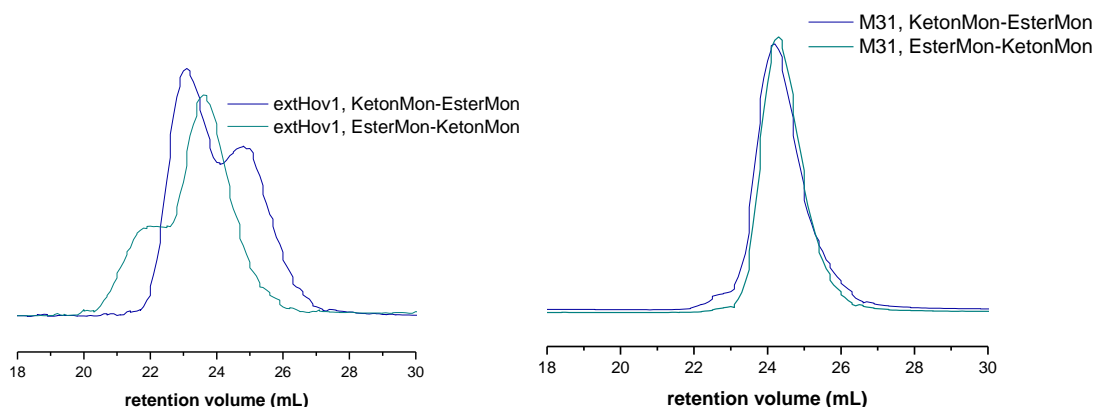
Figure 57: Structure and GPC elugrams of block-copolymers from initiators extHov1 (left) and M31 (right)

As clearly visible in Figure 57, **extHov1** cannot compete with the paramount scope of **M31** in controlled living polymerization of norbornene derivatives[82], but nevertheless its relatively high initiation rate is remarkable when compared to the other derivatives **extHov2**, -**3** and -**4**.

3.4.3 Scope of Latent Initiators extHov2, 3 and 4

Turning attention to the inactive initiators **extHov2**, -**3** and -**4**, their thermal activation was investigated by simultaneous thermal analysis (STA) using monomers bicyclo-[2.2.1]hept-5-ene-2,3-dimethoxymethylen (**EtherMon**) and dicyclopentadiene, (**DCPD**). **EtherMon** is liquid at room temperature, hence easy to handle in small amounts. **DCPD** was chosen as monomer because of its importance regarding large scale industrial processes.[101] As a reference, the pure monomers were submitted to the same thermal analysis, performed at a heating rate of 3°C/min and a constant helium gas flow of 50mL/min. In an open system (as present during the STA measurement), norbornene derivatives decompose at elevated temperatures by a retro Diels Alder reaction, yielding volatile cyclopentadiene,[102] which is removed from the equilibrium by the gas streaming over the sample in an STA machine. The decomposition can be observed by an endothermic peak in the DSC curve going along with a continuous mass loss.
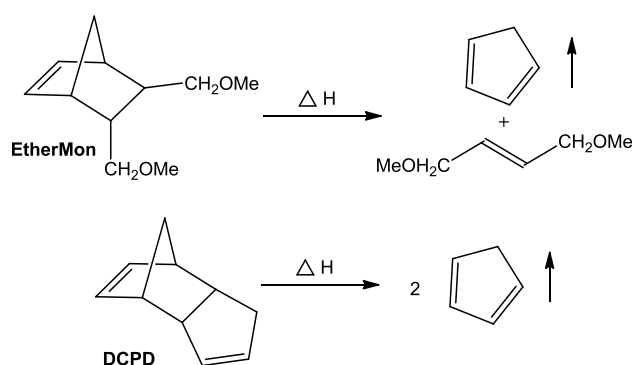
Scheme 17: retro Diels-Alder reaction of dicyclopentadiene (DCPD) to cyclopentadiene (CPD)

---

[101] www.telene.com (2011-10-24)

[102] B. Rickborn, The Retro–Diels–Alder Reaction Part I. C──C Dienophiles in: Organic Reactions *Vol. 52* (**2004**), DOI: 10.1002/0471264180.or052.01
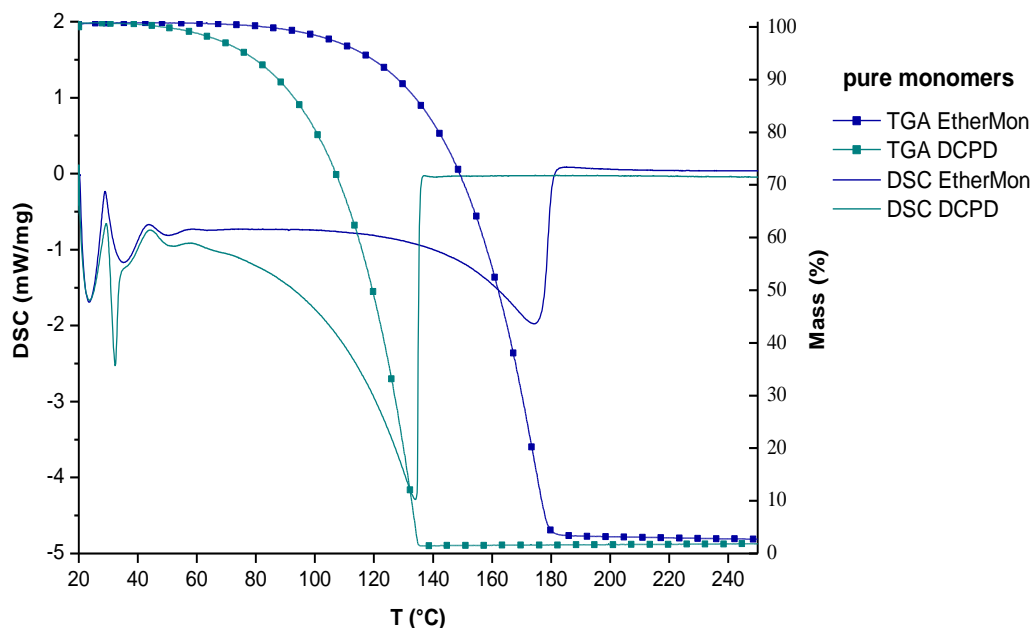
Figure 58: Decomposition of monomers due to retro Diels–Alder reaction monitored with STA

The decomposition temperatures for **EtherMon** and **DCPD** were determined to be 108 °C and 69°C respectively, these are the temperatures where 3% mass loss was observed (*cf.* Figure 58). This information is crucial in order to judge the performance of the initiators. Ideally, polymerization starts well above the processing temperature, but before monomer decomposition occurs. Moreover, it has to be fast enough to not loose monomer during the reaction due to retro Diels-Alder reaction. Although this is not a key issue in industrial curing of **DCPD** in reaction injection molding (RIM) which is performed in closed (pressurized) molds, it is nevertheless crucial for polymerizations in open molds and has to be taken into consideration when testing initiators in the laboratory.

M2 was found suitable as a reference initiator for "App$_{lat}$" (*cf.* Abstract), the thermally triggered ROM polymerization of **DCPD**. All crucial requirements, namely solubility in the monomer, polymerization below decomposition temperature (due to retro-Diels-Alder reaction) as well as thermal switchability (clearly enhanced activity at elevated temperature) are given. The following figure shows the corresponding STA graphs at a heating rate of 3 °C/min. The TGA graph shows mass loss in %, positive values in the DSC stem from exothermic reaction (e.g. polymerization). A loading of 20 ppm of **M2** was found appropriate for the polymerization of **DCPD** under abovementioned conditions. Yet, for the complexes under investigation **extHov2**, **extHov3** and **extHov4** which exhibit a considerably more pronounced latency, a higher loading of 40 ppm (corresponding to a monomer to initiator ratio of 25000/1) was selected in order to

achieve polymerization. Higher loadings were not feasible due to solubility issues.[103] For all STA runs with **DCPD** it has to be taken into account in the mass balance, that the solvent used for the initiator had not been removed before the run. The maximal mass loss due to solvent amounts to about 8 %. Mass losses higher than 8% have to be assigned to monomer decomposition. For reference initiator **M2** a triggering temperature of 60±2°C can be stated for the ROMP of **DCPD** under the described conditions. Nevertheless, a mass loss of 17 % indicates considerable monomer decomposition (*cf*. Figure 59).
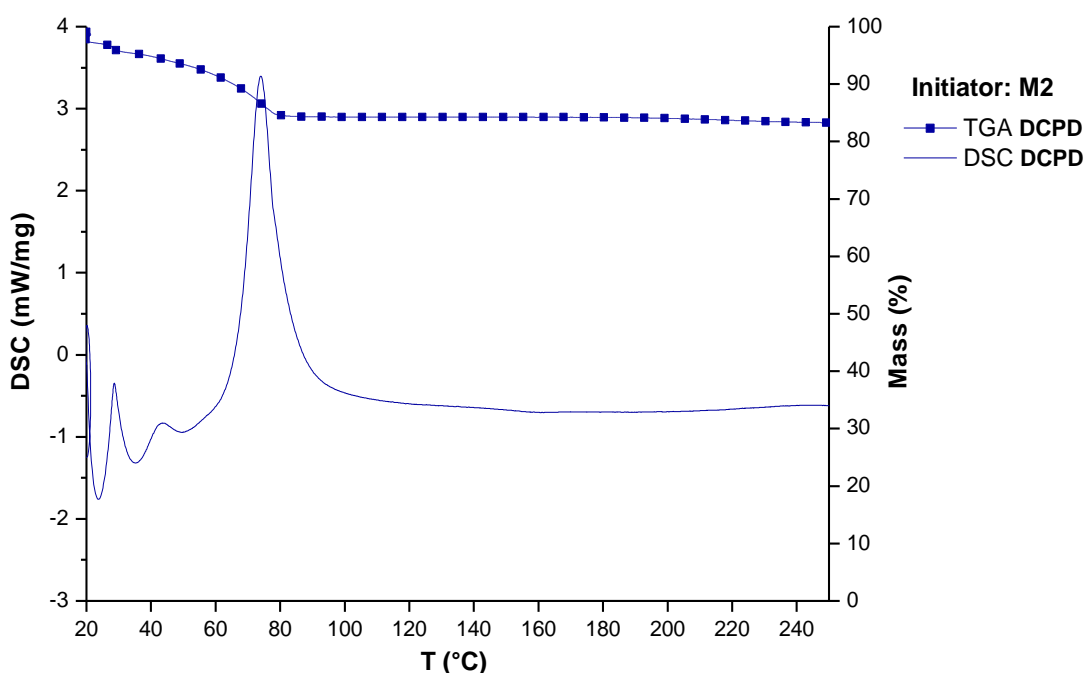
Figure 59: STA of ROMP of DCPD with M2 (20 ppm; heating rate = 3°C/min; Helium gas stream of 50 mL/min)

The polymerization of **EtherMon** was carried out using 2000 ppm of initiator (corresponds to a monomer to initiator ratio of 500/1) and was monitored via STA with each of the latent initiators under investigation. Initiator-monomer mixtures containing 100 mg monomer were prepared and shock-frozen in liquid nitrogen in order to avoid any premature activation. 15-18 mg of this mixture were inserted into the crucible and a heating run employing a rate of 3 °C/min was started at 20°C, in analogy to the previous experiments. Figure 62 shows the results of the STA characterizations for catalysts **extHov2**, -**3** and -**4**. With **extHov2** and **EtherMon**, polymerization starts around 48±2°C, giving the peak of the exotherm at 73±1°C and

---

[103] Jeong, W.; Kessler, M. R. *Chem. Mater*. **2008**, *20*, 7060-7068.

the end of the reaction at about 115°C. Polymerization is accompanied by a minimal mass loss of less than 5%, which can be assigned above all to residual solvent present in the sample. Complexes **extHov3** and **extHov4** are clearly more latent. Polymerization of **EtherMon** starts in both cases at 58±2°C. The maximal heat evolution was found at 90±1°C in case of **extHov3** and 84±1°C in case of **extHov4** meaning that the latter is slightly more reactive. This trend is confirmed by the respective mass losses of the polymerizations, which is about 12 % in case of **extHov3** and <10 % in case of **extHov4** as the initiator. A somewhat different trend is retrieved from the experiments with **DCPD**. Again, initiator **extHov2** is most active. The exothermal signal for the polymerization slightly overlays with the (endothermic) decomposition of **DCPD**, so that an exact starting temperature can not be issued. The maximum of the exothermic peak was found at 90±1°C and a mass loss of about 17 % was determined. With initiator **extHov3** and **extHov4** no polymerization exotherms were observed. Nevertheless polymer was formed to a small extent in both cases, namely 32 % and 13 % respectively. Accordingly, **extHov4** is less active than **extHov3** for the polymerization of **DCPD** under these conditions, and the ranking of initiators is different than for the polymerization of **EtherMon**. A possible explanation for this phenomenon is a reduced solubility of **extHov4** in **DCPD** when compared to **EtherMon**, since the concentration of available, i.e. dissolved, initiator in the reaction mixture determines the polymerization profile.[103]
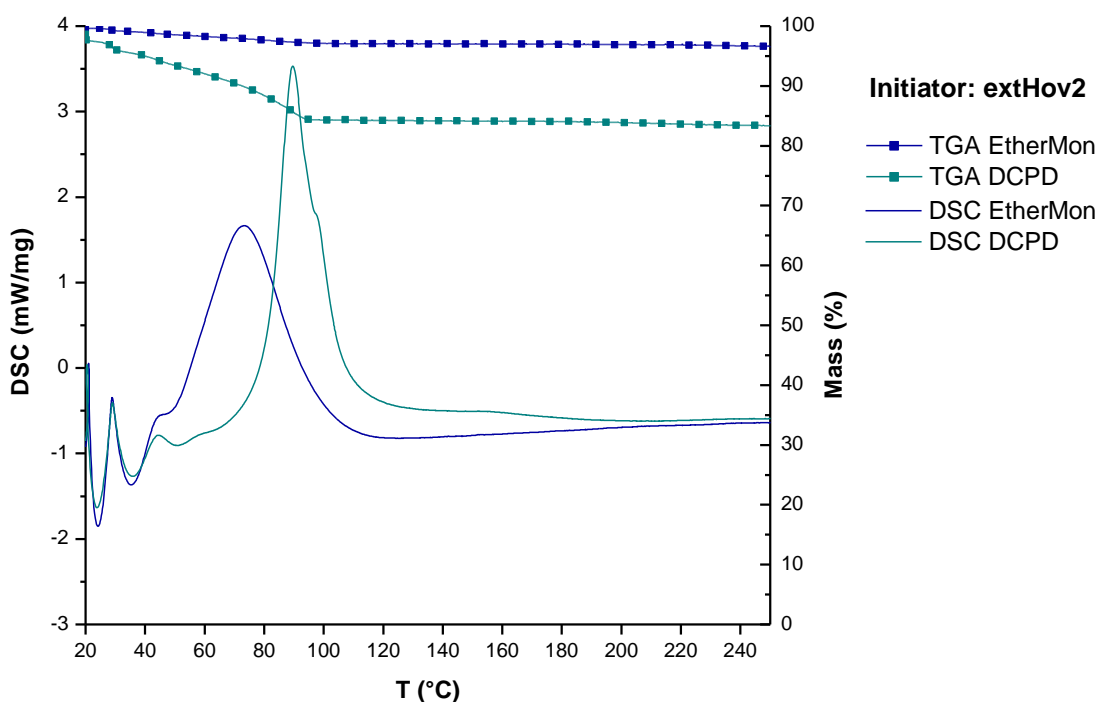
Figure 60: STA of ROMP of EtherMon (blue) and DCPD (turquoise) with initiator extHov2; Heating rate: 3 °C/min; Helium gas stream; 50 mL/min
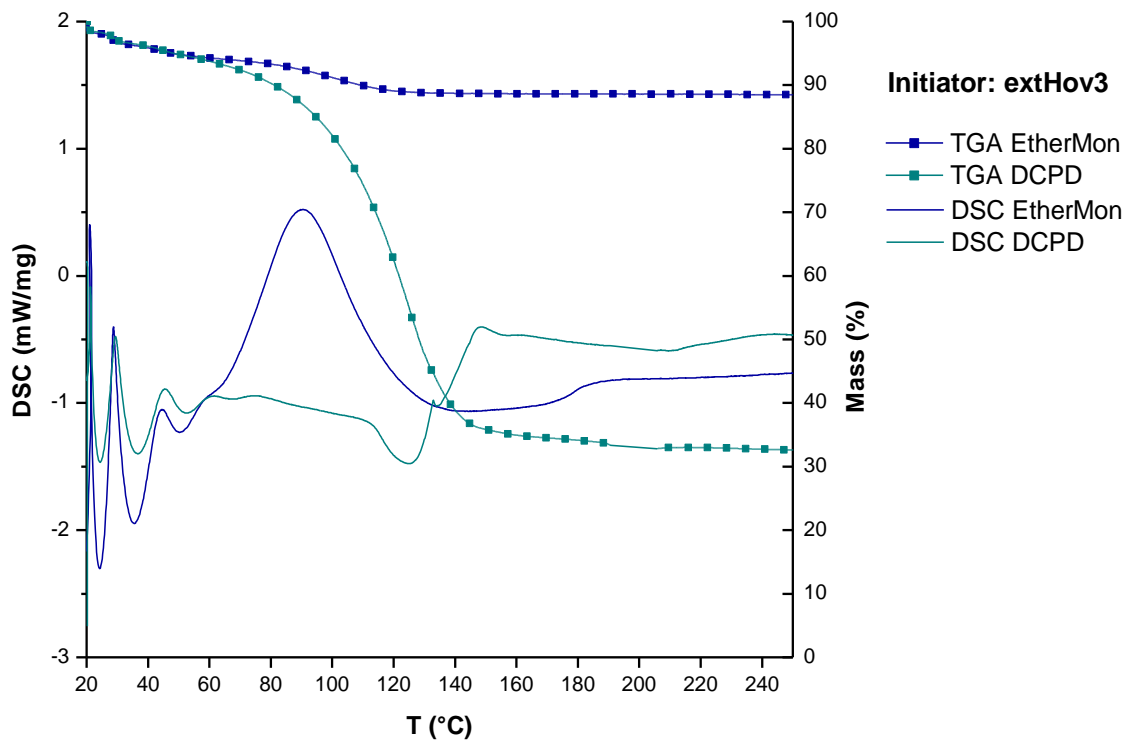
Figure 61: STA of ROMP of EtherMon (blue) and DCPD (turquoise) with initiator extHov3; Heating rate: 3 °C/min; Helium gas stream; 50 mL/min
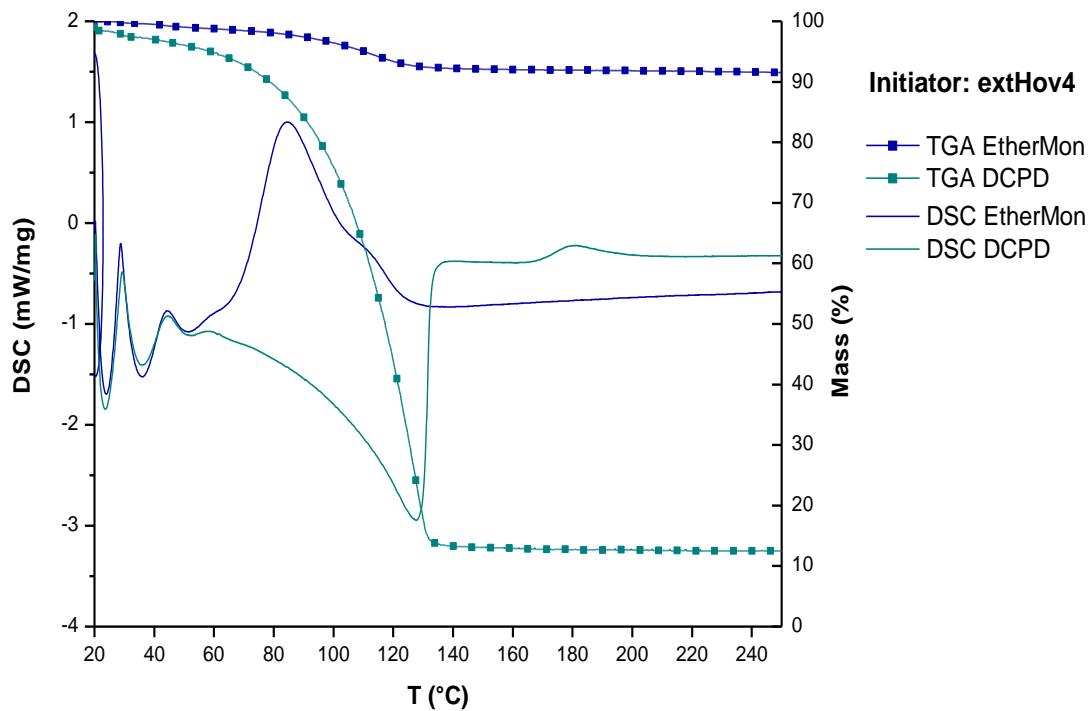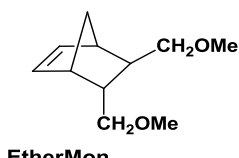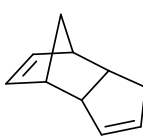
Figure 62: STA of ROMP of EtherMon (blue) and DCPD (turquoise) with initiator extHov4; Heating rate: 3 °C/min; Helium gas stream; 50 mL/min

Table 20: Data from STA of EtherMon curing with extHov2, 3 and 4 (initiator : monomer = 1 : 500)

EtherMon

	Onset (°C)	Peak max (°C)	mass loss (%)
extHov2	47.7	73.5	3.4
extHov3	54.9	90.7	88.5
extHov4	62.3	84.2	91.6

Table 21: Data from STA of DCPD curing with extHov2, 3 and 4 (each 40 ppm), M2 (20 ppm) as reference

DCPD

	Onset (°C)	Peak max (°C)	gross mass loss[a] (%)	net mass loss[b] (%)
M2	67	74	16.7	9.3
extHov2	54.9	89.7	16.6	9.2
extHov3	136.5	147.7	67.3	59.9
extHov4	n.d.	n.d.	88.5	81.1

[a]: total mass loss; [b]: 7.4 % subtracted for solvent (60 µL DCM in 1 mL DCPD)

3.5 Evaluation of the Scope of Latent Initiator M22

A strongly chelating carbene ligand is one way to achieve latency in olefin metathesis. The chelation prevents the ligand from recoordination during the metathesis reaction, and stays attached at one end of the polymer chain, which can be advantageous for some applications (e.g. end group functionalization).[104] Nevertheless, it is also possible to tune latency respectively activity of metathesis catalysts with the isolated leaving ligands, as impressively shown by the introduction of pyridine in 3rd generation complexes. Following the adverse direction, hence increasing latency, the group of Catherine Cazin has developed an **M2** analogue, featuring a phosphite ligand instead of the phosphine.[105] That complex has meanwhile been commercialized as **M22**. Interestingly, the complex exhibits a *cis* dichloro configuration, which is formed as the thermodynamical product after isomerization.

M2: SIMes-PCy$_3$ **M22: SIMes-P(O^{i}Pr)$_3$**
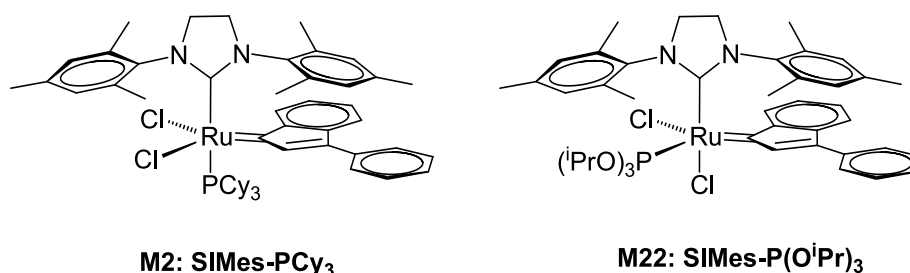
Figure 63: Reference M2 (left) and *cis* dichloro configurated phosphite analogue M22 (right)

3.5.1 Benchmark ROMP

M22 was tested at three different reaction conditions with **EsterMon**. The benchmark reaction employing a monomer to initiator ratio of 300 was carried out in toluene at 80°C in order to get full conversion within reasonable time (*cf*. Table 22). Conditions were identical to those in Scheme 15b. **M22** showed similar results to reference initiator **M2**, reaction time until full conversion was 1h in both cases, and the average molecular weight is slightly lower with **M22** (53000 g/mol compared to 72000 g/mol), indication a higher initiation rate. The PDI value is 2.3 which is typical for 2nd generation complexes.

---

[104] Lexer C.; Saf, R.; Slugovc, C. *J. Polym. Sci. Part A: Polym. Chem*. **2009**, *47*, 299-305.

[105] Bantreil, X.; Schmid, TE.; Randall, R. A. M.; Slawin, A. M. Z.; Cazin, C. S. J. *Chem. Commun.* **2010**, *46*, 7115-7117.

Table 22: GPC results of benchmark reaction with M22

	M_n (g/mol)	PDI	time (h)
M2	72420	2.7	1
M22	52930	2.3	1

toluene 80°C; c(EsterMon) = 0.1 M; initiator:EsterMon = 1:300

A second test reaction was carried out in dichloromethane at 40°C. Conversion was controlled via NMR spectroscopy. Therefore, 200µL were taken from the reaction mixture every few hours, quenched with ethyl vinyl ether (20µL) and dried in vacuum. NMR spectra were recorded in CDCl$_3$ and the integrated olefinic peaks from **EsterMon** (6.28 and 6.07 ppm) were compared to those of the formed polymer (5.49-5.19 ppm). A conversion plot is depicted in Figure 64.
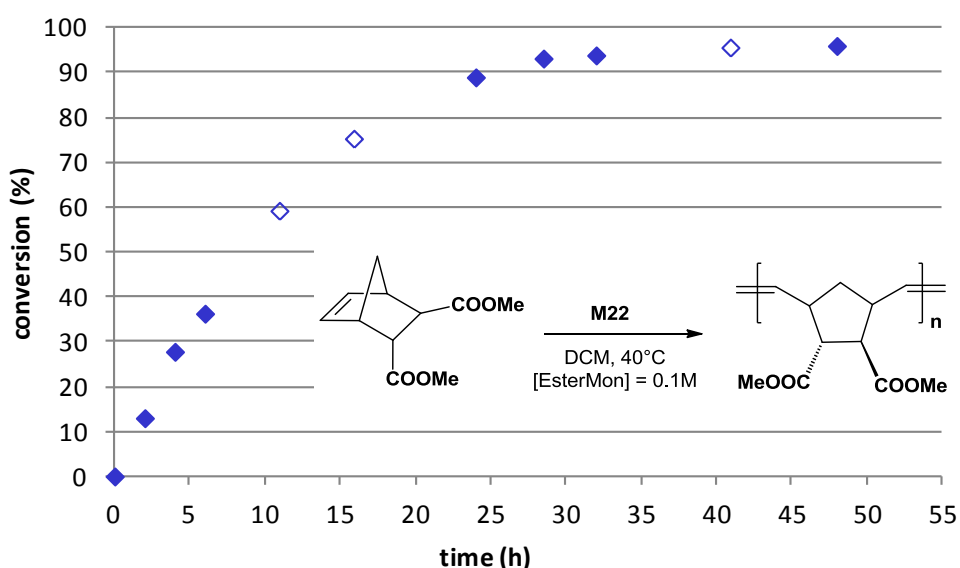
Figure 64: conversion plot of ROMP of EsterMon with M22 (40°C, DCM); empty symbols were added to the measured data (full symbols) for better readability

The conversion plot reveals a half-life (time for 50% conversion) of 10 h and ongoing conversion until 96% are reached after 50h. The experiment was stopped at that time. However, the longevity of **M22** at 40°C constitutes interesting feature that is worth closer investigations. On the one hand, long time stability in solution is beneficial per se, but on the other hand, one of the target applications for latent initiators is the storage of a monomer-initiator mixture at room temperature without any reaction going on. Therefore, a long-time activity study at room temperature was carried out.

Toluene was chosen as solvent in order to prevent evaporation with time. Again, initiator **M22** was employed in a ratio of 1:300 with respect to **EsterMon**. Conversion was followed by TLC and NMR spectroscopy.
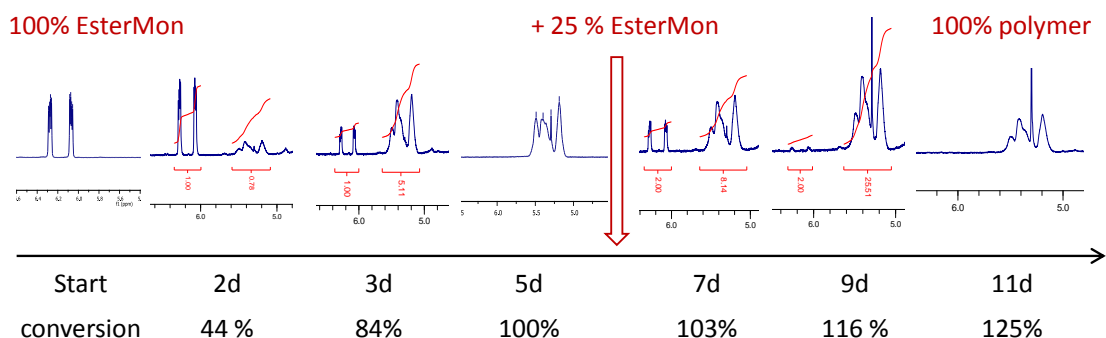
Figure 65: ROMP of EsterMon with M22 at room temperature: Olefin signals at 6.28 and 6.07 ppm for EsterMon and 5.49-5.19 ppm for the polymer

After 5 days, the reaction was completed. An additional amount of monomer (25% of original amount) was added with the corresponding amount of toluene to maintain a monomer concentration of 0.1 M. Again, progress was frequently controlled. After another 6 days, the additional monomer had been consumed to full extent, as clearly visible in Figure 65. Even if the progress had slowed down considerably, this experiment reveals an incredible stability of complex **M22** in solution and in presence of monomer. The fact that polymerization occurs already at room temperature nevertheless excludes the possibility of storing monomer with the initiator and only start polymerization upon an external trigger like heat. Nevertheless it has to be taken into account that the experiments conducted within this series were all performed with **EsterMon** and relatively high initiator ratios corresponding to 3333 ppm. It is well possible, that in different formulations initiator **M22** performs in a switchable manner.

Table 23: conversion times for benchmark reactions at different temperatures with M22 and EsterMon

T (°C)	$t_{1/2}$ 50% conversion	time full conversion
RT (toluene)	50 h[a]	120 h
40°C (DCM)	10 h[a]	50 h
80°C (toluene)	15 min[b]	1 h

[a]: interpolated from data in Figure 64 and Figure 65, [b] estimated from comparison with Figure 30

Table 23 summarized the benchmark reactions for **M22** with **EsterMon**. Activation upon heat is obvious. Therefore, **M22** has also been included in studies concerning the curing of **DCPD** in a thermally triggered fashion. In that case, initiators are employed in far lower loadings, which will decrease activity at room temperature.

3.5.2 Polymerization Details for Initiator M22

Benchmark reactions (Table 22 and Figure 64) were performed as already described (see also experimental). For the room temperature activity study (Figure 65) 1.2 mg of initiator **M22** ($1.4*10^{-3}$ mmol) and 86 mg of **EsterMon** (0.41 mmol, 300 eq.) were dissolved in 4.1 mL of toluene (degassed) to reach a total monomer concentration of 0.1M. Polymerization progress was monitored by TLC and NMR-spectra were recorded daily to determine conversion. After 5 days, the reaction was completed and additional 25 % **EsterMon** (20 mg dissolved in 1 mL toluene) was added. Again, polymerization progress was controlled every day. After another 6 days, the additional monomer was completely consumed. GPC analysis gave the following results: M_n = 362700 g/mol, PDI = 2.62.

4 M2 versus M22 in the Curing of DCPD
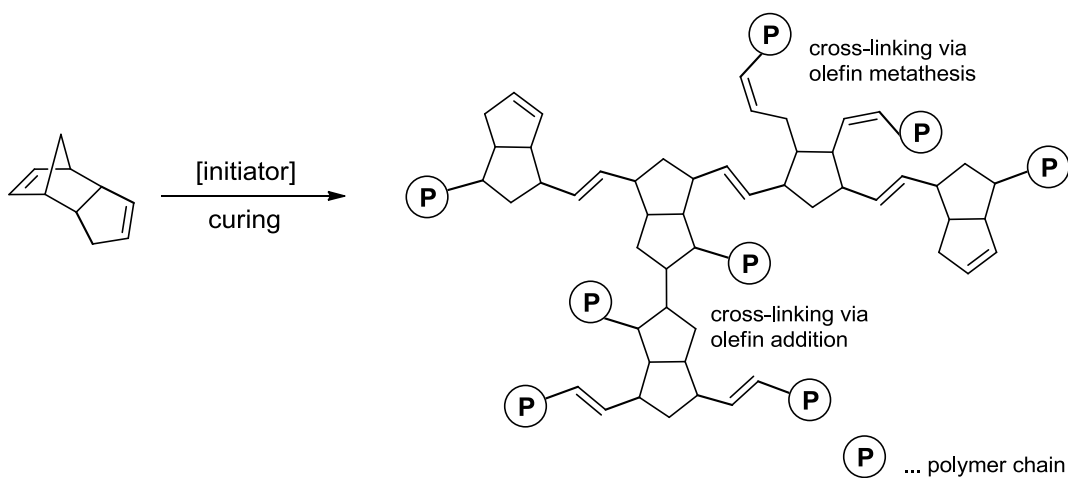
Scheme 18: ROMP of dicyclopentadiene (DCPD). Cross-linking occurs via ROMP or olefin addition
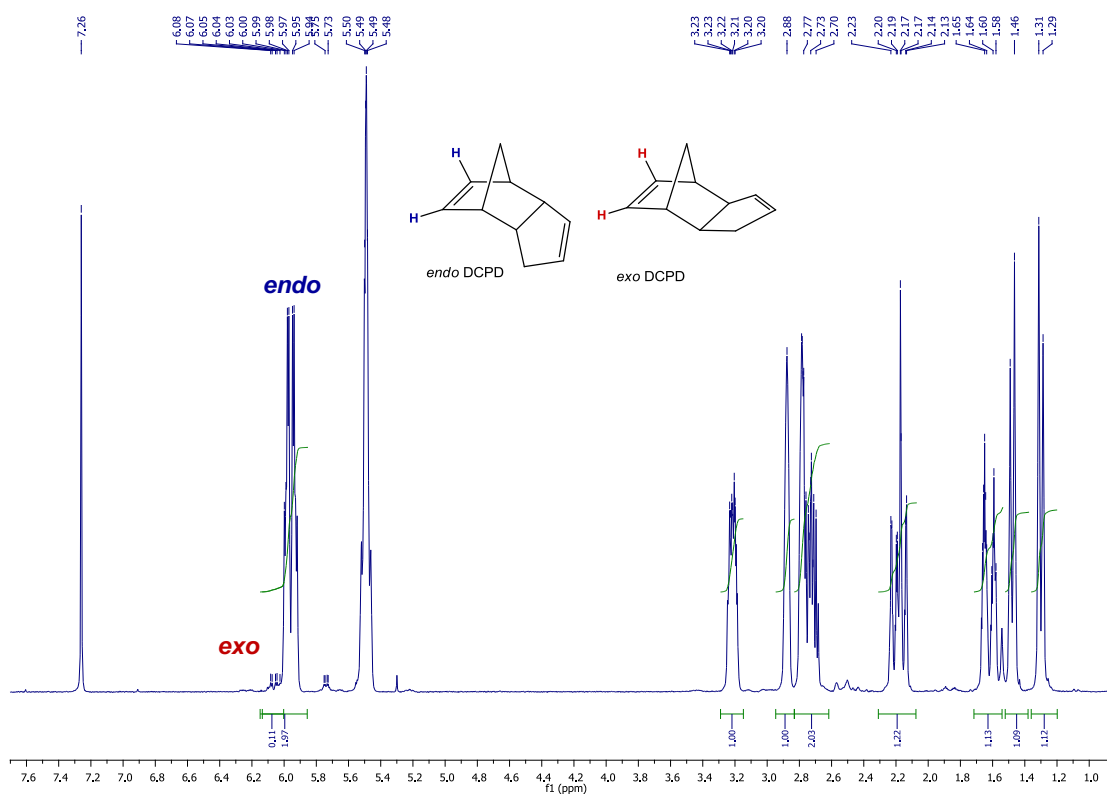
Figure 66: ^{1}H-NMR spectrum of employed DCPD (Sigma Aldrich)

4.1 Preliminary Curing Tests

In order to evaluate the suitability of initiators for the curing of DCPD at low loadings (ranging from 1:30000 down to 1:300000), a preliminary test series was realized for all initiators under investigation. Therefore, a 50 mL polypropylene eppendorf tube was charged with 5 mL of molten DCPD (35°C). The initiator was added dissolved in 300 µL of dichloromethane. Corresponding stock solutions were therefore prepared and diluted upon request. The polymerization mixture was homogenized by shaking and then left for observation of the mixture's consistency at either room temperature, or in case of latent initiators also 60°C (oven). For graphical illustration, the curing progress was scaled from 0 (no reaction, consistency of monomer) to 100 (fully cured, hard and solid polymer block), and classified according to Table 24. **M2** served as reference initiator.

Table 24: Evaluation of curing progress

Category	Consistency of curing mixture
0	**no apparent change in viscosity**
5	slightly viscous
10	viscous
15	more viscous
20	**highly viscous**
25	stacked, highly viscous, sticky
30	gelation, soft & sticky
35	solid, gel-like, slightly sticky
40	solid, gel-like, not sticky
50	solid, very elastic
60	solid, rather elastic
70	**solid, elastic**
80	solid, slightly elastic
90	solid, hardly elastic
100	**solid, fully cured**
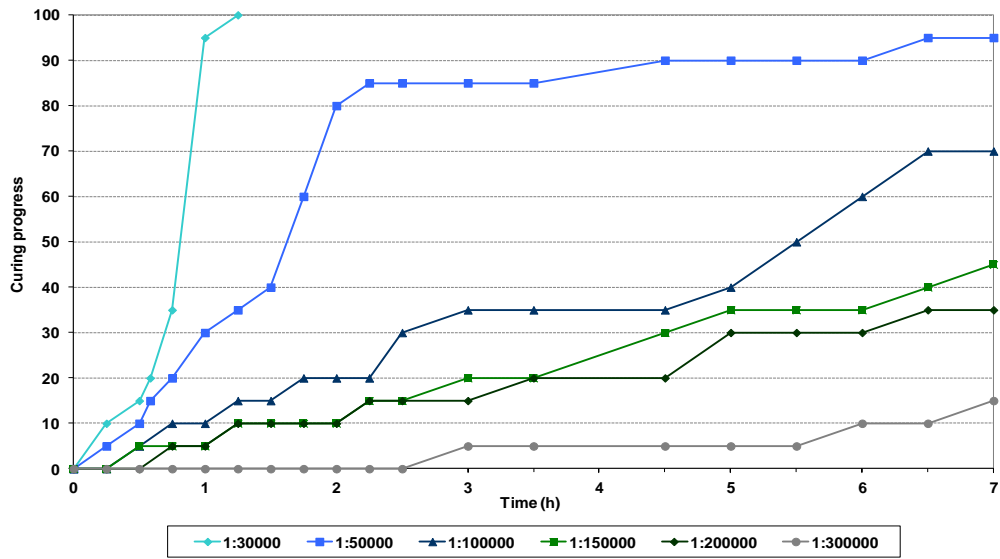
Figure 67: Different loadings of M2 for curing of DCPD at room temperature
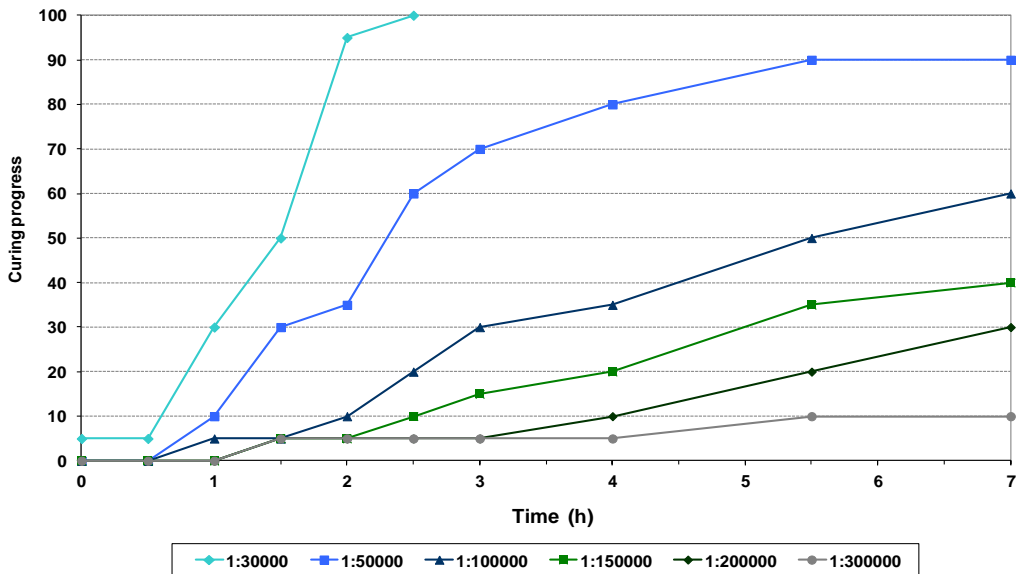
Figure 68: Different loadings of M22 for curing of DCPD at 60 °C

M2 shows polymerization progress at all loadings. Full curing (100 according to Table 24) is reached at the highest loading (33 ppm) after approximately 1 hour, and also with a loading of 20 ppm (1:50000) polymerization proceeds to almost full curing after 7 hours. At the lowest loading (3.3 ppm) no change in viscosity could be determined for 2.5 h, but after this time very slow polymerization was observed resulting in a viscous solution after 7 hours. In the same test setup, **M22** did not show any

95

polymerization progress at room temperature. Thus, the experiments were repeated at 60°C. At 60°C **M22** showed polymerization at all loadings. At 33 ppm (highest loading) full curing was achieved after 2.5 h, and with 20 ppm value 90 on the scale was reached after 7 hours. Indeed, the activity profile for **M22** at 60 °C is very similar to that of **M2** at room temperature, a fact that clearly illustrates the pronounced latency of **M22**.

4.2 Simultaneous Thermal Analysis (STA)

For determining the switching temperature of **M22**, STA measurements were run at different loadings (20, 25, 50, 75, and 100 ppm). A stock solution of **M22** was prepared so that for each loading 60 μL of DCM in total could be used for 1 mL of **DCPD** (*cf.* sample preparation with **extHov**s, chapter 0). For better clearance and direct comparison, the STA graphs of **M2** and **M22** at 20 ppm are exclusively depicted together in one graph (Figure 69).
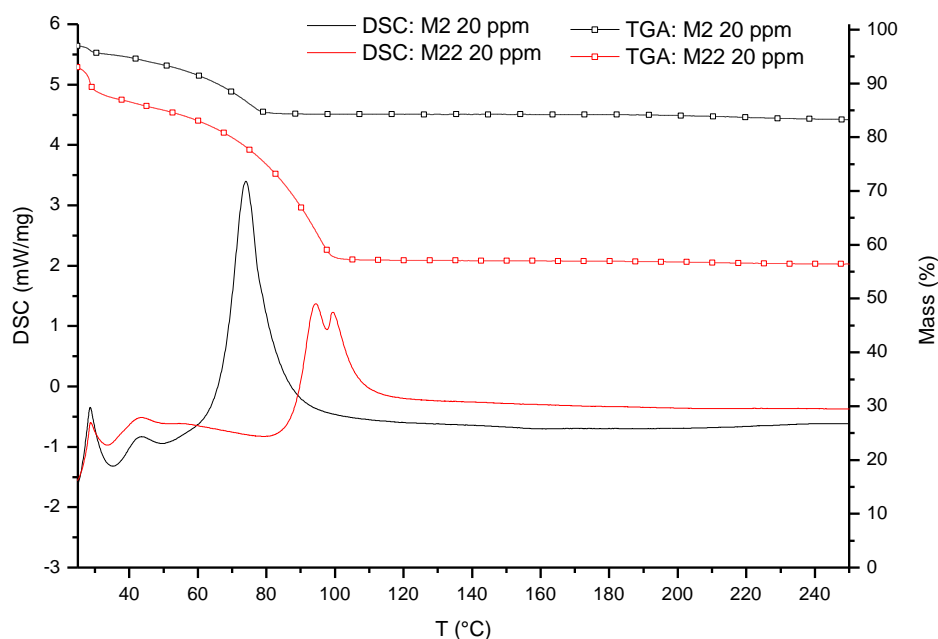
Figure 69: STA of DCPD curing with initiator M2 and M22 with 20 ppm loadings; solvent content = 7.4 %wt
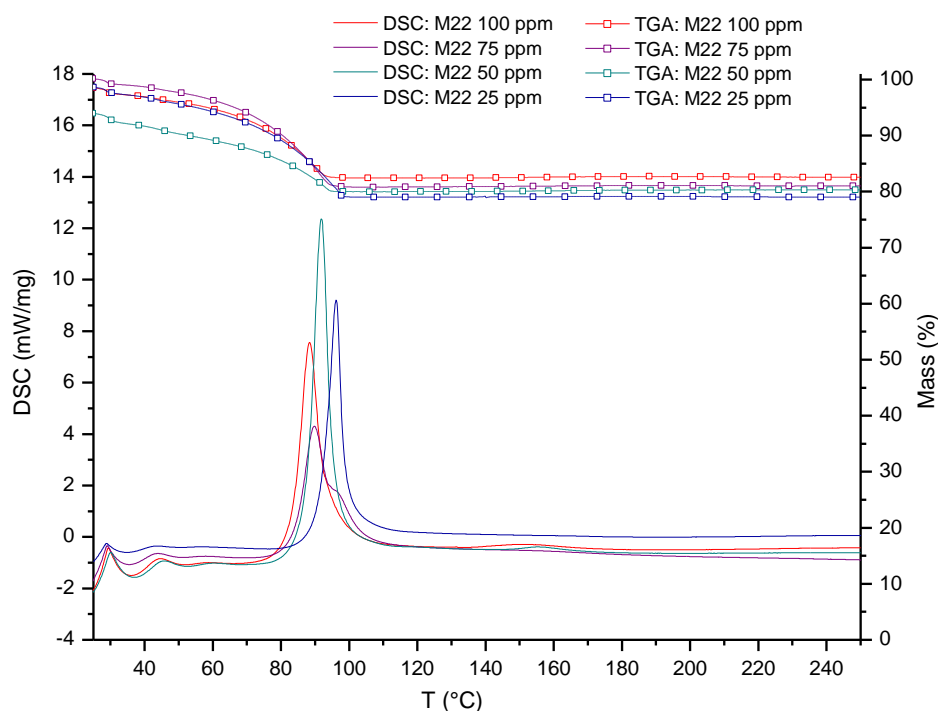
Figure 70: STA of DCPD curing with initiator M22 at different loadings; solvent content = 7.4 %wt

Table 25: characteristic values obtained from STA measurements (*cf*. Figure 69 and Figure 70)

	Onset (°C)	Peak max (°C)	gross mass loss[a] (%)	net mass loss[b] (%)
M2: 20 ppm	67	74	16.7	9.3
M22: 20 ppm	85.1	94.1 / 99.2	43.6	36.2
M22: 25 ppm	92	96	20.9	13.5
M22: 50 ppm	87	92	19.7	12.3
M22: 75 ppm	84	90	19.0	11.6
M22: 100 ppm	83	88	17.4	10.0

[a]: total mass loss; [b]: 7.4 % substracted for solvent (60 μL DCM in 1 mL DCPD)

Clearly, for the herein applied conditions during the STA run, 25 ppm **M22** is the critical loading that is necessary at the minimum to achieve reasonable curing of DCPD. At 20 ppm, being the same loading as used for reference initiator **M2**, polymerization starts at 85 °C (decomposition temperature of 69 °C, *cf*. Figure 58), but after a mass loss of about 30 % (23 % of monomer considering solvent) which increases the actual loading to about 26 ppm. Until that, the DSC curve shows an endothermic progression due to the evaporation of cyclopentadiene. Even after the initiation, mass loss proceeds until a temperature of 103 °C is reached. In the end, the net loss of the monomer is 36.2 % because of the slow curing. At higher loadings, polymerization starts before high mass

loss. No endothermic reaction can be detected in the DSC curves, assuming that the occurring mass loss and starting polymerization compensate each other. Therefore, onset temperatures given in Table 25 are supposedly higher than they actually are. However, the measured onset temperature could continuously be lowered from 92°C (25 ppm **M22**) to 83°C (100 ppm **M22**). Mass loss is still in a relevant dimension, but could be decreased to 10 %wt, which is in the range of reference initiator **M2** (9.3 %wt).

4.3 Shoulder Test Bars

One of the reasons for a vast interest in **polyDCPD** for large scale industrial applications are the outstanding mechanical properties of the polymer. In order to evaluate the scope of latent ROMP initiators in our laboratories, a procedure has been developed for the fabrication of shoulder test bars that are suitable for tensile strength tests. The mold used yields two test bars (Figure 71) of the dimensions listed in Figure 72. Usually, shoulder test bars are prepared from polymers by extrusion or reaction injection molding. Vulcanization of rubbers or blending of polyolefins with fillers etc. are processes that are often combined with this formative process. In the case of **polyDCPD** the formulation to be filled into the mold does not consist of a polymer, but the liquid monomer and dissolved initiator instead. Therefore RIM is not feasible. Also the fact, that ROMP of **DCPD** results in a highly cross-linked thermoset, prohibits the use of RIM. Material in the machine would irreversibly cure and block the function. For this reason, the monomer – initiator formulation was poured into a shoulder test bar mold in liquid form. Molten **DCPD** behaves like water and can be easily distributed homogenously in the mold. Hence, any preferred direction of polymer chains (like in the case of extrusion) is excluded and the resulting three-dimensional polymer network is expected to be randomly oriented.
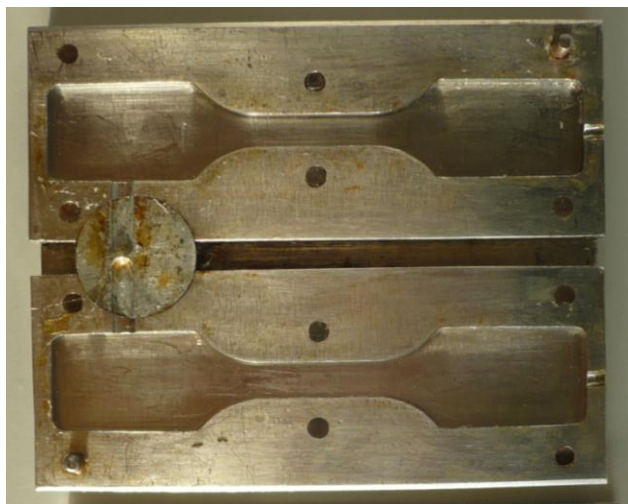
Figure 71: Steel mold yielding two shoulder test bars

$l_1 = 30$ mm
$l_2 = 65$ mm
$l_3 = 140$ mm
$r = 20$ mm
$h = 5$ mm
$b_1 = 9$ mm
$b_2 = 25$ mm
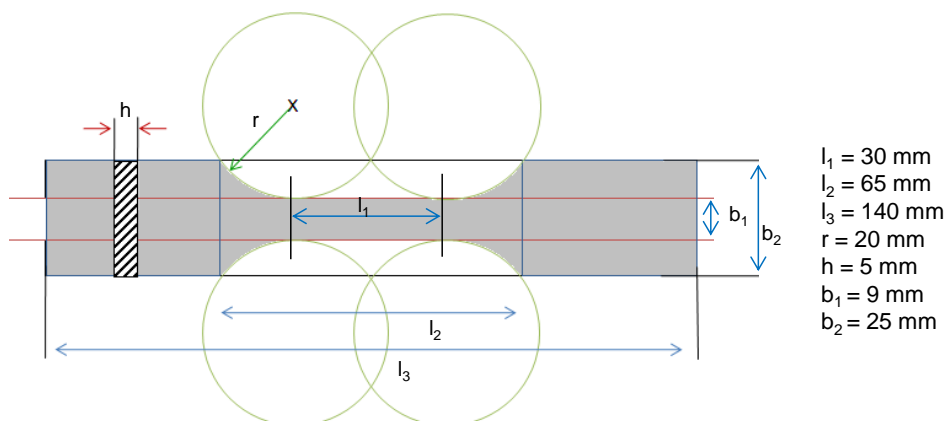
Figure 72: Dimensions of test bar mold

For the preparation of the test bars, a formulation of **DCPD** and the dissolved initiator (exhibiting 60 µL of DCM per 1 mL **DCPD**) was poured into the mold that had been placed in the oven (70°C) shortly before. The mold has to be slightly preheated to approximately 40°C in order to get rid of dichloromethane before the actual curing begins. Otherwise bubbles will be formed due to evaporation through the curing material that continuously increases its viscosity. For the same reason the mold must not be closed. When the mold is too cold, polymerization is prohibited and concurrently DCPD evaporates fast via the large surface area (retro Diels-Alder reaction, *cf*. Scheme 17). With a too hot mold on the other hand, polymerization starts already during the charging resulting in an inhomogeneous piece. Bubbles can also occur because of too high initiator loading. Polymerization is an exothermic process

and higher loadings lead to development of a considerable amount of heat that can also bring residual solvent or even the monomer itself to the boil.
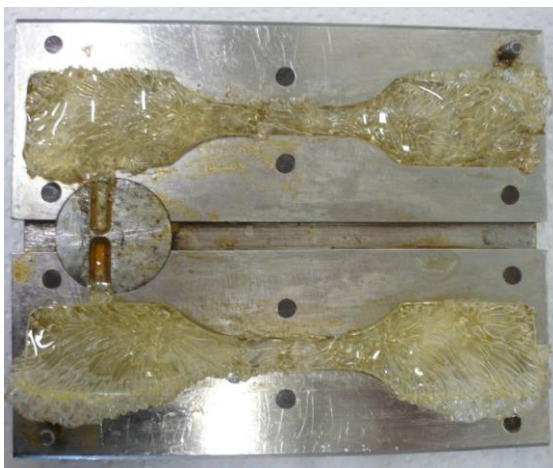
Figure 73: Too high initiator loading leads to bubble formation in shoulder test bars

The ideal loading is individually for each initiator and depends on two main issues, namely solubility and latency: First, the complex has to provide sufficient solubility in dichloromethane for the formulation, which was kept constant in all **DCPD** experiments (60 μL of dichloromethane on 1 mL of **DCPD**). If the complex is not fully dissolved it will be inhomogenously distributed and the experiments are not reproducible anymore. Secondly, the latency of the complex defines the necessary loading for the applied temperature. This means, that a "switching temperature" of a latent initiator is only valid for the respective loading (within a certain limit of tolerance). The probability of initiation at lower temperature increases with the loading. This has already been shown with STA measurements employing the **extHov** series (*cf*. Figure 70). The ideal loading for the test bars may deviate from an ideal loading for the STA measurements, as the formulation will not be shock frozen. Thus premature initiation has to be compensated by lower initiator loading when necessary. Once a suitable loading has been found, the test bars can be easily prepared. The resulting shoulder bars are slightly smaller than the mold due to shrinkage that occurs during the curing. In case of **DCPD** this shrinkage is very low, but still not negligible. Also, some loss of monomer has to be taken into account resulting from evaporation of cyclopentadiene from retro Diels Alder, as the open mold exhibits a large surface area, promoting this undesired effect.

4.3.1 M2 for Shoulder Test Bars from PolyDCPD

Figure 74 shows reference shoulder test bars prepared with different loadings of **M2**; 5, 10 and 20 ppm. Higher loadings were not feasible due to immediate curing at room temperature. The shoulder test bars were cured at 60 °C and showed considerable differences in their appearance. The samples prepared with 5 ppm initiator were barely cured even after 2 hours at 60°C, still soft and flexible, and color of dissolved **M2** was still present. Also, they contained a large amount of monomer, which is easily detectable by the characteristic smell of **DCPD**. Bars containing 10 ppm of **M2** did not smell anymore, indicating full consumption of monomer. They had a solid, tough consistency after 30 min at 60°C. The color was the same as for 5 ppm, but more intensive. This again suggests considerable amounts of non-initiated complex **M2**. For the test bars exhibiting 20 ppm of initiator the situation was different. The curing took only a few minutes to reach solid, fully cured test bars. The color was nearly extinguished during the process. Also the bars got hot. Tiny bubbles were distributed throughout the material.

Figure 74: polyDCPD shoulder test bars (5, 10 and 20 ppm M2)

Obviously, at 20 ppm loading, the initiation rate at 60°C is increased to an amount generating enough exothermic energy (from the polymerization process) that consequently triggers full initiation of **M2**. The reference shoulder test bars were used for tensile strength tests. For the determination of the Young's Moduli of the test bars, an average cross sectional area A_0 of 35.2 mm^2 (corresponding to b_1 = 8 mm and h = 4.4 mm) was assumed after measuring dimensions of 20 test bars. The bars were fixated in the machine with a clamp distance L_0 of 80 mm. The tensile test was

performed with a speed of 1 mm/min. The modulus of elasticity (Young's modulus E) was determined according Equation 1 from the slope within the linear part of the curves. The resulting test curves are depicted in Figure 75.

E (MPa)	Young's modulus
F (N)	tensile force applied
A_0 (mm^2)	cross-sectional area: 35.2 mm^2
ΔL (mm)	elongation
L_0 (mm)	distance between clamps at starting position: 80 mm
σ (MPa)	stress
ε (%)	strain

Equation 1: Young's Modulus
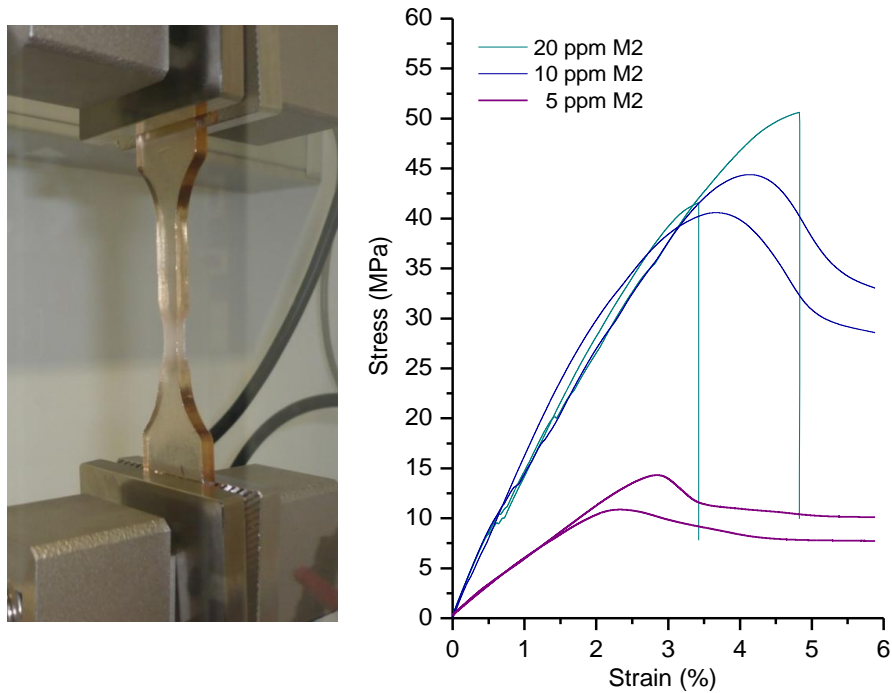
Figure 75: polyDCPD shoulder test bar in testing machine (left) Tensile strength tests with different loadings of M2 (right)

The obtained test curves differ greatly from each other depending on the loading. 5 ppm **M2** yield test bars with a Youngs modulus of 590 MPa. The maximal stress of 12-15 MPa (422 to 528 N) was reached at 2 – 3 % of strain (1.6 - 2.4 mm elongation),and

after that non-elastic deformation occurred. The loading of 10 ppm yielded test bars exhibiting a 3-fold higher Young's modulus (1800 MPa) which perfectly matches typical values for **polyDCPD** from literature. [106] However, non-elastic deformation occurred again after overcoming a maximal applied stress of about 42 MPa at about 4 % strain. The now following elongation was different in value for each measured test bar an reached a total elongation of up to 108 %, depending on minor imperfections like tiny cracks or bubbles in the testing bar. The test bars obtained with 20 ppm **M2** showed a rigid behavior at the maximal applied stress (up to 55 MPa at 5 % strain) and broke at that point. The Young's moduli were in the same range as with 10 ppm **M2**, about 1800 MPa (*cf*. Figure 75). From these observations it can be concluded that a loading of 10 ppm **M2** is necessary to achieve Young's moduli typical for the material. However the non-elastic deformation before break suggests a rather low degree of cross linkage. This might be due to the fact that the cyclopentene ring in **DCPD** is less strained than the unsaturated bicyclus and therefore needs more activation energy to be cleaved by **M2**. As a result, a rather loose network is constructed that can still be oriented along one direction upon tensile stress. In the case of 20 ppm loading, this activation barrier is overcome and the resulting network is dense and rigid. Yet the Young's modulus, determined within the region of elastic deformation at low strain values, is not increased.
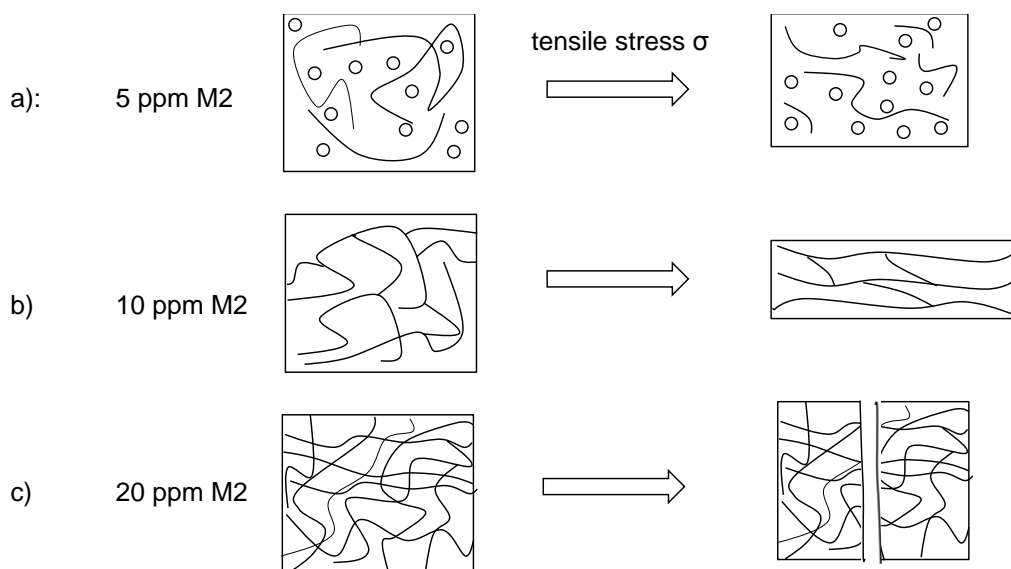
Scheme 19: Schematic illustration of polyDCPD network resulting from different initiator loadings; a): Hardly cross-linked polymer, short polymer chains and residual monomer lead to break at low tensile stress; b): Loosely cross-linked network and full monomer consumption allow high tensile stress before break; c): highly cross-linked rigid network breaks at low strain but bears high tensile stress

---

[106] http://www.matweb.com/search/datasheetText.aspx?bassnum=O3190: MatWeb entry (Nov 2011)

4.3.2 M22 for Shoulder Test Bars from PolyDCPD

4.3.2.1 Preparation of the Test Bars

As a second initiator, **M22** was also employed for making shoulder test bars from **DCPD**. **M22** was considered to be interesting despite the high switching temperature (*cf*. Figure 70) due to its longevity in solution at ambient conditions (*cf*. Figure 65). The pronounced latency was encountered by higher loadings and by adapting the conditions for the shoulder test bar preparation. At first, a change of solvent for the initiator from dichloromethane to toluene was considered. The high boiling point of toluene (110°C) would facilitate curing at high temperatures without bubble formation due to solvent evaporation. However, after ensued polymerization toluene will stay in the polymer and act as softener. Hence, the formulation for the reaction mixture was kept the same as for **M2**. The test bar mold was preheated to 70°C in the oven before being charged with the dark reddish mixture of liquid **DCPD** and dissolved **M22**. The test bars were cured at 70°C until they were ready to be taken out after 45 to 60 min depending on the loading; they were still soft and flexible, but in one piece. These semi-cured bars were then post-treated with a heat-gun (*cf*. Figure 76). Thus, high temperatures (up to 300 °C) could be applied without losing monomer, as residual monomer was already trapped in the existing network. By this procedure **M22** could be exhaustively initiated, which was confirmed by the discoloration from dark reddish-brown to slightly yellow (*cf*. Figure 77). Also, the rigidity of the test bars was massively increased.
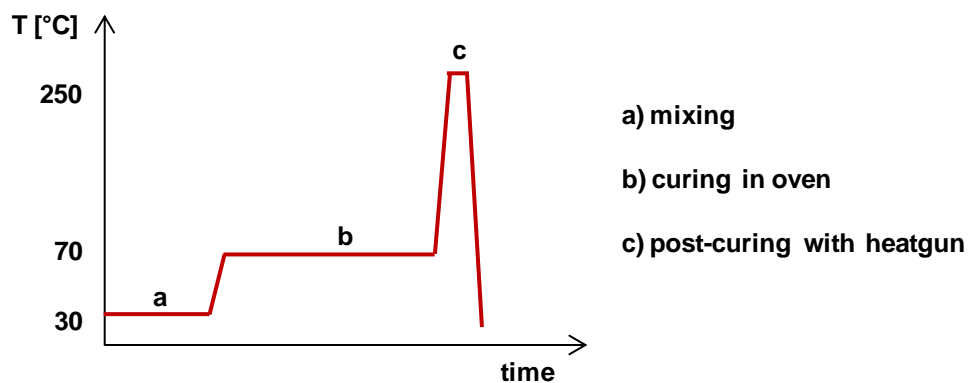
Figure 76: Two-step curing process for DCPD with M22
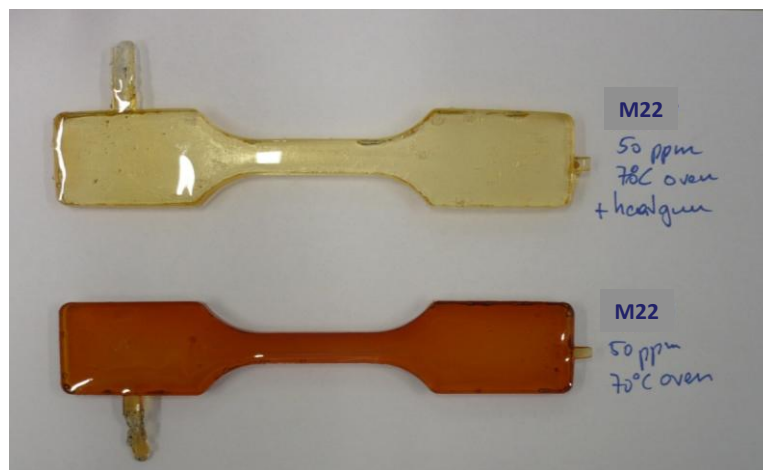
Figure 77: Shoulder test bars cured at 70°C in the oven; above: post treatment with heatgun

A series of test shoulder bars was produced employing different ratios of **M22**. They were primarily used for tensile strength tests (Figure 78), but also swelling in toluene was examined in order to compare the degree of cross linking (Figure 79). A second series of test bars was kept at ambient conditions for 6 weeks before being exposed to tensile stress, in order to determine the influence of aging through oxidation processes.

4.3.2.2 Tensile Strength Tests

The tensile strength tests show similar results to those where reference initiator **M2** was employed. In Figure 78 one representative test curve (of four measured) for each loading (5, 10, 25, 50, 75 and 100 ppm) is depicted.
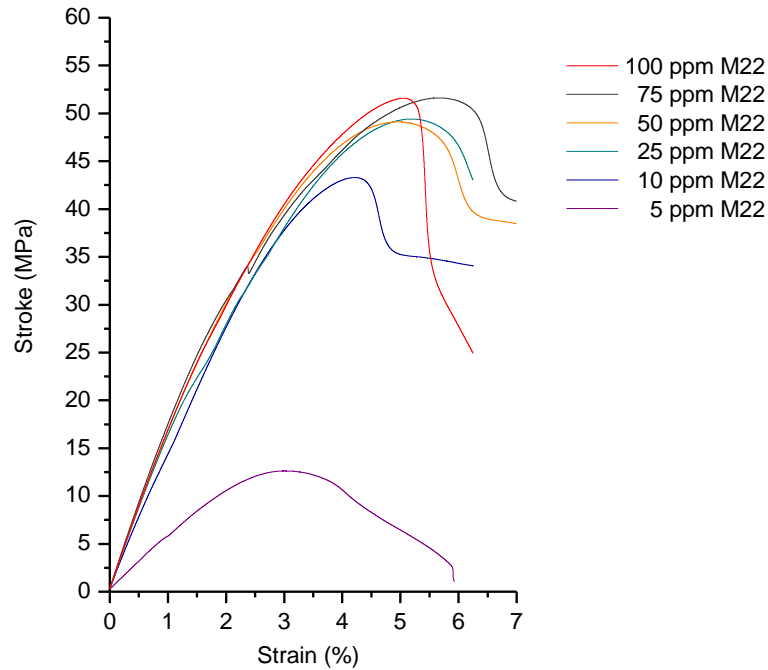
Figure 78: Tensile strength tests of test specimen produced with different loadings of M22

The bars prepared with 5 ppm **M22** clearly achieved the lowest values for Young's modulus (600 MPa) and maximal stress (10 MPa at 3 % strain). These results resemble the corresponding 5 ppm bars prepared with **M2**. For higher loadings, the Young's moduli range from 1660 (10 ppm) to 1830 MPa (100 ppm). The curves are very similar to each other and it has to be pointed out that apart from the 10 ppm bars which constantly achieved slightly lower values, the deviation within one loading (four bars each were tested) was in the same range as the differences between different loadings. For direct comparison of **M22** with reference **M2**, results from the tensile strength test are summarized in Table 26. Average values for higher loadings of **M22** are quoted, which once more emphasizes the minimal differences in the determined mechanical properties.

Table 26: Summarized results from tensile strength tests with M2 an M22 (rounded average values)

	Young's modulus E (MPa)	maximal stress σ_{max} (MPa)
M2: 5 ppm	600	12
M2: 10 ppm	1800	42
M2: 20 ppm	1800	50
M22: 5 ppm	600	12
M22: 10 ppm	1660	43
M22: 25-100 ppm	1800	50

4.3.3 Influence of Aging in Air on Mechanical Properties

As mentioned above, shoulder test bars were kept at ambient conditions before being tested. However, these experiments did not show any effect arising from aging (*cf*. experimental). Obviously the oxidation in air does not proceed deeper into the material after the formation of a thin layer at the surface that is formed immediately during curing in air.[107]

4.3.4 Swelling Experiments

For swelling tests a small piece (approximately 1 g) of the specimen was cut off, weighed and covered with toluene. Regularly, the specimen was taken out, toluene from the surface was carefully removed with a paper towel and the swelled piece was weighed again, until no further weight increase was observed. The increase of weight from toluene uptake is documented in Figure 79 for all loadings under investigation. The obtained curves perfectly match the results from the tensile strength tests. Whereas specimen with loadings of 10-100 ppm **M22** only show minor deviation from each other, the sample exhibiting only 5 ppm of **M22** steps out of line in terms of mass increase. After being covered in toluene for 18 h, the sample had more than doubled its weight, and after 60 hours the final weight (approximately 270 % of the initial weight) had been reached. The toluene uptake for samples with initiator loadings ranging from 10-100 ppm is slower, but proceeds according to their respective loadings in the beginning. After 18 h initial weights are increased between 40 % (100 ppm) and 80 % (10 ppm). After 60 h the final weights had again been reached. They were then close together amounting for 217 % to 222 % of the initial weights.

---

[107] Mühlebach, A.; van der Schaaf, P. A.; Hafner, A.; Setiabuti, F. *J Mol Catal* **1998**, *132*, 181-188.
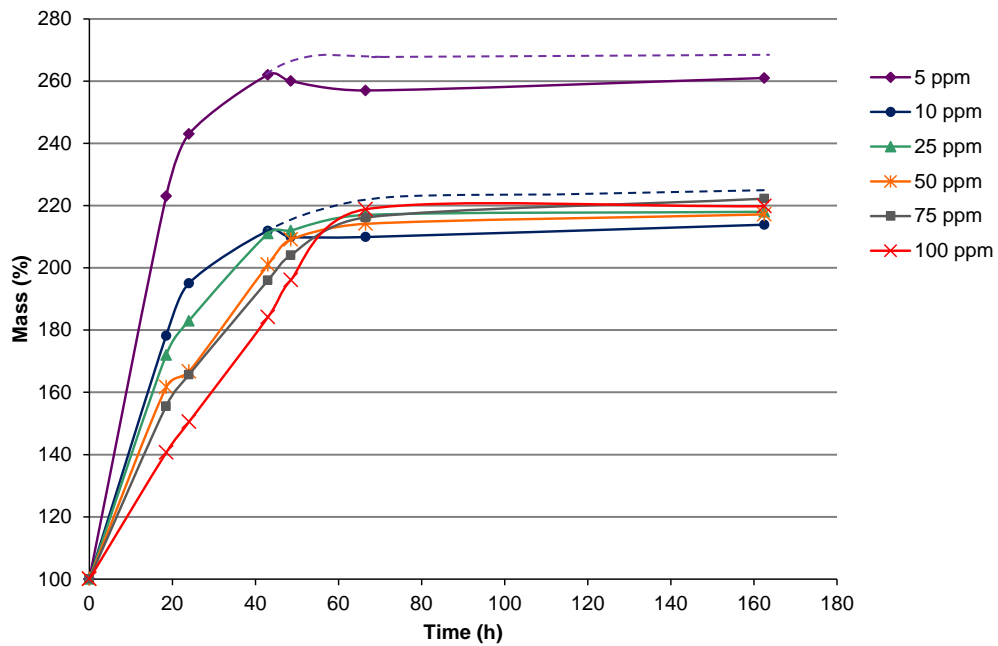
Figure 79: Weight increase of polyDCPD cured with different amounts of M22 due to swelling in toluene; connecting lines were added for clarity; dashed lines were introduced manually.

The weight decrease after 43 h for the 5- and 10 ppm samples are attributed to the loss of tiny polymer pieces that broke off when getting hold of the – by then – sloppy samples. In Figure 79 the respective curves are manually extended in dashed lines, following the trend of the remaining curves.
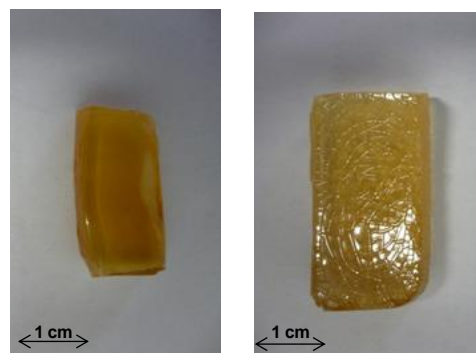
Figure 80: polyDCPD (initiator: 50 ppm M22) before and after swelling in toluene

Figure 80 exemplarily shows photos of the 50 ppm sample before and after swelling in toluene in the same magnification. Besides of the apparent volume increase, the swollen sample shows fine fissures on its surface. Obviously the oxidized surface layer cannot be penetrated by toluene and cracks during the swelling procedure.

5 M31 for ROMP-ATRP graft-co-POLYMERS

The synthesis of well defined, organic-inorganic hybrid graft co-polymers employing ROMP and ATRP was targeted in cooperation with Dr. Georg Witek, at that time working with Krzysztof Matyjaszewski from Carnegie Mellon University (Pittsburgh). A schematic overview of the project is provided in the following (Scheme 20). Various PDMS-based macro-monomers for ROMP had been synthesized in order to follow either the "ROMP first" approach followed by a "grafting-from" step, or the "ATRP first" approach followed by ROMP in a "grafting-through" process (*cf*. chapter 2.3.3.3).
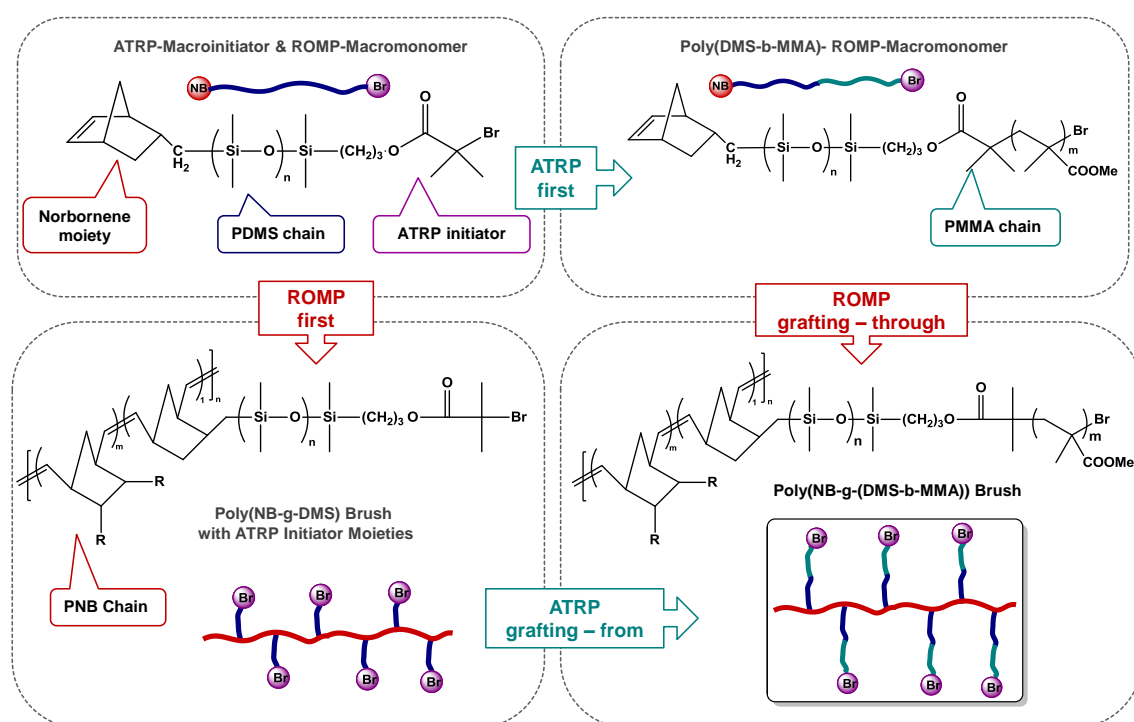
Scheme 20: Strategies to achieve brush-graft-co-polymers employing ROMP and ATRP

For this endeavor, initiator **M31** was employed which has proven its applicability for living polymerization of various ROMP monomers.[14,17a] The macromonomer for the "ROMP first" approach (**MonGW21**) consists of a norbornene which is mono-functionalized with a polydimethylsiloxane chain (PDMS) bearing an ATRP initiator at its end. By means of NMR spectroscopy the molecular weight was determined to be 5050 g/mol, which roughly corresponds to GPC data (M_n=5577 g/mol). With ring opening metathesis polymerization, homo-polymers of **MonGW21** as well as statistical block-copolymers with **EsterMon** in various ratios were synthesized. For the "ATRP first" approach **MonGW21** had been subjected to ATRP with either

metyhlmethacrylate or butylacrylate to yield **MonGW31** (11193 g/mol) and **MonGW32** (10663 g/mol) respectively. Molecular weights were again determined by NMR spectroscopy and by GPC. The (block-co-polymer)-macromonomers **MonGW31** and **MonGW32** were again employed in ROMP using **EsterMon** as co-monomer.
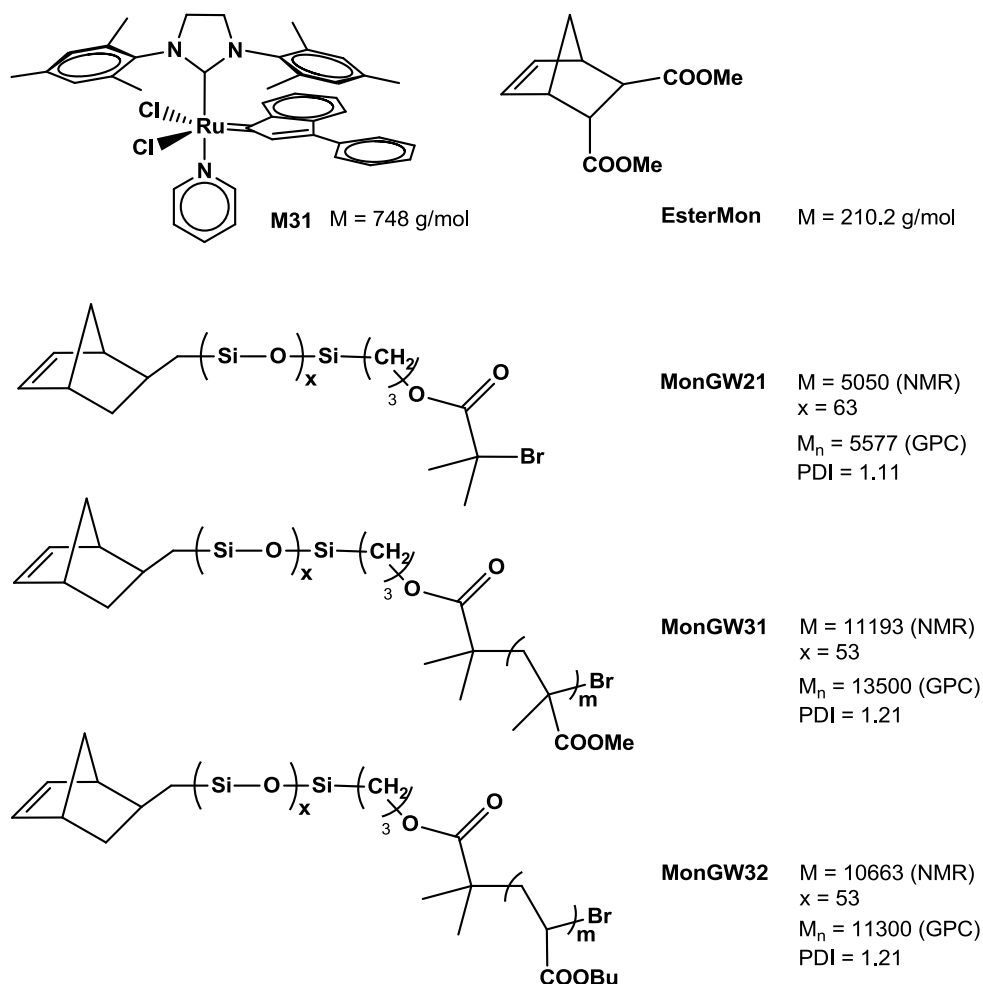
Figure 81: Initiator and monomers employed for organic-inorganic hybrid brush-copolymers

All experiments were carried out at room temperature and under oxygen-free conditions with Schlenk technique, with dichloromethane as the solvent. The concentration was adapted in each reaction due to the diverging characteristics of the monomers. (*cf*. Experimental, chapter 0) Monomer(s) were put into a Schlenk flask and dissolved before an aliquot of a freshly prepared **M31** stock solution was added under vigorous stirring. The targeted molecular mass is given from the stoichiometric ratio of the monomer(s) to the initiator. Conversion was followed by TLC and/or ^{1}H-NMR spectroscopy (TLC was only feasible for **MonGW21**). When maximum conversion was

reached the polymerization was quenched with excess ethylvinylether. The solution was concentrated to approximately 1 mL and the polymer was then precipitated in cold, vigorously stirred MeOH. The product was then characterized by ^{1}H-NMR spectroscopy and GPC (calibrated with poly styrol standards).

5.1 The "ROMP first" Approach

5.1.1 Homo-Polymerization

First, homo-polymerization of **MonGW21** according to Scheme 21 was performed. Monomer concentration was decreased to 0.01 M (standard benchmark conditions = 0.1 M) in order to account for its high molecular weight compared to usual monomers. Immediate initiation was observed, indicated by the sudden color change from orange (dissolved **M31**) to light yellow (active initiator species).
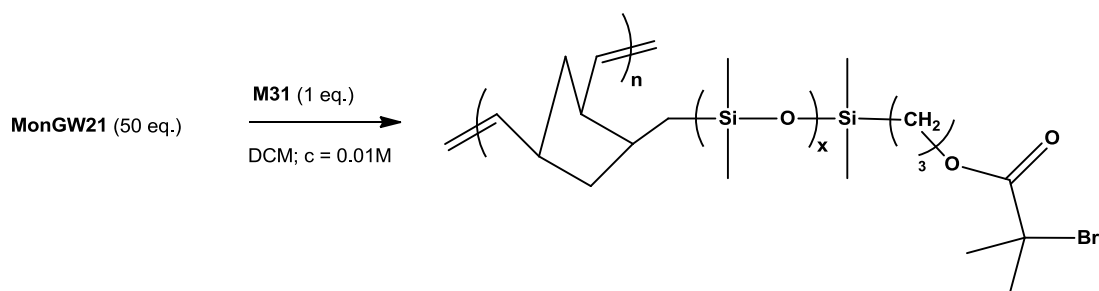
Scheme 21: Homopolymerization of MonGW21

After 24 hours, the reaction was still not quantitative (~ 70 %), but no further progress could be noted by TLC. Precipitation in MeOH did not yield solid polymer, but separated most of residual monomer anyway, as no more trace of monomer was detectable by GPC. The average number molecular weight was determined to be 103600 g/mol suggesting a degree of polymerization around 20. The molecular weight distribution is rather broad (PDI = 1.32), supposedly due to steric hindrance during polymerization. No further investigations regarding homopolymerization were performed.

5.1.2 Co-Polymerization with EsterMon

EsterMon was employed to "dilute" the macro-monomer **MonGW21**. Hence steric hindrance caused by the PDMS chain is reduced and it is expected to reach higher

degrees of polymerization (DP). Either four or nine equivalents of **EsterMon** were used with respect to **MonGW21**, so that overall ratios of monomer to initiator of 50, 100, 250 or 1000 could be realized (*cf*. Scheme 22).
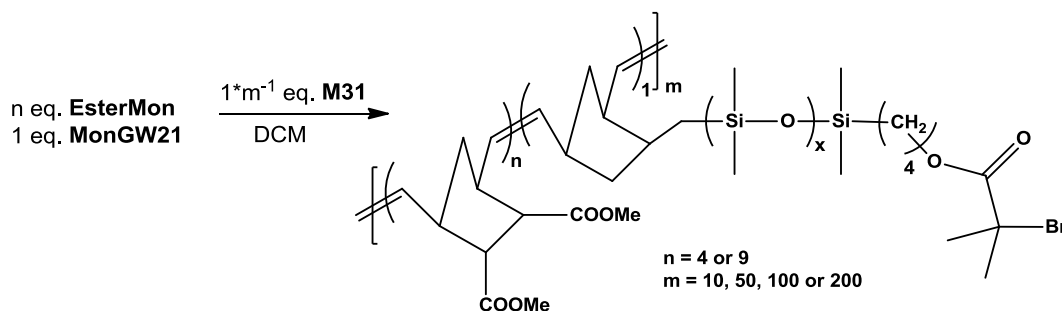
Scheme 22: Co-polymerization of EsterMon and MonGW21 with different ratios

For m = 10, (*cf*. Scheme 22), ROMP could be performed in a well-controlled manner for both stoichiometric monomer ratios (PDI = 1.12 for n = 4 and PDI = 1.13 for n = 9). For full conversion, reaction times were between 2.5 h and 4 h for n = 4, and up to 15 h for n = 9. It has to be noted that in case of n = 4, prolonged reaction times (> 4 h) lead to backbiting and degradation of the polymer by the active initiator species as indicated by broad molecular weight distributions. Also, higher DPs were not achieved in equal quality. For DP_{Target} = 250 (m = 50) a PDI of 1.25 was determined and for DP_{Target} of 1000 (m = 200) the molecular weight distribution even yielded a PDI of 1.70. However, upon increasing the share of **EsterMon** (m = 9), polymers with DP_{Target} = 1000 were achieved exhibiting PDIs below 1.5 (1.47) and for DP_{Target} = 100 perfect control was maintained resulting in a PDI value as low as 1.13. Detailed experimental results are summarized in Table 27 and the GPC elugrams are shown in Figure 82.

Table 27: Results of the co-polymerizations of $[(EsterMon)_n(MonGW21)_1]_m$

ratios			GPC results	
n	m	DP target	M_n	PDI
4	10	50	40200	1.12
4	50	250	109200	1.25
4	200	1000	390200	1.70
9	10	100	46500	1.13
9	100	1000	204600	1.47

Comparison of the target molecular weight and Mn determined by GPC is unrewarding, as grafted copolymers are generally underestimated by GPC. Moreover, the hydrodynamic radii of these polymers in comparison to the PS standards used for GPC calibration, contribute to this deviation. Hence, the molecular weight distribution (represented by the PDI value) and mutual comparison of the co-polymers give the most valuable information for these experiments. The obtained co-polymers were also analyzed by NMR-spectroscopy to confirm the applied ratio of the monomers (exemplary shown for $[(EsterMon)_9(MonGW21)_1]_{10}$ in Figure 83).
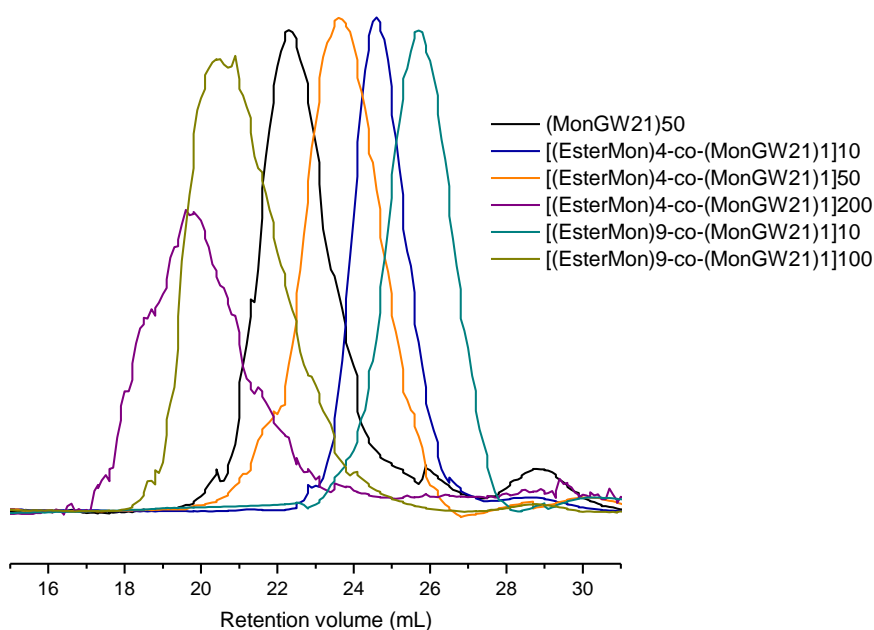
Figure 82: GPC elugrams of homopolymer $(MonGW21)_{50}$ and copolymers $[(Mon1)_n(GW021)_1]_m$
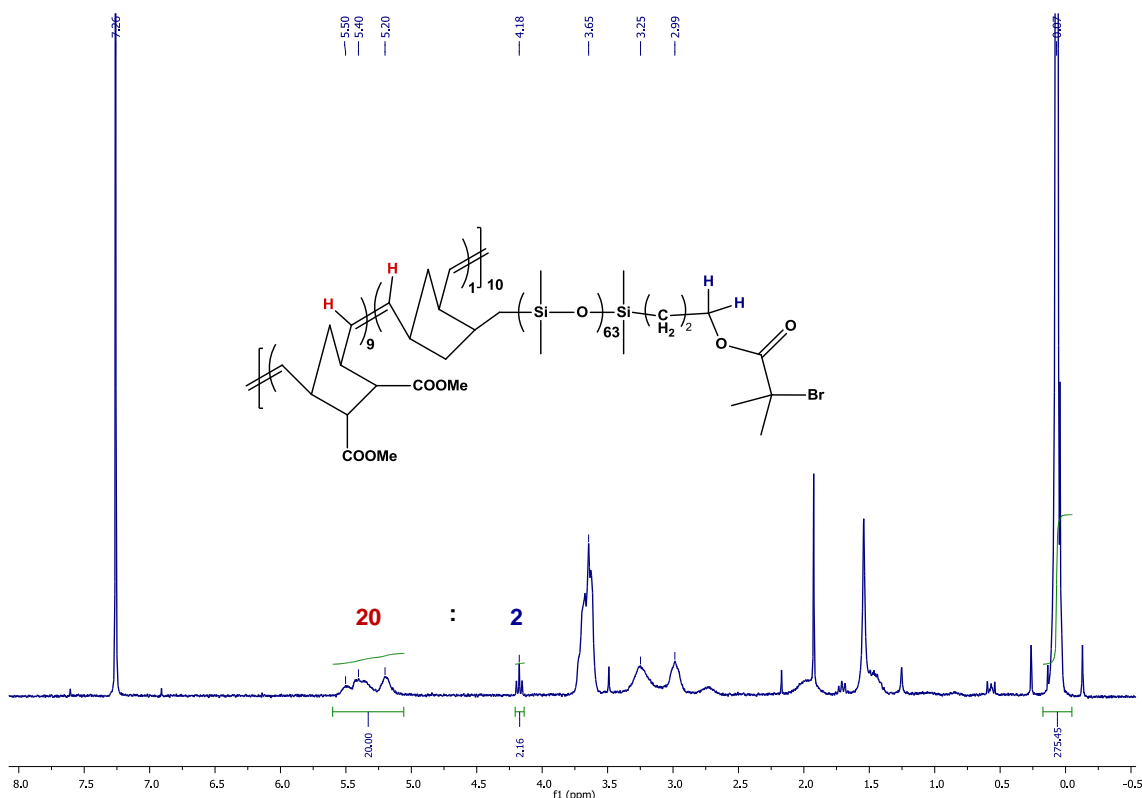
Figure 83: ^{1}H-NMR (CDCl$_3$, 300MHz) spectrum of [(EsterMon)$_9$(MonGW21)$_1$]$_{10}$

5.2 The "ATRP first" Approach

5.2.1 Homo-Polymerization

ROMP of PDMS-acrylate block copolymers (**MonGW31**: PDMS-*b*-PMMA and **MonGW32**: PDMS-*b*-PBA) was performed with **M31** in dichloromethane according to Scheme 23 and Scheme 24. Generally, conversion control by means of TLC is no longer feasible for these polymeric macro-monomers, as they will not move on the TLC plate. Hence, mostly GPC was used for analysis of the isolated polymers. Residual monomer can't be separated and is therefore co-analyzed. NMR spectroscopy for reaction control is also critical, as the characteristic olefinic peaks are of minimal relevance in the spectra due to the high-molecular-weight-tether.
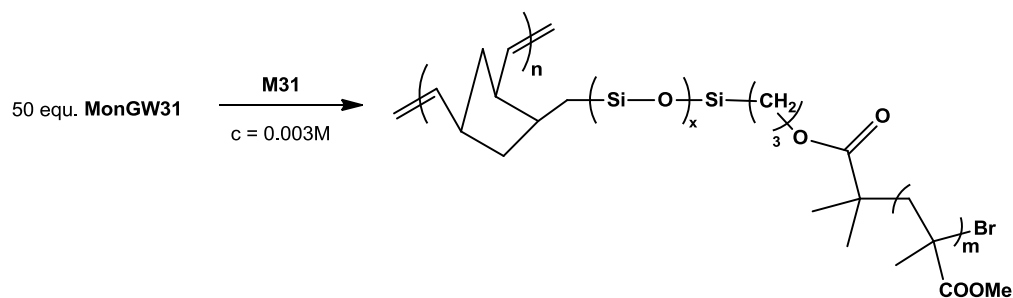
Scheme 23: Homo-polymerization of MonGW31
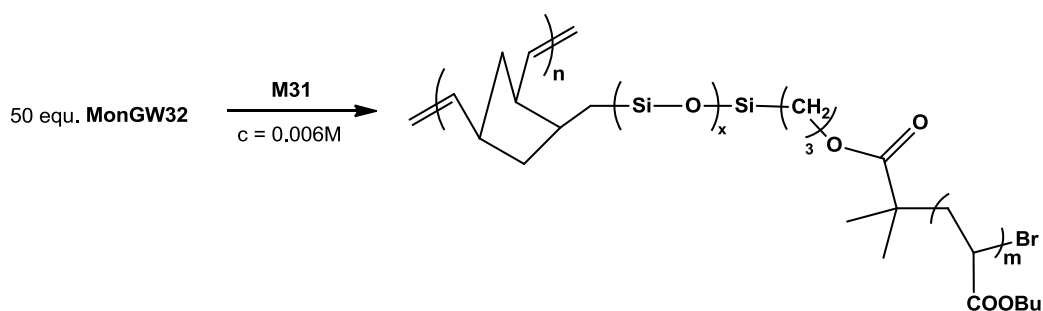
Scheme 24: Homo-polymerization of MonGW32

As already observed with **MonGW21**, homo-polymerization of the polymeric macromonomers was problematic and did not reach full conversion. Interestingly, polymers from **MonGW31** (featuring a PDMS-b-PMMA tether) was more prone to backbiting even when polymerized in higher dilution. Also, only low conversion was reached (estimated to 50% according GPC elugram, *cf.* Figure 84). Homo-polymerization of **MonGW32** (featuring a PDMS-b-PBA tether) was more successful and according to GPC only a small amount of monomer was left unpolymerized (*cf.* Figure 86). As a consequence, only **MonGW32**, the butylacrylate blockcopolymer (PDMS-*b*-PBA) was further employed for copolymerization experiments with **EsterMon**.
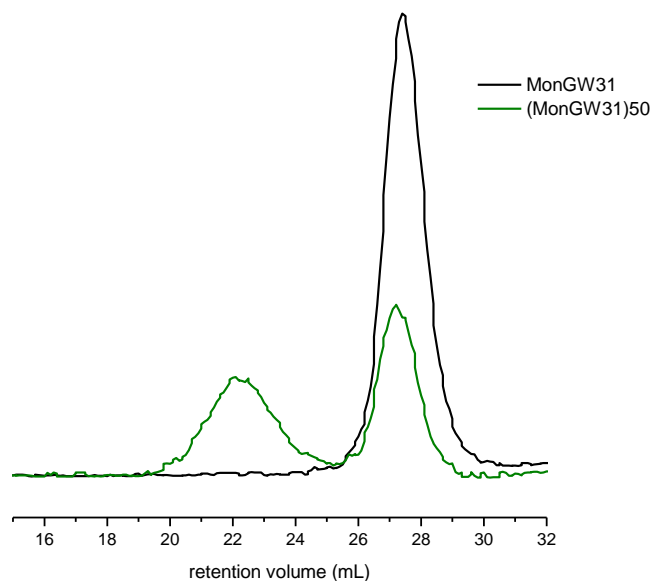
Figure 84: GPC elugrams: macromonomer MonGW31 and homo-polymer thereof.

5.2.2 Co-Polymerization with EsterMon

Deduced from results of the "ROMP first" copolymerization experiments with **MonGW21** (PNB-*g*-PDMS), nine equivalents of **EsterMon** with respect to **MonGW32** were used and overall ratios of monomer to initiator **M31** (corresponding to DP$_{Target}$) of 100 and 1000 were employed as shown in Scheme 25. Results are summarized in Table 28.
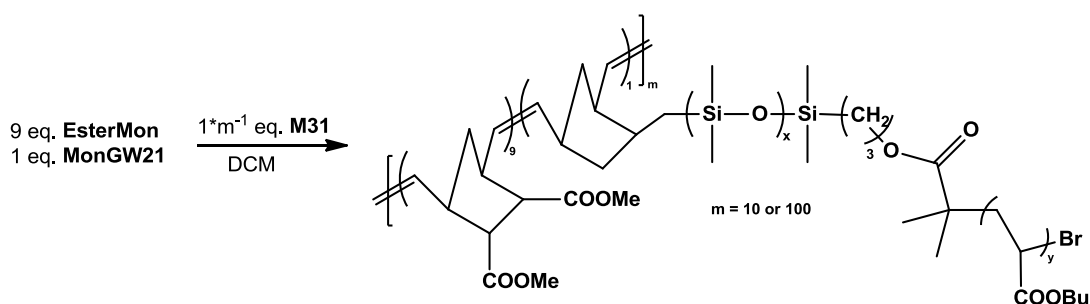
Scheme 25: Co-polymerization of EsterMon and MonGW32 with different ratios

Table 28: Results of the co-polymerizations of [(EsterMon)$_9$(MonGW32)$_1$]$_m$

ratios		GPC results	
m	**DP$_{Target}$**	**M$_n$**	**PDI**
10	100	65400	1.19
100	1000	225700	1.60
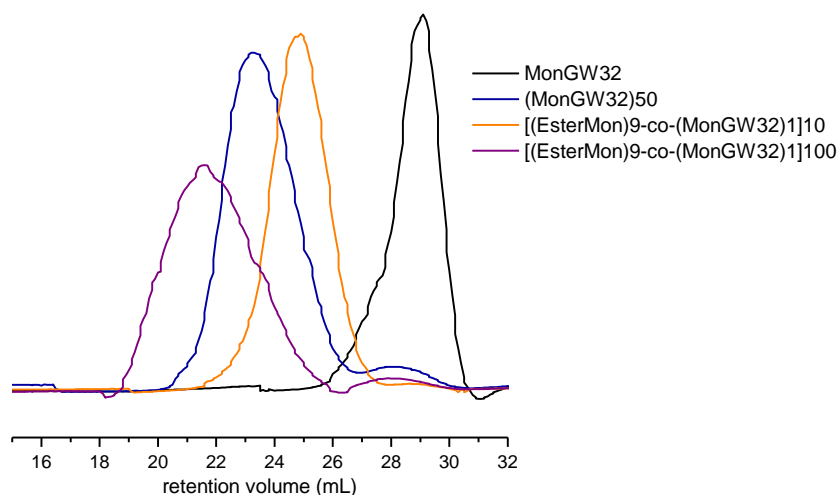
Figure 85: GPC elugram of the homo- ((GW032)$_{50}$) and copolymerization [(Mon1)$_9$(GW032)$_1$]$_m$ (m = 10 or 100) of the macromonomer PDMS-*b*-PBA via "grafting through" ROMP

Figure 85 shows the GPC elugrams of the ROMP homo- and co-polymerization experiments with the PDMS-*b*-PBA macromonomer. The elugram of the pure monomer is added as a reference (black line). As can be seen from the blue line – the homopolymerization – monomer conversion was incomplete. **MonGW32** was only fully consumed in the co-polymer with a targeted degree of polymerization of 100 (orange line). Here also the PDI value is satisfactorily low (1.19). For DP$_{Target}$ = 1000 (violet line) the weight distribution is rather high with a PDI value of 1.60.

5.3 Comparing "ROMP-first" with "Grafting-Through ROMP"

Regarding homo-polymerization it is stated that with none of the three macromonomers under investigation full conversion was achieved, even when only 50 equivalents of monomer were used with respect to initiator **M31**. Figure 86 shows the corresponding GPC elugrams. In all cases a second peak originating from the monomer can be observed at higher retention volumes, most pronounced for the PDMS-*b*-PMMA macromonomer **MonGW31**. Still, the results can compete with published works: Examples from literature employing initiator **G2** with cyclobutene based ROMP-

macromonomers exhibiting ATRP tethers (resulting in polybutadiene-g-(polystyrene-b-poly(acrylic acid)), report a maximal initiator to monomer ratio of 1:10, prolonged reaction times up to 76 hours and high temperatures of 70°C for reasonable PDI values below 1.2 for the grafting-through process.[108]
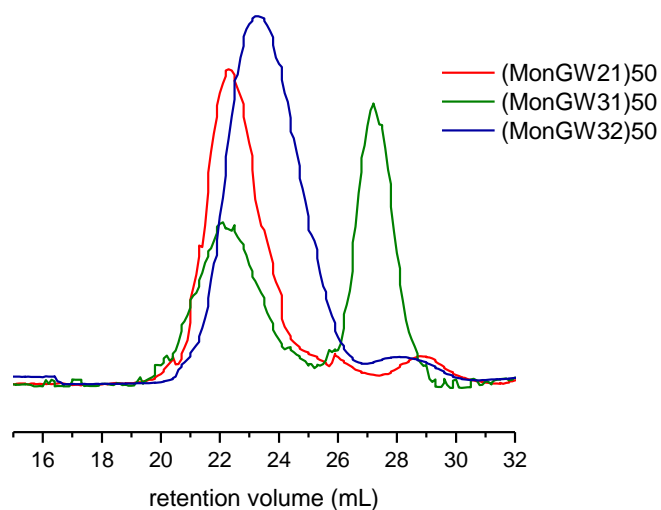
Figure 86: GPC elugrams of the ROM homopolymerizations of MonGW21 (Nbe-PDMS), MonGW31 (Nbe-PDMS-*b*-PMMA) and MonGW32 (Nbe-PDMS-*b*-PBA), (50 eq. each)
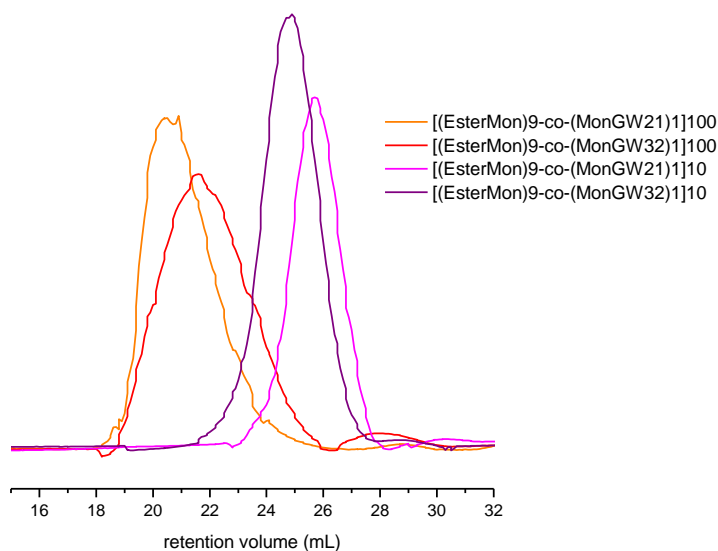
Figure 87: GPC elugrams of the copolymerization experiments of PDMS (GW021) and PDMS-*b*-PBA (GW032) with Mon1 with Mon1/GW = 9 and DP$_{Target}$ = 100 or 1000

Higher or even quantitative monomer consumption was achieved when the macromonomers **MonGW21** (Nbe-PDMS) and **MonGW32** (Nbe-PDMS-*b*-PBA) (**MonGW32**)

---

[108] Morandi, G.; Montembault, V.; Pascual, S.; Legoupy, S.; Fontaine, L. *Macromolecules* **2006**, *39,* 2732-2735.

were "diluted" with **EsterMon**. Also, polymer degradation by backbiting could successfully be prohibited, resulting in generally satisfactorily narrow molecular weight distributions (*cf*. Table 27 and Table 28). For direct comparison, GPC elugrams of the copolymerization experiments with a monomer ratio of **EsterMon/MonGW** = 9 and a DP_{Target} = 100 or 1000 are shown in Figure 87. Only for the "grafting-through" polymerization of the PDMS-*b*-PBA with a targeted DP of 1000 incomplete monomer consumption (estimated 95 % conversion) was observed. Generally, better polymerization control was achieved in all "ROMP first" approaches. For DP_{target} = 100, both approaches yielded quantitative monomer conversion for different monomer ratios, and PDI values were below 1.2. In contrast, for DP_{Target} = 1000, only the "ROMP first" method led to quantitative monomer conversion and a PDI < 1.5. However, polymers from the "ROMP first" approach still have to be subjected to the "grafting-from" step (*cf*. Scheme 20) so that a relevant comparison of the final target-product, namely the brush-graft-co-polymer **Poly(Nbe-g-(DMS-b-MMA))** and **Poly(Nbe-g-(DMS-b-BA))** can be conducted from both approaches. Also, it has to be taken into account, that the macromonomers used for the "grafting-through" process already exhibited PDI values of 1.2 (*cf*. Figure 81), which of course, is impossible to reduce by further polymerization.

6 Concluding Remarks

In the previous chapters 0 and 4, different aspects that are relevant for the development of new ruthenium based initiators for olefin metathesis, in particular for their application in ring opening metathesis polymerization – ROMP – have been evaluated. In this context, ROMP has largely been employed as an analytical tool or amplifier, rather than for the sake of producing polymers. In most metathesis reactions like ring closing metathesis (RCM), the active catalytical species is the perpetually regenerated ruthenium-methylidene, and the pre-catalyst is only relevant for the very first initiating step. Thus, catalytic activity of the complex can be portrayed by conversion, longevity or calculated turn-over numbers; however, initiation rates are difficult to be determined. In contrast to that, ROMP yields different products (i.e. polymers exhibiting different molecular weight distributions) depending on the activity of the ruthenium pre-catalyst (initiator). Hence, initiation rate and propagation behavior (the latter reflecting activity of the actual active species) can be roughly estimated by determination of the number molecular weight and the polydispersity, and by following conversion with time, respectively. Sterical and electronic tuning of the various initiators' ligands and subsequent testing in ROMP has confirmed some expected effects, but has also revealed some surprising facts and correlations.

All phosphine-tuned initiators under investigation (*cf*. chapter 0) showed improved initiation efficiency compared to reference initiator **M2**, which bears PCy_3 and produces polymers with the highest M_n and PDI values for the employed monomers **EsterMon** and **EtherMon** (c*f.* Table 5). Complex **PPh₃CF₃** featuring the most electron-withdrawing group, *i.e.* the CF_3 group, showed the best results in terms of initiaton and propagation behavior. Regardless of the respective phophsine, none of the complexes under investigation outperforms the pyridine bearing initiator **M31** in this respect. The presented results are in line with previous works carried out by Grubbs *et al.* who compared initiation constants in polymerization of 1,4-cyclooctadiene (COD) with analogous benzylidene complexes. It is to note, that back-biting occurs in COD polymerizations and a correlation of the electronegativity χ with molecular weight M_n is not possible in this case.

In chapter 0, three different NHC ligands, namely **SIMes**, **SIPr** and **SI-o-Tol** have been investigated. The conducted experiments clearly show that the NHC ligand severely interferes in the metathesis process, which can be visualized by judicious ROMP experiments and careful analysis of the resulting polymers. Both, initiation and propagation rate are affected by the nature of the NHC ligand, resulting in distinctly different molecular weight distributions within the different complex classes.

Recapitulating, it is stated that the increased steric bulk of SIPr leads to facilitated initiation compared to SIMes. The opposite effect is observed for the propagation rate which is lower for SIPr complexes but enormously high for SI-o-Tol, the smallest NHC ligand within the series. Bimodality of the molecular weight distribution is occurring in all experiments employing SIPr complexes; however the reason therefore could not be clearly made out. For further investigations on that matter, the employment of MALDI-TOF mass spectroscopy of growing oligomers in order to determine a potential second active species is currently being explored. The NHC ligand also influences the *cis/trans* ratio of the formed double bonds. As the nature of the monomer plays a major role, a general trend is difficult to be claimed. The only consistent observation was that SIPr complexes generally yield more *trans* double bonds compared to SIMes complexes with the same monomer.

By the example of closely related ruthenium based metathesis catalysts featuring a chelating ester carbene ligand, chapter 0 revealed surprising correlations and facts on structure and activity related differences. The impact of the NHC ligand and the electronic features of the benzylidene ester ligand led to unexpected synthetic differences regarding the number and accessibility of possible products. Once more, the yet unproven hypothesis that the SIPr NHC ligand exclusively yields *trans* dichloro geometry in the resulting complexes, was strengthened: Synthesis of complex **6: OMe-SIPr** was clearly the easiest and most straight forward process within this study, showing 100% conversion, highest isolated yield (72 %) and extraordinary stability, which indicates a pronounced thermodynamical preference in contrast to its *cis* dichloro counterpart **5a: OMe-SIMes** (77% conversion according to NMR, 35% isolated yield: *cf*. reference 72b, supporting information). ROMP benchmark reactions revealed considerable deviations in activity (and stability) at moderate temperature; in particular higher activity (resulting from a weaker chelate) of NO_2-compounds can be stated. However, this effect is negligible at 80°C, where all complexes perform rather similar as initiators for ROMP. As for RCM reactions, the poor reproducibility within the experimental series is most striking. Ten experiments with complexes **5a** and **6** each resulted in a conversion of the substrate under investigation, 4-methyl-N,N-bis(2-methylallyl)benzenesulfonamide, of 64.7±14 % and 73.8±9 % respectively. The deviation is incredibly high and most clear when comparing experiment number 4 and 5 (Table 15) featuring complex **5a** (93 % versus 50 % conversion). Obviously, the active methylidene species in RCM is extremely sensitive to minimal changes regarding oxygen and moisture, suggesting the use of a glove-box for these experiments.

Also chapter 0 evaluates a family of ruthenium initiators featuring chelating carbene ligands. The characteristics of four complexes based on the Hoveyda-Grubbs catalyst

design exhibiting ligands with an extended π-system was disclosed for ROMP.[109] Huge differences in their activity were found, depending on the position of the condensed phenyl ring(s). Complex **extHov1** was shown to be a highly active initiator at ambient conditions and a potential candidate for controlled polymerization of certain norbornene based monomers. In contrast, complexes **extHov2**, **extHov3** and **extHov4** are inactive at room temperature, but can be turned active upon heating. Especially complex **extHov2** is a promising initiator for the polymerization of **DCPD**, as the trigger temperature is in the right temperature range. It was made clear that at first sight minor changes of the initiator's chelating carbene ligand can have a distinct effect on its performance in ROMP. Even clearly disparate applications, namely **App$_{act}$** and **App$_{lat}$** (*cf*. Abstract) can be targeted with different members of the same initiator family.

For **App$_{lat}$,** the thermally triggered polymerization with latent initiators, a test procedure has been developed to evaluate the scope of latent ROMP initators for their applicability in the curing of dicyclopentadiene (**DCPD**) – *cf*. chapters 0 and 4. For this monomer, analysis by GPC is no longer feasible as polymerized DCPD yields a heavily cross-linked and therefore insoluble thermoset. A first impression of the initiators' activity was gained by simply following the curing process at room temperature or 60°C in open tubes. Then, simultaneous thermal analysis (STA), combining differential scanning calorimetry (DSC) and thermo-gravimetric analysis (TGA) was used for determining the switching temperature for different loadings. **DCPD** was also cured in larger scale for the production of shoulder test bars which are used for tensile strength tests. Commercially available initiator **M2** was screened first as a reference and turned out to perform well beyond expectations. Good mechanical properties of the test specimen could be achieved with low loadings (10-20 ppm). Yet, the low switching temperature (**M2** is active at room temperature and only latent at very low loadings) is an obstacle for homogenous systems, as the time frame for processing is very low. In that context, the much more latent initiator **M22** was thoroughly tested. After optimization of the test parameters, shoulder test bars with similar mechanical properties could be prepared. A minimal loading of 25 ppm initiator was found to be necessary for reproducible results. Swelling in toluene resulted in a weight increase of up to 220 % of the initial weight. This suggests that even highly cross-linked material can incorporate considerable amounts of solvent. However, it seems that the oxidized layer on the surface potentially prohibits this effect and toluene was supposedly taken via the freshly cut areas. This section can be summarized as an important contribution to currently ongoing investigations on the use of single-component, robust initiators for the curing of DCPD. Initiator **M22** that has been developed within the EUMET

---

[109] Leitgeb, A., Szadkowska, A., Michalak, M., Barbasiewicz, M., Grela, K., Slugovc, C. *J. Pol. Sci. Part A: Polym. Chem.* **2011**, *49*, 3448-3454.

project constitutes a successful example of a thermally switchable initiator that on the one hand provides enough processing time without premature initiation, but on the other hand will get highly active and polymerize fast when exposed to enough thermal energy. The herein applied and necessary two-step-curing (Figure 76) can definitely be evaluated advantageously regarding post-treatment of semi-cured specimen (e.g. cutting etc.).

Finally, an impressive and unprecedented example for the applicability of initiator **M31** for tailored polymer architectures (**App$_{act}$**) is given in chapter 5. **M31** was used for the synthesis of organic-inorganic hybrid brush-co-polymers, whereas ROMP was either used before or after an ATRP step. Low conversions and broad molecular weight distributions could be largely avoided by co-polymerization with **EsterMon** and higher amounts of solvent. Thus, polymers with satisfactorily high molecular weights and low PDI values have been realized.

7   EXPERIMENTAL PART

7.1 Syntheses of Ruthenium Complexes
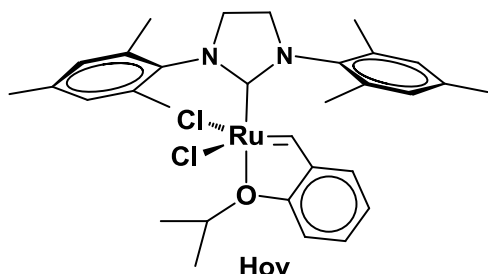
Hov

(SPY-5-31) - Dichloro-(κ^2(C,O)-2-isopropylether-benzylidene) - (1,3-bis(2,4,6-trimethylphenyl) 4,5-dihydroimidazol-2-ylidene)ruthenium: Preparation of complex **Hov** has already been published in: Wappel, J.; Urbina-Blanco, C. A.; Abbas, M.; Albering, J. H.; Saf, R.; Nolan, S. P.; Slugovc, C. *Beilstein J. Org. Chem.* **2010,** *6,* 1091–1098 (Reference 71b).
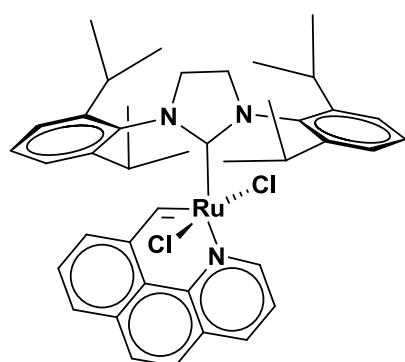
SIPr-benzoquinoline

(SPY-5-31) - Dichloro-(κ^2(C,N)-2-(benzo[h]quinolin-10-yl) methylidene) - (1,3-bis(2,6-diisopropylphenyl) 4,5-dihydroimidazol-2-ylidene)ruthenium: SIPr-py complex **M32** (150 mg, 0.18 mmol, 1 eq) was dissolved in 9 mL of freshly degassed dichloromethane. Benzoquinoline ligand L-1 (1.5 eq, 55 mg, 0.26 mmol) was added. The mixture was stirred for 48 h at room temperature, whilst the colour turned from red to bright green. The solvent was evaporated, and the crude product was subjected to column chromatography (silica, cyclohexane: ethylacetate 3+1, TLC r_f = 0.43). The final clean complex was isolated as light green powder in 81% yield (110 mg). The structure was confirmed by NMR spectroscopy and elemental analysis.

^{1}H-NMR (δ, 20°C, CDCl$_3$, 300 MHz): 19.06 (s, 1H, Ru=C*H*); 8.61-8.60 (d, $^3J_{HH}$ = 5.2 Hz, $^4J_{HH}$ = 3.67 Hz, 1H, bq^2); 8.15-8.12 (d, $^3J_{HH}$ = 8.1 Hz, 1H, bq^7); 8.09-8.06 (d, $^3J_{HH}$ = 8.1 Hz, 1H, bq^4); 7.91-7.86 (d, $^3J_{HH}$ = 8.8 Hz, 1H, bq^5); 7.67-7.59 (m, 4H, bq^{6,8}, Ar^{SIPr}); 7.52-7.44 (dd, $^3J_{HH}$ = 8.1 Hz, $^3J_{HH}$ = 5.2 Hz, 1H, bq^3, m, 4H, Ar^{SIPr}); 6-97-6-95 (d, $^3J_{HH}$ = 6.87 Hz, 1H, bq^9); 4.20 (s, 4H,NC*H$_2$*); 3.77 (bs, 4H, C*H*^{Pri}); 1.35-1.16 (24H, C*H$_3$*^{Pri}).

^{13}C-NMR (δ, 20°C, CDCl$_3$, 125MHz): 306.2 Ru=C*H*; 217.7 (1C, N*C*N); 149.4, 148.6, 145.9, 141.7, 137.2, 136.1, 129.9, 129.8, 129.5, 129.3, 128.6, 127.0, 125.4, 124.7, 122.8, 121.3 (25C, bq$^{2-10}$, Ar$^{1-6}$); 54.8 (2C, N*C*H$_2$); 27.06 (8C, Pr^i); 23.9 (4C Pr^i).

^{1}H-NMR (δ, 20°C, CD$_2$Cl$_2$, 300 MHz): 19.00 (s, 1H, Ru=C*H*); 8.71-8.69 (d, $^3J_{HH}$ = 5.2 Hz, 1H, bq^2); 8.22-8.20 (d, $^3J_{HH}$ = 8.0 Hz, 1H, bq^7); 8.17-8.15 (d, $^3J_{HH}$ = 8.0 Hz, 1H, bq^4); 7.99-7.96 (d, $^3J_{HH}$ = 9.0 Hz, 1H, bq^5); 7.75-7.61 (m, 4H, bq^{6,8}, Ar^{SIPr}); 7.56-7.45 (dd, $^3J_{HH}$ = 8.0

Hz, $^3J_{HH}$ = 5.2 Hz, 1H, bq^3, m, 4H, Ar^{SIPr}); 6-99-6-98 (d, $^3J_{HH}$ = 7.1 Hz, 1H, bq^9); 4.18 (s, 4H,NCH_2); 3.37 (bs, 4H, CH^{Pr^i}); 1.35-1.16 (24H, C$H_3^{Pr^i}$).

Elemental analysis of **SIPr-benzoquinoline** calculated for $C_{41}H_{47}Cl_2N_3Ru$ (753.8 g/mol) C, 65.33; H, 6.28; N, 5.57; found (Ø): C, 65.21; H, 6.20; N 5.51.
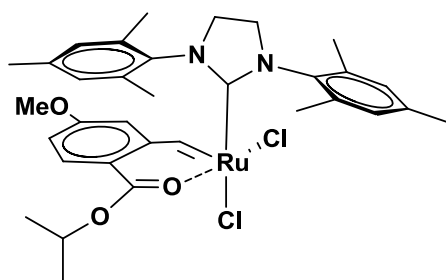
5a: OMe-SIMes

(SPY-5-34) – Dichloro - (κ^2(C,O) - (2-isopropyl ester-5-methoxy benzylidene) - (1,3-bis(2,4,6-trimethylphenyl) - 4,5-dihydroimidazol-2-ylidene) - ruthenium: Preparation of complex 5a has already been published in: Zirngast, M.; Pump, E.; Leitgeb, A.; Albering, J. H.; Slugovc, C. *Chem. Commun.* **2011**, *47*, 2261-2263 (Reference 72b).
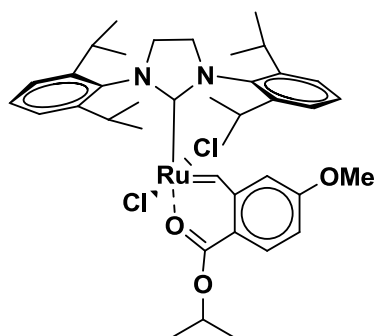
6: OMe-SIPr

(SPY-5-31) – Dichloro - (κ^2(C,O) - (2-iso-propyl ester-5-methoxy benzylidene) - (1,3-bis(2,6-diisopropylphenyl) - 4,5-dihydroimidazol-2-ylidene) - ruthenium: SIPr-py complex **M32** (400mg, 0.48 mmol, 1 eq) was dissolved in 15 mL of freshly degassed DCM. Vinyl ligand **3** (1.3 eq, 137 mg, 0.63 mmol) were added. The mixture was stirred for 48 h at room temperature, whilst the colour turned from red to green. The solvent was reduced to 3 mL, precipitation with n-pentane yielded a light green powder. Several washings using ultrasonic wave completely removed residual ligand and other impurities. The final clean complex was isolated 72% yield (267 mg). Crystals were obtained by dissolving a small amount of the complex in DCM and overlaying it with n-pentane in a loosely closed glass vial. XRD revealed 1 eq of DCM in the crystal structure, which is also confirmed by elemental analysis.

^{1}H-NMR (CDCl$_3$): 18.49 (s, 1H, Ru=C*H*); 8.00-7.97(d, 1H, $^3J_{HH}$ = 8.7 Hz, lig^5); 7.53 (t, 2H, $^3J_{HH}$ = 7.3 Hz, SIPr^4); 7.39-7.37 (d, 4H, $^3J_{HH}$ = 7.5 Hz, SIPr^3); 7.26-7.01 (dd, 1H, $^3J_{HH}$ = 6.1 Hz, $^4J_{HH}$ = 2.6 Hz, lig^4); 6.13-6.12 (d, 1H, $^4J_{HH}$ = 2.6 Hz, lig^2); 5.30 (s, CH$_2$Cl$_2$); 5.15 (hep, 1H, lig$^{Pr^i}$); 4.12 (s, 4H, NCH$_2$); 3.83 (s, 3H, OMe); 3.69 (bhep, 4H, SIPr$^{Pr^i}$); 1.35-1.18 (30H, lig^{Me}, SIPr^{Me}).

^{13}C-NMR (CDCl$_3$) 299.3(1C, Ru=*C*); 214.2 (1C, NCN); 172.8 (1C, C=O); 165.0, 160.1, 149.7, 149.1, 137.3, 134.2, 129.5, 124.8, 115.0, 113.9, 109.0 (18C, 2mes$^{1-6}$, bz$^{1-6}$); 71.7 (1C, OPr^i); 55.9 (1C, OMe); 54.6 (2C, NCCN), 53.6 (CH$_2$Cl$_2$); 28.7 (2C, mesPr^i); 26.6 (2C, mesPr^i), 24.2 (8C, C*H*$_3^{mes}$); 21.7 (2C, OC(CH$_3$)$_2$).

Elemental analysis of **6** calculated for $C_{40}H_{54}Cl_4N_2O_3Ru$ (853.75 g/mol): C, 56.27; H, 6.38; N, 3.28; found (∅): C, 56.34; H, 6.37; N, 3.59.
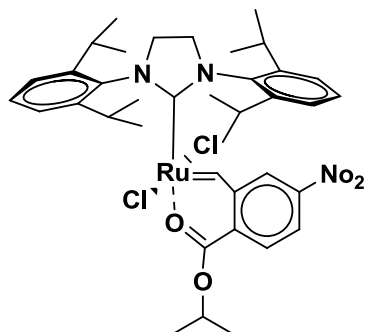
(SPY-5-31) – dichloro - (κ^2(C,O) - (2-iso-propyl ester-5-nitro benzylidene) - (1,3-bis(2,6 - diisopropylphenyl) - 4,5-dihydroimidazol-2-ylidene) - ruthenium: SIPr-py complex **M32** (120 mg, 0.144 mmol, 1 eq) was dissolved in 5 mL of freshly degassed DCM. Vinyl ligand 4 (1.3 eq, 44 mg, 0.187 mmol) were added. The mixture was stirred for 48 h at room temperature, whilst the colour turned from red to brownish-green. The solvent was evaporated, and the crude product was subjected to

7: NO$_2$-SIPr

column chromatography (silica, cyclohexane: ethylacetate 5/1, TLC rf = 0.37) The final clean complex was isolated as golden powder in 52% yield (60 mg). The structure was confirmed by NMR spectroscopy and elemental analysis.

^{1}H-NMR (CDCl$_3$, 300MHz) 18.47 (s, 1H, Ru=C*H*); 8.40-8.36 (dd, 1H, $^3J_{HH}$ = 8.7 Hz, $^4J_{HH}$ = 2.3 Hz, lig^4); 8.19-8.16 (d, 1H, $^3J_{HH}$ = 8.7 Hz, lig^5); 7.63 (t, 2H, $^3J_{HH}$ = 7.6 Hz, SIPr^4); 7.48-7.47 (d, 1H, $^4J_{HH}$ = 2.3 Hz, lig^2); 7.42-7.40 (d, 4H, $^3J_{HH}$ = 7.6 Hz, SIPr^3); 5.23 (hep, 1H, lig^{Pri}); 4.15 (s, 4H, NCH$_2$); 3.625 (bhep, 4H, SIPr^{Pri}); 1.34-1.32 (d, 6H, $^3J_{HH}$ = 6.2 Hz, lig^{Me}); 1.29-1.20 (d, bd, 24H, SIPr^{Me}).

^{13}C-NMR (CDCl$_3$, 125MHz) 292.8 (1C, Ru=*C*); 211.1 (1C, NCN); 172.3 (1C, C=O), 152.2, 149.1, 148.3, 136.8, 133.7, 130.2, 125.2, 125.1, 120.8, 119.6 (18C, 2mes$^{1-6}$, bz$^{1-6}$); 73.8 (1C, OPr^i); 54.7 (2C, NCCN); 28.9 (2C, mesPr^i); 26.7 (2C, mesPr^i), 24.2 (8C, *C*H$_3^{mes}$); 21.7 (2C, OC(*C*H$_3$)$_2$).

Elemental analysis of **7** calculated for $C_{38}H_{49}Cl_2N_3O_4Ru$ (784.8 g/mol): C, 58.23; H, 6.30; N, 5.36; found (∅): C, 57.89; H, 6.12; N, 5.40.
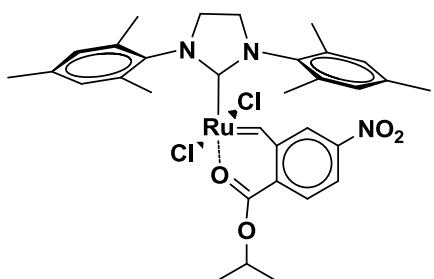
(SPY-5-31) – dichloro - (κ^2(C,O) - (2-iso-propyl ester-5-nitro benzylidene) - (1,3-bis(2,4,6-trimethylphenyl) - 4,5-dihydroimidazol-2-ylidene) - ruthenium: SIMes-py complex **M31** (287 mg, 0.383 mmol, 1 eq) was dissolved in 10 mL of freshly degassed DCM. 2-Vinyl-4-nitrobenzoesäureisopropylester 4 (1.5 eq, 135 mg, 0.574 mmol) were added. The mixture was stirred

8a: NO$_2$-SIMes

for 20 h at room temperature. The solvent was reduced to 3 mL, precipitation with n-pentane yielded a reddish-brown powder (179 mg) (crude NMR revealed a product mixture (two carbene species, one corresponding to *cis* dichloro structure (19.09 ppm,

25%) and one to the *trans*-py-adduct (18.78 ppm, 75%). Column chromatography (silica, DCM/MeOH = 20/1 to DCM/MeOH = 5/1) yielded clean product **8a** (, carbene signal at 18.71 ppm, corresponding to the *trans* dichloro complex without coordinated pyridine) and two mixed fractions. Total yield: 35 mg, 17.2%.

^{1}H-NMR (CDCl$_3$, 300MHz) 18.71(s, 1H, Ru=C*H*); 8.44-8.40 (dd, 1H, $^3J_{HH}$ = 8.7 Hz, $^4J_{HH}$ = 2.3 Hz, lig^4); 8.20-8.18 (d, 1H, $^3J_{HH}$ = 8.6 Hz, lig^5); 7.61-7.60 (d, 1H, $^4J_{HH}$ = 2.3 Hz, lig^6); 7.13 (s, 4H, Mes); 5.27 (hep, 1H, lig^{Pri}); 4.14 (s, 4H, NCH$_2$); 2.48 (s, 6H, SIMes^{Me4}); 2.48 (s, 12H SIMes^{Me2,6}); 1.32-1.30 (d, 6H, $^3J_{HH}$ = 6.3 Hz, iPr^{Me}).
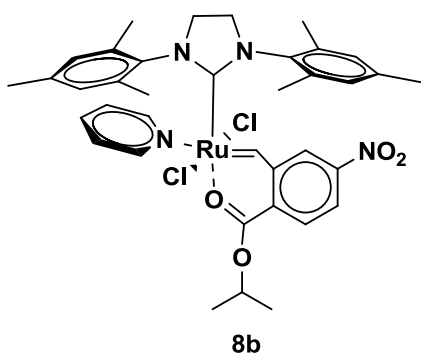
8b

(SPY-5-31) – dichloro - (κ^2(C,O) - (2-iso-propyl ester-5-nitro benzylidene) - (1,3-bis(2,4,6-trimethylphenyl) - 4,5-dihydroimidazol-2-ylidene) - 1-pyridyl- ruthenium: This complex occurs during the synthesis of **8a** (see above) and is in equilibrium with the same as long as pyridine from the parent complex M31 is present. **8b** was not purely isolated but detected in the raw NMR sprectrum. Crystals that were found in the NMR tube confirmed the proposed structure (see above). The pyridine ligand is lost upon purification with column chromatography, which then yields complex **8a**.

7.1.1 Syntheses of Chelating Carbene Ligands

L-1
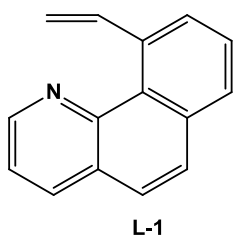
10-vinylbenzo[h]quinoline: Preparation of ligand **L-3** has already been published in: Szadkowska, A.; Gstrein, X.; Burtscher, D.; Jarzembska, K.; Wozniak, K.; Slugovc, C.; Grela, K.; *Organometallics* **2010**, *29*, 117–124 (Reference 77).

L-3
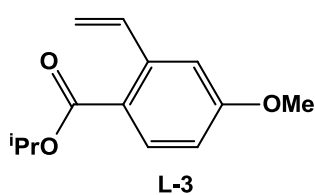
Isopropyl 4-methoxy-2-vinylbenzoate: Preparation of ligand **L-3** has already been published in: Zirngast, M.; Pump, E.; Leitgeb, A.; Albering, J. H.; Slugovc, C. *Chem. Commun.* **2011**, *47*, 2261-2263 (Reference 72b, electronic supporting information).
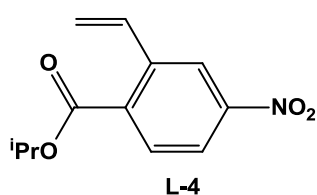
Isopropyl 4-nitro-2-vinylbenzoate: 2-Bromo-4-nitrobenzoic acid (1 eq, 600 mg, 2.44 mmol) was dissolved in 5 mL of *iso*-propanol. The mixture was cooled to 0°C before $SOCl_2$ (3.6 eq., 0.64 mL, 8.78 mmol) was added dropwise. The reaction was heated slowly to 80°C and stirred for 20 h. Excess $SOCl_2$ and *iso*-propanol were removed by distillation and the residue was dissolved in diethylether and extracted with water twice. The organic phase was then extracted with $NaHCO_3$ (sat) twice and dried over Na_2SO_4. After evaporation of the solvent isopropyl 2-bromo-4-nitrobenzoate was isolated as a yellow solid (604 mg, 95% yield). In the second step 2-bromo-4-nitrobenzoate (1 eq., 500 mg, 1.74 mmol), vinylboronic anhydride pyridine complex (3 eq., 501 mg 2.08 mmol) and K_2CO_3 (2 eq., 479 mg, 4.50 mmol) were dissolved in 15 mL degassed DME/H_2O (3:1). $Pd(PPh_3)_4$ (0.03 eq, 60 mg, 0.070 mmol) was added and the reaction mixture was heated to 90°C and stirred for 18 hours. The reaction mixture was extracted with water, Et_2O, 10% HCl- and saturated $NaHCO_3$ solution. The organic layer was dried with Na_2SO_4, filtered and evaporated. The orange, oily residue was purified by column chromatography, using cyclohexane/ethyl acetate 5:1 (v:v). Yield: 327 mg (80%), yellowish oil.
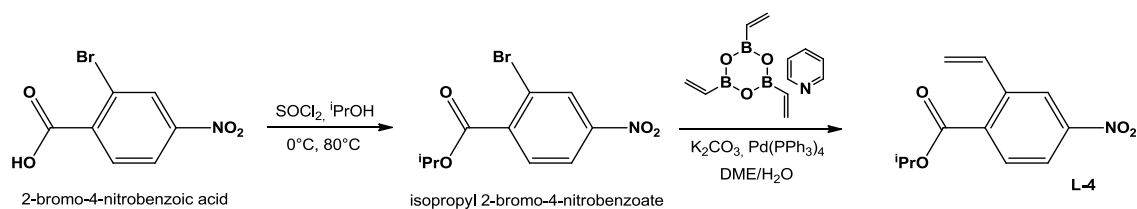
Scheme 26: Synthesis of ligand L-4

^{1}H-NMR (δ, 20°C, $CDCl_3$, 300 MHz): 8.41 (d, 1H, $^4J_{HH}$ = 2.6 Hz, ph[6]); 8.14-8.10 (dd, 1H, $^3J_{HH}$ = 8.8 Hz, $^4J_{HH}$ = 2.6 Hz, ph[4]); 7.98 - 7.95 (d, 1H, $^3J_{HH}$ = 8.7 Hz , ph[3]); 7.46 - 7.36 (q, 1H, $^3J_{HH}$ = 11.1 Hz, C*H*CH$_2$); 5.85-5.80, 5.55-5.51 (2d, 1H, $^3J_{HH}$ = 17.2 Hz, 1H, $^3J_{HH}$ = 10.9 Hz CHC*H$_2$*); 5.28 (m, 1H, $^3J_{HH}$ = 6.2 Hz, C*H*(CH$_3$)$_2$); 1.41 (d, 6H, $^3J_{HH}$ = 6.2 Hz, CH(C*H$_3$*)$_2$). ^{13}C{^{1}H}-NMR (δ, 20°C, $CDCl_3$, 75 MHz): 165.6 (1C, COO[i]Pr), 149.8 (1C, ph[4]), 140.8 (1C, ph[2]), 134.9 (1C, *C*HCH$_2$), 133.9 (1C, ph[1]), 131.5, 122.0, 121.86 (3C, ph[3,5,6]), 119.3 (1C, *C*H$_2$CH), 69.9 (1C, *C*H(CH$_3$)$_2$), 21.9 (2C, CH(*C*H$_3$)$_2$).

7.2 Syntheses of Substrates
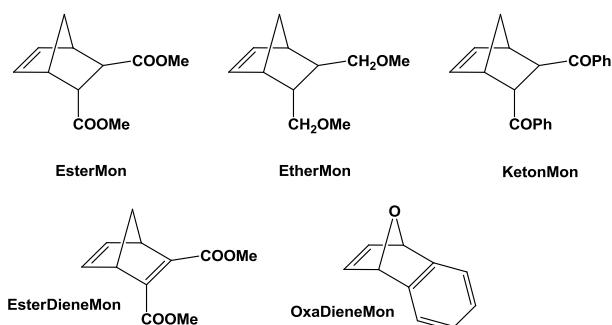
The norbornene based monomers *exo,endo*-Dimethylbicyclo[2.2.1] hept-5-ene-2,3-dicarboxylate (**EsterMon**), *exo,endo*-5,6-bis(methoxymethyl)-bicyclo[2.2.1]hept-2-ene (**EtherMon**), *exo,endo*-5,6-bis(phenylketon)-bicyclo[2.2.1]hept-2-ene (**KetonMon**), Dimethylbicyclo [2.2.1]hept-2,5-diene-2,3-dicarboxylate (**EsterDieneMon**) and 7-oxabenzonorbornadiene (**OxaDieneMon**) were synthesized according to literature procedures with Diels-Alder reactions of cyclopentadiene or furan and the corresponding Diels-Alder counterpart.[110]
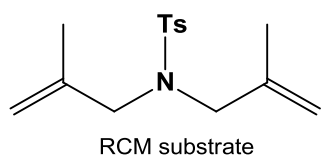
The RCM substrate 4-methyl-N,N-bis(2-methylallyl)benzenesulfonamide was synthesized according to literature.[111] 4-methylbenzenesulfonamide (1-58 g, 9.04 mmol, 1 eq), 3-bromo-2-methylprop-1-ene (2.6 mL, 25.8 mmol, 2.85 eq) and potassium carbonate (4.75 g, 27.12 mmol, 3 q) were put into a reactor together with 50 mL of acetonitrile and a stirring bar. The reactor was closed and the reaction was allowed to stir for 48 h at 110°C. After that time it was cooled to room temperature, K_2CO_3 was filtered off, and the solvent was rota-evaporated. The crude product was purified with column chromatography (silica, cyclohexane/ acetylacetate: 3+1) to yield a yellow oil (2.35 g, 93%). (TLC: r_f = 0.61)

7.3 Standard Benchmark ROMP Reactions

The standard benchmark reaction for all initiators investigated within this work was performed according Scheme 27. This reaction was performed as a preliminary test employing first of all the monomer **EsterMon** in order to judge activity and potential application fields of the initiators. For highly active initiators KetonMon was employed in subsequent reactions. All reactions were performed under nitrogen conditions using Schlenk technique.

---

[110] Kirmse, W.; Mrotzeck, U.; Siegfried, R. *Chem. Ber*. **1991**, *124*, 241-245.
[111] Elias, X.; Moreau, J. *Ad. Synth. Catal*. **2006**, *348*, 751-762.
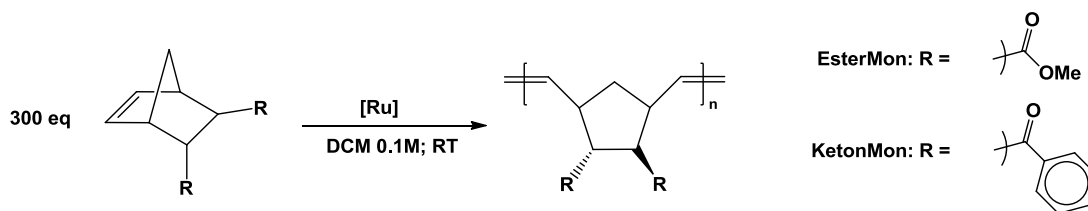
Scheme 27: standard benchmark reaction for ROMP

In general, 100 mg monomer and corresponding amount of freshly degassed DCM have been used (0.475 mmol and 4.8 mL for **EsterMon;** 0.331 mmol, 3.3 mL for **KetonMon**). Initiators stock solutions were used in order to be more precise. Usually, 2 eq were weighed into a small vial, put under nitrogen and dissolved in 1000 µL of solvent. 500 µL (1eq) thereof were put into a Schlenk flask and the dissolved monomer was added while stirring. The reaction was then monitored by TLC and $KMnO_4$ staining (silica, cyclohexane/acetylacetate (3+1)). While the monomers exhibit an r_f- value of ~0.4, the polymers don't move on the TLC plate. Thus, conversion can be easily followed. Table 29 lists the amount of initiators required (1 eq), for the benchmark, see Scheme 27.

Table 29: Required amounts of initiators for benchmark reaction (Monomer : initiator) = 300

initiator	[M] (g/mol)	for EsterMon[a] (mg)	for KetonMon[b] (mg)
M31	748	1.18	0.75
M2	948	1.50	0.95
Hov	627	0.99	0.63
SIPr-PCy₃	1033	1.63	1.03
SIPr-Py	832	1.31	0.83
SIPr-BrPy	911	1.44	0.91
SI-o-Tol	893	1.41	0.89
SIPr-benzoquinoline	753	1.19	0.75
OMe-SIMes	684	1.08	0.68
OMe-SIPr	768	1.21	0.77
NO₂-SIMes	699	1.10	0.70
NO₂-SIPr	784	1.24	0.78
extHov1]	676	1.07	0.68
extHov2	676	1.07	0.68
extHov3	676	1.07	0.68
extHov4	726	1.15	0.73
M22	874	1.38	0.87

[a] $1.58*10^{-3}$ mmol initiator for 300 eq **EsterMon**; [b] $1.10*10^{-3}$ mmol initiator for 300 eq **KetonMon**

7.4 Reaction Profiling NMR spectroscopy

7.4.1 NHC Study (SIMes, SIPr, SI-o-Tol)

Polymerization profiling using ^{1}H-NMR spectroscopy (CDCl$_3$, 500 MHz, 25°C): abovementioned experiments were performed using a ratio of initiator to monomer of 1:50 and CDCl$_3$ as solvent in a concentration of 0.1 M with respect to the monomer. CDCl$_3$ was degassed for 15 min before use. 0.0033 mmol of the respective initiators (corresponds to 3.42 mg for **SIPr-PCy$_3$**, 2.75 mg for **SIPr-Py**, 2.95 mg for **SI-o-Tol**, 2.47 mg **M31**, and 3.12 mg for **M2**) was weighed into a vial, purged with argon and dissolved in 600 µL of degassed CDCl$_3$. 300 µL of this solution was transferred to an NMR tube (purged with argon). **KetonMon** (25 mg, 0.0825 mmol) was dissolved in 1060 µL CDCl$_3$ and 530 µL thereof were added quickly to the initiator with a micropipette. After fast mixing, the ^{1}H-NMR spectrum of the reaction was immediately recorded (500 MHz). An automatic program measured subsequent spectra in predefined frequency until complete conversion to the polymer was reached. The conversion was determined by integration of the respective NMR peaks stemming from the double bond in **KetonMon** (6.43 and 5.95 ppm) and the corresponding polymer (5.67 – 4.67 ppm).

7.4.2 Extended Hoveyda Initiators

Polymerization profiling using ^{1}H-NMR spectroscopy (CDCl$_3$, 300 MHz, 25°C) (Figure 54): abovementioned experiments were performed using a ratio of initiator to monomer of 1:50 and CDCl$_3$ as solvent in a concentration of 0.1 M with respect to the monomer. CDCl$_3$ was degassed for 15 min before use. 0.0033 mmol of the respective initiators (corresponds to 2.2 mg for **extHov1-3**, 2.4 mg for **extHov4**, 2.1 mg for **Hov**, 2.5 mg **M31**, and 3.1 mg for **M2**) was weighed into a vial, purged with argon and dissolved in 600 µL of degassed CDCl$_3$. 300 µL of this solution was transferred to an NMR tube (purged with argon). **KetonMon** (50 mg, 0.165 mmol) was dissolved in 1060 µL CDCl$_3$ and 530 µL thereof were added quickly to the initiator with a micropipette. After fast mixing, the ^{1}H-NMR spectrum of the reaction was immediately recorded (300 MHz). Subsequently, spectra were recorded at regular intervals until complete conversion to the polymer was reached. The conversion was determined by integration of the respective NMR peaks stemming from the double bond in **KetonMon** (6.43 and 5.95 ppm) and the corresponding polymer (5.67 – 4.67 ppm).

7.5 Scope in Controlled Polymerization

7.5.1 NHC-Study (SIMes, SIPr, SI-o-Tol)

Evaluation of the scope in controlled polymerization - variation of polymer chain length (Figure 31, Figure 32, Table 7): For the evaluation of **SIPr-Py**, stock solutions of the initiator in dichloromethane were freshly prepared. Experimental details are given in Table 30and Table 31. For the evaluation of **SIPr-PCy$_3$**, stock solutions of the initiator in dichloromethane were freshly prepared. Experimental details are given in Table 32. Data for **M31** were extracted from reference 72a.

Table 30: test series controlled polymerization: KetonMon, SIPr-Py (*cf*. Figure 31)

monomer	SIPr-Py[a]		KetonMon		Solvent[b]
equivalents	µL	mmol	mg	mmol	mL
200	400	0.23	139	0.46	4.6
450	200	0.46	157	0.52	5.2
600	150	0.86	156	0.51	5.1
900	100	0.57	157	0.52	5.2

[a]: (5.7*10^{-3} M: 7.65 mg SIPr-Py in 1600 µL DCM); [b] total amount

Table 31: test series controlled polymerization: EsterMon, SIPr-Py (*cf*. Figure 31)

monomer	SIPr-Py[a]		EsterMon		Solvent[b]
equivalents	µL	mmol	mg	mmol	mL
200	400	1.88	79.1	0.37	3.7
450	300	1.42	134	0.63	6.3
600	200	0.94	119	0.56	5.6
900	200	0.94	178	0.852	8.5

[a]: (4.71*10^{-3} M: 6.27 mg SIPr-Py in 1600 µL DCM); [b] total amount

Table 32: Test series controlled polymerization: EsterMon, SIPr-PCy$_3$ (*cf*. Figure 31)

monomer	SIPr-PCy$_3$[a]		EsterMon		Solvent[b]
equivalents	µL	mmol	mg	mmol	mL
200	400	1.92	80	0.38	3.8
450	300	1.44	136	0.65	6.5
600	200	0.96	121	0.57	5.7
900	150	0.72	136	0.65	6.5

[a]: (4.81*10^{-3} M: 7.95 mg SIPr-PCy$_3$ in 1600 µL DCM); [b] total amount

7.5.2 Extended Hoveyda Initiators

Evaluation of the scope in controlled polymerization - variation of polymer chain length (Figure 55, Table 19): 100 mg of **KetonMon** and a total amount of 4.7 mL of dichloromethane (freshly degassed) were used for all experiments in this series in order to maintain a concentration of 0.1 M with respect to the monomer. Stock solutions of **KetonMon** (100 mg*mL^{-1}, 0.33 M) and the initiators **M31**, **Hov** (each 0.0022 M) and **extHov1** (0.0032 M)[112] were prepared. A Schlenk flask with a stirring bar was charged with dichloromethane and the corresponding amount of initiator solution to achieve the envisaged chain length. One milliliter of the monomer solution was quickly added. The used amounts are exemplarily listed in Table 33 for **M31**. Reactions were run at room temperature and progress was frequently monitored by TLC until complete conversion had been reached (all reactions were completed within 24 hours). After quenching the initiator with a large excess of ethyl vinyl ether (200 μL), the solvent was reduced to 1 mL, the polymer was precipitated in methanol, dried in vacuum and subjected to GPC analysis in order to determine the molecular weight and polydispersity.

Table 33: test series controlled polymerization: M31 (*cf*. Figure 55)

monomer equivalents	M31[a]	KetonMon[b]	DCM
150	1000 μL	1000 μL	2700 μL
300	500 μL	1000 μL	2200 μL
450	333 μL	1000 μL	3367 μL
600	250 μL	1000 μL	3450 μL
900	167 μL	1000 μL	3533 μL

[a]: 2.2*10^{-3} M: 5.76 mg in 3500 μL DCM [b] 522 mg in 5220 μL DCM

Evaluation of the scope in block-co-polymer synthesis (Figure 57): Complex **extHov1** (0.75 mg, 1.1*10^{-3} mmol) was dissolved in 1.7 mL of dichloromethane. 150 equivalents of the first monomer (**EsterMon**: 34.7 mg; **KetonMon**: 50.0 mg) was added and the reaction was monitored via TLC until no monomer could be detected anymore. Then, 150 equiv of the second monomer, dissolved in 1.7 mL DCM, was added. Again, the reaction was monitored until completion, before being quenched with excess ethyl vinyl ether. The polymer was collected upon precipitation in cold methanol, GPC analysis followed. The same procedure was accomplished using reference initiator

---

[112] Polymers with different chain lengths were prepared with **extHov1** (*cf*. Table 12)

M31 (0.82 mg, $1.1*10^{-3}$ mmol). ^{1}H-NMR spectra were recorded which did not differ depending on the monomer order or initiator used, as expected. ^{1}H-NMR (300 MHz, CDCl$_3$): 7.8-7.1 (m, 10H, Ph), 5.3_4.7 (m, 2H + 2H, HC=CH), 3.7-3.6 (m, 6H, COOCH$_3$), 4.3_2.3 (m, 4H + 4H, c^{Pen}), 2.1_1.1 (m, 2H + 2H, c^{Pen});

7.6 Sample preparation for STA

7.6.1 STA measurements with EtherMon

Sample preparation for STA measurements with EtherMon (Figure 62): Complexes **extHov2**, **extHov3** (each 3.4 mg), and **extHov4** (3.7 mg) were dissolved in 1 mL dichloromethane (each $5.02*10^{-3}$ mmol*mL^{-1}). 220 µL of this solution was transferred into a small glass vial and almost dried with an N$_2$-stream. **EtherMon** (100 µL, 100 mg, 0.55 mmol) was added and then the residual solvent was removed by an N$_2$-stream, thus perfectly mixing the batch. The mixture was immediately shock-frozen in liquid nitrogen to avoid any premature activation. For transportation the vial was stored in a Styrofoam container. About 15–18 mg of the mixture was transferred into a cooled DSC pan, which was then subjected to the STA run. The analysis was run with a constant helium gas stream of 50 mL*min^{-1} at a heating rate of 3 K*min^{-1}, starting at 20 °C.

7.6.2 STA measurements with DCPD

Sample preparation for extHovs (Figure 62 3.4.3): As **DCPD** is solid at room temperature; it was molten in a 35 °C water bath before use. Initiators **extHov2**, **extHov3** (each 3.4 mg), and **extHov4** (3.7 mg) were dissolved in 1 mL dichloromethane (each $5.02*10^{-3}$ mmol*mL^{-1}). 60 µL of this stock solution ($0.3*10^{-3}$ mmol catalyst) was transferred into a small glass vial, and 1.0 mL of liquid DCPD (7.4 mmol) was added with a syringe, so that the batch was well mixed. The total content of solvent in the mixture is 7.4 %wt (d$_{DCM}$ = 1.33 g*mL^{-1}, d$_{DCPD}$ = 0.98 g*mL^{-1}). The vial was immediately put into liquid nitrogen to shock-freeze the mixture. For transportation the vial was stored in a Styrofoam container. About 15–18 mg of the mixture was transferred into a cooled DSC pan, which was then subjected to the STA run. The analysis was run with a constant He gas stream of 50 mL*min^{-1} at a heating rate of 3 K*min^{-1}, starting at 20 °C.

Sample preparation for M22 (chapter 4.1): Initiator **M22** (11.01 mg) was dissolved in 1 mL dichloromethane ($12.67*10^{-3}$ mmol*mL^{-1}). This stock solution was used for total initiator loadings of 100, 75, 50 and 25 ppm respectively. For the highest loading, 60 µL

of this stock solution ($0.75*10^{-3}$ mmol catalyst) was transferred into a small glass vial, and 1.0 mL of liquid DCPD (7.4 mmol) was added with a syringe, so that the batch was well mixed. For lower loadings the stock solution was diluted accordingly. The total content of solvent in the mixture is 7.4 %wt (d_{DCM} = 1.33 g*mL^{-1}, d_{DCPD} = 0.98 g*mL^{-1}). The vial was immediately put into liquid nitrogen to shock-freeze the mixture. For transportation the vial was stored in a Styrofoam container. About 15–18 mg of the mixture was transferred into a cooled DSC pan, which was then subjected to the STA run. The analysis was run with a constant He gas stream of 50 mL*min^{-1} at a heating rate of 3 K*min^{-1}, starting at 20 °C.

Sample preparation for M2 (chapter 4.1): Initiator **M2** (3.59 mg) was dissolved in 1500 µL dichloromethane ($2.52*10^{-3}$ mmol*mL^{-1}). 60 µL of this stock solution ($0.75*10^{-3}$ mmol catalyst) was transferred into a small glass vial, and 1.0 mL of liquid DCPD (7.4 mmol) was added with a syringe, so that the batch was well mixed. The total content of solvent in the mixture is 7.4 %wt (d_{DCM} = 1.33 g*mL^{-1}, d_{DCPD} = 0.98 g*mL^{-1}). The vial was immediately put into liquid nitrogen to shock-freeze the mixture. For transportation the vial was stored in a Styrofoam container. About 15–18 mg of the mixture was transferred into a cooled DSC pan, which was then subjected to the STA run. The analysis was run with a constant He gas stream of 50 mL*min^{-1} at a heating rate of 3 K*min^{-1}, starting at 20 °C.

7.7 ROMP-ATRP graft co-polymers

7.7.1 Macro-Monomer Synthesis

Macro-monomers **MonGW21**, **MonGW31** and **MonGW32** have been synthesized by Georg Witek.[113] A schematic draft is given in Scheme 28. The synthesis was started from bicyclo[2.2.1]hept-5-ene-2-carboxylic acid (predominantly *endo*). The acid was reduced to the alcohol by using lithium aluminum hydride (LAH). In the next step the corresponding chloride was synthesized by use of triphenylphosphine and CCl_4 (Appel reaction). The lithiation was achieved using the arene-adducts (Li(naph)) (corresponding to either lithium-naphthalene or lithium-4,4'-di-*tert*-butylbiphenyl (Freeman's reagent)). Finally, hetero-difunctional PDMS (**MonGW21**) was obtained by *in situ* ring opening polymerization of cyclic hexamethyl trioxatrisilinane and termination by an adequate chlorosilane (*cf*. Scheme 28). The corresponding ^{1}H-NMR spectrum is given in Figure 88. **MonGW31** and **Mon GW32** have been achieved by ATRP of methyl methacrylate (*cf*. Scheme 29) or butyl acrylate (*cf*. Scheme 30) respectively, using **MonGW21** as initiator.
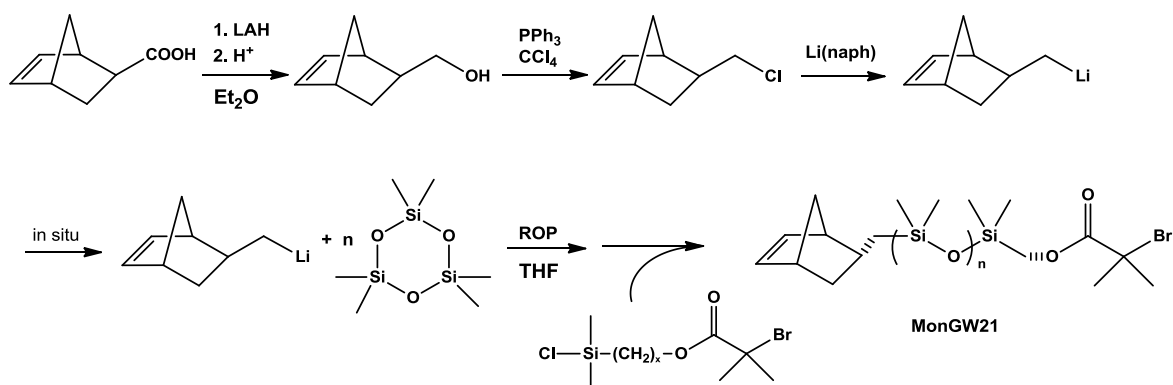
Scheme 28: Overview for the synthesis of MonGW21[113]; (1): LAH/Et₂O; (2): PPh₃/CCl₄; (3): Li(naphthalene)/Et₂O; (4): THF

---

[113] Witek G.; Leitgeb, A.; Uhlig, F.; Matyjaszewski, K. *unpublished results*
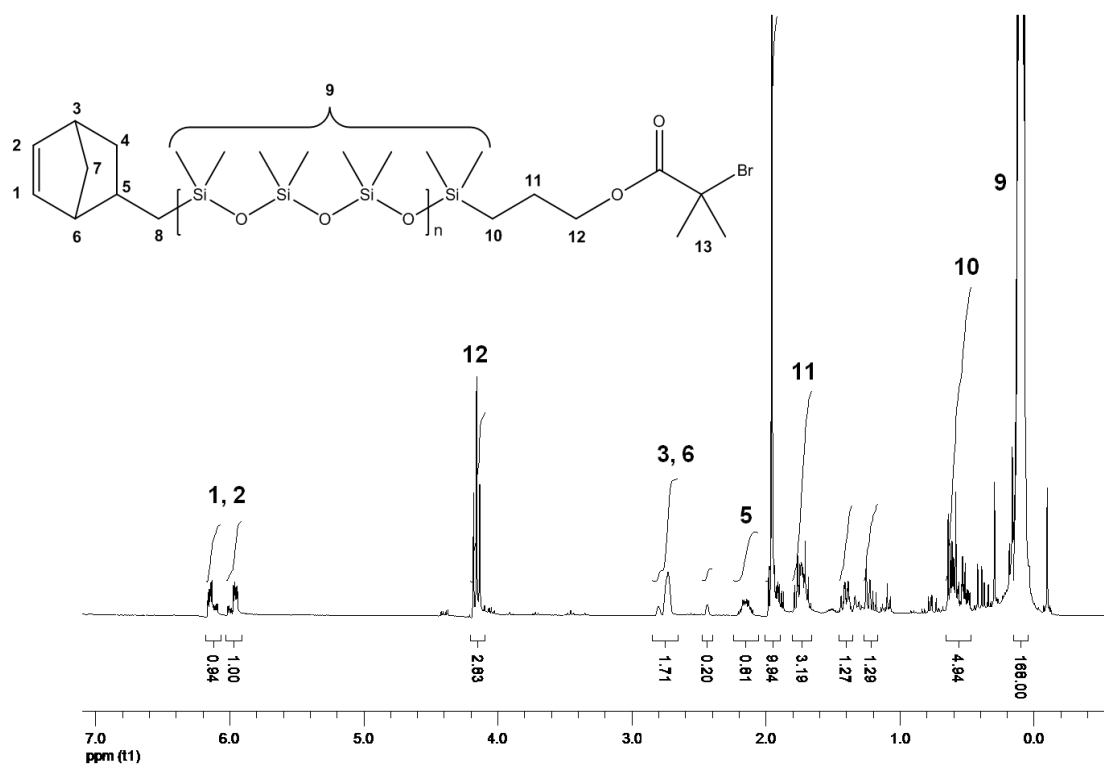
Figure 88: ^{1}H-NMR spectrum of MonGW21
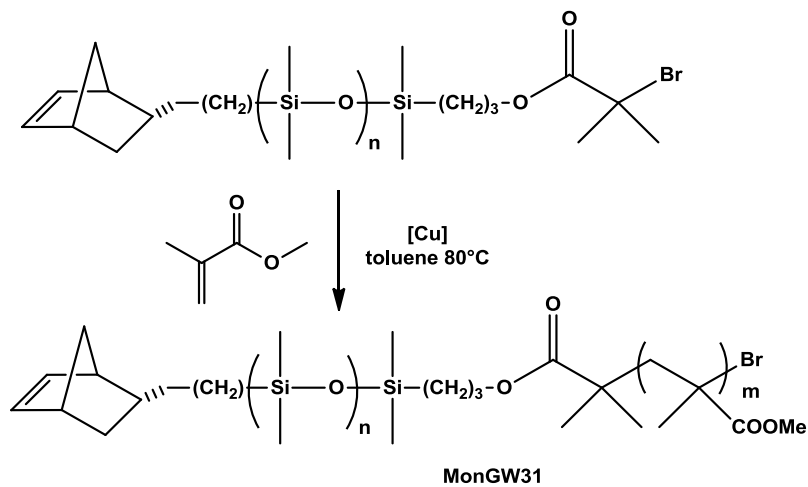
Scheme 29: Synthesis of MonGW31[113] by ATRP of methyl methacrylate using MonGW21 as initiator
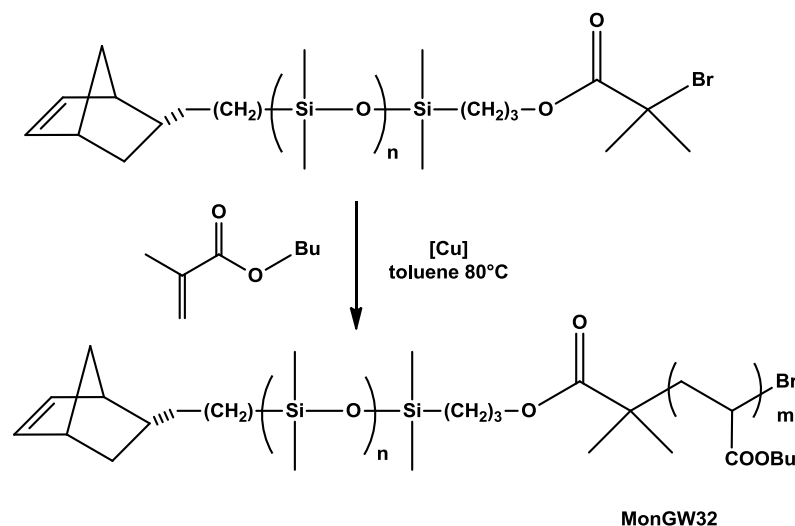
Scheme 30: Synthesis of MonGW32[113] by ATRP of butylacrylate using MonGW21 as initiator

7.7.2 ROMP Homo-Polymerizations

Homo-polymerization of **MonGW21:** 1.0 mL of a stock solution of **M31** in dichloromethane was freshly prepared (1.2 mg, $1.6 \ast 10^{-3}$ mmol). A Schlenk flask was charged with **MonGW21** (100 mg, 2.0 mmol) dissolved in DCM (1750 µL). 250 µL of the stocksolution (resulting in a monomer to initiator ratio of 50) were added, immediately yielding the yellowish colour of initiated **M31**. The mixture was stirred for 24h maintaining regular TLC control (silica, cyclohexane, ethylacetate (3+1), r_f (monomer) = 0.71). After that time no further progress was noted and the reaction was quenched with ethylvinylether and stirred for another 20 min. Solvent was reduced to 1 mL and the mixture was precipitated in cold stirred methanol (yielded turbid solution). The methanol was rota-evaporated and the polymer was dried in vacuo before GPC and NMR analysis.

Homo-polymerization of **MonGW31** and **MonGW32:** Again, a monomer to initiator ratio of 50 was applied. 1.0 mL of a stock solution of **M31** in dichloromethane was freshly prepared (1.9 mg, $2.5 \ast 10^{-3}$ mmol). A Schlenk flask was charged with **MonGW31** (140 mg, $1.3 \ast 10^{-2}$ mmol) dissolved in DCM (3900 µL). 100 µL of the stock solution were added yielding an overall concentration of $3.0 \ast 10^{-3}$M with respect to the monomer. The reaction was quenched after 3 h and usual work-up followed (cf. MonGW21). The same procedure was accomplished with **MonGW32** (133 mg, $1.3 \ast 10^{-2}$ mmol) dissolved in 1900 µL of DCM for an overall concentration of $6.0 \ast 10^{-3}$M with respect to the monomer. After 6 h the reaction was quenched and worked up for analyses.

7.7.3 ROMP Co-Polymerizations

Co-polymerizations of **EsterMon** with **MonGW21**, **MonGW31** and **MonGW32:** For all co-polymerizations a Schlenk flask was first charged with the two monomers dissolved in dichloromethane. **M31** was added from a freshly prepared stock solution. Concentration with respect to the monomer was adapted individually to the reaction. The experimental details are summarized in the following tables.

Table 34: Experimental details of the copolymerization of $[(Mon1)_4(GW021)_1]_m$

ratios		EsterMon		MonGW21		M31[a]	DCM[b]	c[c]	time[d]
m	DP_{target}	mg	mmol	mg	mmol	µL	mL	M	h
10	50	16.6	8.0E-2	100	2.0E-2	1000	6.5	1.5E-2	2.0
50	250	33.6	0.16	202	4.0E-2	400	6.0	3.3E-2	4.0
200	1,000	42.05	0.20	252	5.0E-2	200	5.0	2.0E-3	1.5

[a] stock solution: 3.0 mg **M31** in 2.0 mL of DCM (corresponding to $2.0*10^{-3}$ M); [b] total amount including stock solution; [c] concentration with respect to (EsterMon + MonGW21); [d] reaction time until quenching

Table 35: Experimental details of the copolymerization of $[(Mon1)_9(GW021)_1]_m$

ratios		EsterMon		MonGW21		M31[a]	DCM[b]	c[c]	time[d]
m	DP_{target}	mg	mmol	mg	mmol	µL	mL	M	h
10	100	47.3	0.23	126.2	2.5E-2	1000	8.0	3.0E-2	3.0
100	1000	94.6	0.45	252.3	5.0E-2	400	15.0	3.3E-2	15.0

[a] stock solution: 3.75 mg **M31** in 2.0 mL of DCM (corresponding to $2.5*10^{-3}$ M); [b] total amount including stock solution; [c] concentration with respect to (EsterMon + MonGW21); [d] reaction time until quenching

Table 36: Experimental details of the copolymerization of $[(Mon1)_9(GW032)_1]_m$

ratios		EsterMon		MonGW21		M31[a]	DCM[b]	c[c]	time[d]
m	DP_{target}	mg	mmol	mg	mmol	µL	mL	M	h
10	100	30	0.14	169	1.6E-2	1000	3.0	5.3E-2	2.0
100	1000	45	0.21	253.5	2.4E-2	150	8.0	3.0E-2	4.0

[a] stock solution: 2.4 mg **M31** in 2.0 mL of DCM (corresponding to $1.6*10^{-3}$ M); [b] total amount including stock solution; [c] concentration with respect to (EsterMon + MonGW21); [d] reaction time until quenching.

8 APPENDIX

8.1 Chemicals and Instrumental Details

Complexes **M31**, **M2** and **M22** were purchased from Umicore AG and used as received. Complexes **M32** and **SIPr-PCy₃** were prepared by the Nolan group according to their procedures and used as received. All other chemicals were purchased from established commercial resources (Alfa Aesar, Sigma Aldrich, Roth) and used as received.

NMR spectra were recorded either on a Bruker Avanze 300 MHz spectrometer or on a Varian INOVA 500 MHz spectrometer operating at 499.803 MHz (^{1}H) and 125.687 MHz (^{13}C) respectively. Chemical shifts are given in ppm relative to a SiMe$_4$ standard. The solvent peak of CDCl$_3$ was used for referencing the NMR spectra to 7.26 (^{1}H) and 77.16 ppm (^{13}C), respectively.

GPC measurements for determination of molecular weights and the PDI of the polymers were carried out in tetrahydrofuran (THF) with the following arrangement: a Merck Hitachi L6000 pump, separation columns of Polymer Standards Service (5 µm grade size) and a refractive-index detector from Wyatt Technology, model Optilab DSP Interferometric Refractometer. For calibration Polystyrene Standards purchased from Polymer Standard Service were used.

Simultaneous thermal analysis (**STA**) was performed with a Netzsch Simultaneous Thermal Analyzer STA 449C (crucibles: aluminum from Netzsch). A helium flow of 50 mL*min^{-1} was used in combination with a protective flow of 8 mL*min^{-1}.

XRD measurements to obtain crystal structures were performed on a Bruker AXS Kappa APEX II diffractometer using Mo Kα radiation. The structures were solved by direct methods using SHELXS and refined with SHELXL. The absorption correction was performed using the program SADABS.

Tensile strength tests were performed on a Shimadzu Autograph AGS-X, with a force measuring range from 10-10 kN. Clamping length of the samples was 80 mm; an initial tension of 10.0 N was applied. The area of the shouldered test bars was 35.2 mm^2 in the reduced section; samples were measured with a speed of 1 mm/min.

8.2 List of Figures

8.3 List of Schemes

8.4 List of Tables

8.5 Abbreviations

ADMET	acyclic diene metathesis polymerization
ATRP	atom transfer radical polymerization
CM	cross metathesis
COD	cyclooctadiene
DCM	dichloromethane
DCPD	dicyclopentadiene
DP	degree of polymerization
DSC	differential scanning calorimetry
GPC	gel permeation chromatography
HIPE	high internal phase emulsion
IMes	1,3-dimesityl-imidazole-2-ylidene
MALDI-TOF	matrix assisted laser deposition ionization – time of flight
Mon	monomer
NHC	N-heterocyclic carbene
NMR	nuclear magnetic resonance spectrometry
OLED	organic light emitting diode
PBA	poly butyl acrylate
PDMS	poly dimethylsiloxane
PEG	poly ethylene glycol
PMMA	poly methylmethacrylate
PS	polystyrol
RAFT	reversible addition–fragmentation chain transfer polymerization
RCM	ring closing metathesis
RIM	ring injection molding
ROMP	ring opening metathesis polymerization
ROP	ring opening polymerization
rt	room temperature
SIMes	1,3-dimesityl-4,5-dihydroimidazole-2-ylidene
SI-o-Tol	1,3-di(*ortho*-tolyl-4,5-dihydro-imidazole-2-ylidene
SIPr	1,3-di(2,5-di-isopropyl-phenyl)-4,5-dihydroimidazole-2-ylidene
STA	simultaneous thermal analysis
TGA	thermal gravimetric analysis
TLC	thin layer chromatography
TMSD	trimethylsilyldiazomethane
V$_{Bur}$	buried volume
XRD	X-ray diffractometry